Computational study on prediction and reduction of aerodynamic noise from fans

LIM, Tae-Gyun / 林, 泰均

(開始ページ / Start Page)
1
(終了ページ / End Page)
154
(発行年 / Year)
2018-03-24
(学位授与番号 / Degree Number)
32675乙第229号
(学位授与年月日 / Date of Granted)
2018-03-24
(学位名 / Degree Name)
博士(工学)
(学位授与機関 / Degree Grantor)
法政大学 (Hosei University)
(URL)
https://doi.org/10.15002/00014768

Doctoral Dissertation Reviewed by

Hosei University

Computational study on prediction and reduction of aerodynamic noise from fans

（ファンから生じる空力騒音の予測と低減に関する計算的研究）

Tae-Gyun Lim

林　泰均

Supervisor : Professor **Gaku Minorikawa**, Hosei University

Abstract

Turbomachinery is machinery device in which energy is delivered either to or from fluid that is continuously moving due to action of moving blades. Performance and flow noise are two major indices for evaluation of turbomachinery. In terms of energy transfer, researches on performance of turbomachinery have been conducted since long time ago; and these researches for performance improvement are still ongoing currently. In addition, flow noise produced by turbomachinery came to the fore as turbomachinery has been used in various fields and everyday life closely and frequently. Especially, consumers' demand on improvement in affective quality has been increased and regulation on noise has been being reinforced due to damages and adverse effects caused by noise. Therefore, development of high performance and low noise turbomachinery is highly required.

Meanwhile, experimental methods have been used to develop low noise turbomachinery; however, the experimental methods solely are not sufficient to achieve such aim since measuring in small turbomachinery is challenging. Hence, prediction technique, to which the numerical analysis method that yields complementary effects in combination with the experimental methods is applied, is required.

This study was conducted with the aim of applying numerical analysis method for noise reduction in turbomachinery. Therefore, three-dimensional unsteady Navier-Stokes equations were solved to simulate the flow field. Turbulence models used to predict the flow field were SST k–ω model that provides outstanding simulation of separation and adverse pressure gradient in boundary layer and LES model that presents excellence in turbulence intensity modeling, respectively. Computational Aeroacoustics (CAA) used to predict the flow noise in this study was acoustic analogy that is one of the hybrid methods; and the acoustic analogy is the method analyzing unsteady flow field by using Computational Fluid Dynamics (CFD) and then predicting noise by using the information of unsteady flow field obtained from the results of CFD simulation. To conduct acoustic analogy, Lowson equation, which can be used to predict sound pressure for point force that is moving in a free field, was calculated. Despite of disadvantage that influence of an object including scattering, diffraction, and reflection

within acoustic field is difficult to be considered, this method that directly reduces noise sources was able to be drawn since the locations of the noise source can be seen by numerical approach. Because predicting the location of the noise source is able to figure out the unsteady flow which causes the noise. As a result, the reduction method of flow-induced noise in this study is to find the way to reduce or remove the unsteady flow generating the noise, based on CAA and CFD.

In order to indicate the location of the noise source, "Aeroacoustic source strength, A_{st}" was defined and compared with the location of the noise source measured by the acoustic camera to which beamforming technology is applied; and they were agreed qualitatively well each other.

Due to miniaturization of electronics and maintenance of fan performance, whereas size of fan is getting smaller, the rotational speed of it getting higher. In this study following the current trend, three fans with each other different type were used for adopting numerical method to noise reduction; i) a small axial fan of rotor's diameter D = 0.166 m and a rotation speed 2860 rpm with circular shroud, ii) a small axial fan of rotor's diameter D = 0.076 m and a rotation speed 7000 rpm with square-type shroud used in a rack mount server computer, iii) a small centrifugal fan with rotor's diameter D = 0.032 m and a rotation speed 10460 rpm used as a cooling fan in portable home electronics such as a small laptop computer. The noise of each type fan was predicted and compared with the measured noise. The predicted noise and measured noise presented agreement in tonal noise of the blade passing frequency (BPF) and its harmonic frequencies and in the broadband noise at low frequency. Although the broadband noise at high frequency was somewhat different due to random broadband noise, the shapes for noise reduction were able to be drawn effectively by predicting the location of the noise sources. Low noise models suggested for noise reduction provided the result of noise reduction from the prediction and specific noise level was used to evaluate the noise reduction considering the changes in fan performance.

In case of the axial flow fan with circular shroud, the interaction between the rotating rotor blades and the flow separated from the inlet of the shroud was found to be the major cause of the noise through the analysis on the location of the noise sources and unsteady flow field. Consequently, reduction of the flow noise was predicted by correcting the shape of the shroud inlet.

Abstract

In the small axial flow fan installed in the rack mount server computer, the tonal noise occurring by irregular clearance between the blade tip and the shroud due to the square-shaped shroud was well predicted. In addition, coherence analysis was conducted to identify the relationship between the surface pressure fluctuation due to the flow and the sound pressure predicted from the microphone. As a result, the correlation for each frequency was well presented.

For a centrifugal fan that is used as a cooling fan in home electronics such as a portable small laptop computer, the flow structure of the centrifugal fan was simulated by setting the condition to be analogous to the operating condition within the actual product. And then the reduction of the flow noise was predicted by correcting the tip of the impeller blades based on the location of the noise sources.

This study aimed to apply the method of numerical analysis to the noise reduction in turbomachinery. For this, the unsteady flow field was analyzed, the result of noise prediction obtained from the flow filed information was compared and validated, and the location of the noise sources and the structure of the flow field causing the noise were understood; hence, the low noise design was able to be drawn effectively and properly. In this study, the reduction of the flow noise was successfully achieved by adopting the method of numerical analysis and the flow noise of the fan that were improved for noise reduction was predicted to be reduced by 0.8 and 3.7 dB, respectively.

Table of Contents

Nomenclature

A_{st}	:	aeroacoustic source strength
a_0	:	speed of sound
C_s	:	Smagorinsky model constant
D	:	diameter of the rotor
dB	:	decibel
F	:	force, blending function
G	:	Green's function, filter function
H	:	head of the impeller
H_n	:	helicity
K_{sa}	:	specific noise level
L	:	length
M	:	Mach number
n	:	unit normal vector
p	:	pressure, acoustic pressure
Q	:	strength of point source, flow rate
r	:	vector from source to observer
Re	:	Reynolds number
S_ϕ	:	source term
T	:	torque, Lighthill stress tensor
t	:	time
V	:	angular velocity vector

Greek letters

δ	:	delta function
ϕ	:	dependant variable
ρ	:	density
Γ	:	diffusion coefficient
μ	:	viscosity coefficient
τ	:	shear stress, time

Subscript

fluid	:	caused by the fluid flow
ref	:	reference
ret	:	quantity evaluated at the retarded time
SGS	:	Sub-Grid Scale

Symbol

∂	:	partial derivative
Δ	:	filter size

List of figures

List of figures

List of figures

List of tables

Chapter 1. General introduction and literature review

1.1 Background

Turbomachines are defined as all those devices which exchange energy either to, or from, a continuously flowing fluid through the dynamic motion of one or more moving blade rows. The word "*turbo*" or "*turbinis*" is from Latin origin and implies that which spins or whirls around [1]. Especially, the rotating blade row changes the pressure of the fluid by either doing work on the fluid (as a pump) or having work done on the blade row by the fluid (as a turbine), depending upon the purpose required of the machine [2].

The fan with the purpose of air conditioning was invented by Ding Huan who was a master artisan and engineer of Han Chinese in around the second century. The fan was in diameter of 3 *m* and manually rotated. Since then, Chinese in dynasty era used fan more frequently and they sometimes used water power to rotate fans [3]. The first rotating fan used in Europe was used to ventilate the inside of a mine during the 16th century as described by Georg Agricola (1494-1555) [3]. In 1727, Dr. John Théophile Desaguliers who was a British engineer designed the fan system for ventilation of mine in Westmorland by using the theory of chimney; and installed further improved device in Houses of Parliament in 1745. However, it was not utilized much due to difficulties in finding power source for operation of the fan. Afterwards, power-operated fans were begun to be used and the use was rapidly increased since the electric powered fan was invented at the end of 1800s. Now, fans are the most frequently used turbomachinery in everyday life as the one cannot find the field including the field of electric/electronic, automobile, and aviation where fans are not used. Examining the classification of fluid machinery, these can be divided by depending on the purpose of use such as displacement, kind of fluid, direction of energy or flow and so on. Figure 1-1 shows the classification of fluid machinery in detail. The turbomachines are classified by direction of energy as a pump and a turbine, can be divided again by direction of flow as axial flow type, radial flow type and mixed flow type, respectively. For instance, axial flow fans present uniform direction of the flow in general and are used where with high flow rate and small pressure difference. However, many axial flow fans were stacked in multi-layer for cases where large pressure difference and high flow rate are required

such as the engine of the air planes (Figure 1-2). Meanwhile, centrifugal fans have been used in vacuum cleaners, automobile HVAC and ventilation system for buildings where pressure difference rather than flow rate needs to be increased in small space. With the increased use of fans, issues of the fan noise that had not been considered before came to the fore. In particular, the sound source of the fan noise is in the space where people works in; hence, the radiation within the closed building and inside a room causes major noise issues. Predicting the noise source and the radiation patterns of the noise is essential since such noise has various influences including sleep interruption and the decrease in work efficiency.

In terms of energy, fans are the devices that transform the momentum energy to flow energy by delivering energy to flow through rotation of fan blades. In other words, the aim of a fan is to deliver energy to flow; hence, the primary interest is still in its performance. Various researches through experiments or numerical analysis have been conducted to improve fan performance up to date. Owing to the rapid development of calculation capacity of computers in the late 1990s, researches of numerical analysis on flow field of a fan have been being conducted particularly.

Interest in the noise caused by a fan is growing due to the increase in the use of fans as these are used in wide range of industrial field. For axial flow fans, the noise caused by airplanes was drawn attention relatively earlier as axial flow fans were used in the jet engines of airplanes. Consequently, a good number of results have been communicated by numerous researchers studied on the cause of noise and prediction methods in the 1960s and 1970s [4-7]. As a result, the fan noise mechanisms which explain the noise type generated by each source were summarized by Neise [8] in 1992 as following figure 1-3. Blade thickness noise or monopole noise is known, as giving a significant influence to fan noise only when the blade tip speed is over Mach number 0.5. The source of monopole noise is due to the volume displacement effect which generates repeatedly the disturbance in the flow field when the moving fan blade displaces fluid mass. The dipole noise is called loading noise and generates discrete and broadband noise. It can be explained as the noise generated by forces acting on the fluid. The quadrupole is related to Lighthill’s term and represents the sound radiation by fluctuating Reynolds stresses within fluid layers. According to Morfey [4], it becomes dominant issue only when the blade tip of rotational speed is greater than the Mach

number 0.8. It's well-known to be generated typically by shear stresses.

Fans that are used in field of home appliances and automobiles are operated in subsonic domain; hence, the cause of the noise is different from the cause of the airplane's noise and the size of the noise is relatively smaller than that caused by airplanes. Therefore, the practical noise reduction method through experiment has been studied. Since then, fans have been being widely used in closed area or near life space and thereby, consumers' demand on affective quality has also been increased according to overall improvement in quality of products in the late 1990s. As a result, numerous researches adopting experiment or numerical analysis have been conducted. In addition, researches measuring and visualizing noise sources by utilizing beamforming are being conducted recently. Beamforming is one of microphone array locating technology. It can be considered as one of the usual acoustics visualizing method and is frequently used in industrial field to detect noise sources owing to its advantage of high speed, contactless, and high resolution. Researchers have been trying to find continuously the sound source, because it's very important to find the place at where the source is located, in order to reduce the noise. However, only experimental methods are not enough to find and understand the unsteady flow field generating the noise. The numerical analysis is necessary to find and figure out the location of the sound source and the unsteady flow field generating the noise. Therefore, prior to adopting numerical analysis method for reduction of the flow noise, the locations of noise sources predicted by the numerical analysis in this study was compared with that measured by a equipment like a sound camera which has been developed based on a beamforming technology.

In summary so far, the noise of fans used in the industrial part except the aviation field was taken late relatively the customer's attention and the main focus of the flow-induced noise in this study became the dipole noise. The application of the numerical analysis based on the main focus can provide the high feasibility for noise reduction in the turbomachines.

Meanwhile, the acoustics at dictionary is the branch of physics that deals with sound and sound waves in gases, liquids, and solids. Sound waves are classified by infrasound (f < 20 Hz), audible sound (20 Hz < f < 20 kHz) and ultrasound (20 kHz < f < 5 MHz) depending on frequency range. In audible sound, the classification of noise or music is

divided by whether giving people displeasure or not, when people listen to the sound. Though the noise is divided as structure borne noise and airborne noise depending on the transmission medium of the sound waves, aeroacoustics was covered in this study. The aeroacoustics is a branch that studies the noise generated by the turbulent flow, the periodically varying flow, the aerodynamic force interacting with a surface and so on. Ffowcs Williams [9] defined that flow noise is the term used to describe the pressure fluctuations associated with unsteady flow, particularly turbulent flow. Therefore, the numerical method, which is called as Computational Aeroacoustics (CAA), as well as Computational Fluid Dynamics (CFD) to predict the unsteady flow field were required to understand or predict the flow noise in detail. CAA is a part of aeroacoustics to analyze the flow-induced noise generated in the flow field through numerical methods. The numerical method predicting noise caused by flow is majorly classified into two kinds: direct method in which flow field and acoustic field that may be the noise source are analyzed simultaneously and hybrid method in which flow field that is the region of the noise source and acoustic field where the noise propagates are analyzed separately under the assumption that the influence of the acoustic field on the flow field is ignorable (Figure 1-4).

The direct method of the noise prediction is the method in which the sound pressure that causes noise is directly calculated by using the numerical method. However, the researches on this method were started to be conducted in the 1990s for the first time and have not been utilized wieldy even nowadays due to two reasons. The first reason is the physical causes including the differences in scale of the length between the flow field and the acoustic field and the difference in perturbation size between the flow field and the acoustic field. The second reason is caused by the demand of the numerical techniques requiring the high-order accuracy in the frequency-wavenumber domain as well as in the time-space domain.

The hybrid method of noise prediction analyzes the unsteady flow field, as the noise source region, by using Computational Fluid Dynamics (CFD) and then predicts noise propagation by utilizing acoustic analogy, boundary element method, and linear/nonlinear acoustic propagation equation. In this study, the hybrid method that has been known to be more efficient than the direct method was used. After obtaining unsteady flow field by utilizing CFD, the noise was predicted by using acoustic analogy

which is the one of hybrid methods. In general, it has been known that the appropriate model among numerous acoustic analogies should be applied by taking account of the environment where the flow noise of interest occurs because noise prediction based on acoustic analogy proposes a kind of approximate solution through the modeling of major noise sources. This study utilized the acoustic analogy derived from the Lighthill equation [10, 11]. The method using acoustic analogy allows obtaining accurate solution up to farther distance; however, the influence of scattering or reflection is difficult to be considered in case of having scattering or reflection due to an object when the object is inside the acoustic field. Notwithstanding this problem, the acoustic analogy can sufficiently propose the efficient and direct method for flow noise reduction by predicting the location of noise sources. The method of flow noise reduction with the numerical analysis is composed of the following procedures; first is the validation of the noise prediction value obtained from the aeroacoustic noise analysis utilizing acoustic analogy, second is the analysis on the locations of the predicted noise sources, third is the analysis and identification of unsteady flow causing the noise sources, and fourth is the prediction of the noise reduction by taking account of the shape that can reduce the unsteady flow related to the noise sources.

The fundamentals of aeroacoustic analogy was established by the sound wave equation in free space proposed by Lighthill in 1952 and 1954 and Curle [12] revised the equation so that it can be valid even in case of having object surface. In 1965, Lowson [13] induced the equation predicting sound pressure caused by moving point force and Ffowcs Williams and Hawkings [14] defined the flow noise sources occurring from moving objects with arbitrary velocity within the flow by expanding the acoustic analogy proposed by Lighthill and Curle.

In this study, acoustic field caused by the turbomachinery in a free space was predicted through the numerical analysis by using Lowson equation based on the information of unsteady flow field due to the turbomachinery. In addition, application of the numerical analysis to reduce the flow noise of the turbomachinery used practically was focused by describing the distribution of the noise sources through defining “Aeroacoustic source strength” from the result of the aeroacoustic noise analysis.

1.2 Literature review

In case of considering the operating fluid as gas, fans can be defined as the machineries with an impeller or a rotor that exerts mechanical work letting the gas to flow with arbitrary energy and is the turbomachinery that is the most frequently used in everyday life. The rotation velocity of a fan can be increased to maintain the performance depending on its operating condition, size, and shape. This complicates the flow field, increases the flow noise, and thereby causes serious problems in products. Therefore, researches on fans were reviewed after classified into the flow analysis and the flow noise.

The flow analysis of a fan can be distinguished into the simple way analyzing the performance only and the method analyzing the flow field. Initially, only the performance of the impeller that supplies energy was studied in order to predict fan performance. Since then, the method that predicts the head of turbomachinery in a simple manner by using a velocity triangle with infinity blade theory was developed in the early 20^{th} century. Afterwards, the method that predicts performance based on finite blade theory where the slip factor was introduced was developed and numerous equations with regard to the slip factor have been studied. As shown in figure 1-5, Wiesner [15] provided the information for determination of slip factors within limitation of the mean radius ratio of the impeller in centrifugal impeller applications. Exceeding the limitation, an empirical correction was proposed.

Weissgerber and Carter [16], Takagi et al. [17] and Rathod and Donovan [18] proposed a prediction method for centrifugal pumps in different types and with specific rotation speeds. Such method used a simple velocity triangle combined with several experimental equations and could predict somewhat accurate values for impellers in simple shape only in a narrow range near the best efficiency point, due to the causes of the inadequate flow modeling and without the consideration of all possible losses. Nevertheless, they have been still used by many business entities.

Aforementioned method predicts the performance only; therefore, it does not offer information about the flow field including velocity or pressure on the blade surface. The origin of such method for the flow field analysis can be recognized as shown in figure 1-6 that Wu [19] divided the three-dimensional passage flow into S_1 and S_2 surface and calculated for each case in 1954. The method was further developed by Katsanis [20] in

1964 and numerous studies have been done based on Katsanis's method. However, such methods were useful only when analyzing impellers at steady state and had the disadvantage that it was not able to be used when analyzing impellers at unsteady state or considering fans with the fixed parts including the casing and diffuser.

With the development of computers since the 1980s, studies on transient characteristics of two-dimensional inviscid unsteady state impeller had been conducted with the use of vortex panel by Tsukamoto and Ohashi [21], Imaichi, et al. [22], Tsukamoto, et al. [23], and Shoji and Ohashi [24]. Figure 1-7 shows the characteristics for the stopping transients through comparison of the calculated and measured data by Tsukamoto, et al. Afterwards, Kiya and Kusaka [25] conducted a numerical research on characteristics of the unsteady flow that was separated from the leading edge of the blade of the centrifugal impeller in the flow field of the two-dimensional inviscid incompressible fluid by using discrete vortex method in 1989. Owing to the rapid development of computer performance since the late 1990s, the three-dimensional flow field caused by the turbomachinery was simulated with the numerical analysis method and a good number of researches aiming for the improvement in fan performance have been conducted [26-28]. Panigrahi and Mishra [26] simulated the flow field near the airfoil produced by the angle of attack by using k–ε turbulence model in order to improve the efficiency of the axial fan for mine ventilation. In order to identify the effect of the vortex design and blade lean of the nozzle guide vane at turbine inlet, Zhang et al. [27] conducted the numerical analysis with SST k–ω turbulence model, analyzed the loss occurring in the guide vane according to the cause, and showed the distribution of each loss component based on the direction of the axis in figure 1-8. Pogorelov et al. [28] conducted a large scale numerical analysis on the influence of the clearance in the tip leakage flow generated at an axial flow fan and analyzed the tip leakage vortex by using LES model. Figure 1-9 shows the unsteady flow field depending on time about each clearance.

Looking at a turbulence model used to simulate the flow field for fan performance prediction of the previous studies in recent years, Reynolds-Averaged Navier-Stokes (RANS) turbulence model established with the approach in terms of time-average is still being used. Because the reason presents excellent stability of convergence even though the number of grids used is small. Recently, the frequency of using LES model that

allows identification of turbulence eddy in various sizes by conducting direct analysis without physical modeling about turbulence eddy which is larger than a mesh size has been being increased.

The below is a brief review on acoustic analogy that is the fundamentals of the aeroacoustic noise. From the study reported by Lynam and Webb [29] in 1919, the acoustic noise by turbomachinery has been concentrated to predict the acoustic noise caused by rotor sand propellers of helicopters. Thereafter, his study by Gutin [30] shown in figure 1-10 made a significant progress in the field of acoustic noise prediction. However, Gutin noise caused by the steady loading generating on propellers was not useful for fan noise prediction. In 1952, Lighthill [10] established aeroacoustics theory through conducting the dimensional analysis on the acoustic noise generation by using flow velocity and shape variables. Tyler and Sofrin [31] analyzed the noise radiation of rotating sources in a duct by simplifying the rotating fan as the acoustic source arranged to circumferential direction on the disk plane with using mode theories They reported that each blade number of rotor and stator is the most dominant factors in noise occurred by the interaction between the rotor and the stator. In 1965, Lowson induced the formula calculating the acoustic pressure produced by a moving point force [13]. Ffowcs Williams and Hawkings (FW-H) [14] drew an equation for a moving acoustic source by expanding the Curle's study [12] which could not consider a moving acoustic source.

Meanwhile, the initial studies on the flow noise produced by the interaction between a rotating object such as a fan and the surrounding structures focused on the development of the method for noise reduction and noise prediction based on the experiments rather than the numerical analysis. The researches [32-37] related to the noise of centrifugal fans were more focused on the noise reduction by adjusting the increase of cut-off intervals, the lean of the impeller blades and cut-off edges, the mesh installation on leading and tailing edges of the impeller blades, and the placement of impeller blades asymmetrically. Figure 1-11 shows the effect of impeller with sloping blades in the noise reduction.

With the improvement of computational performance in 1990s, direct calculation based on Lighthill equation was enabled to predict the aeroacoustic noise. However, it is

still challenging to conduct the direct method of the noise field analysis due to the numerical methods requiring the high capacity grids and the accuracy of higher order. Researches for noise prediction are still being conducted by utilizing CFD or taking the hybrid method yet [38-44].

In figure 1-12, Chen and Wu [38] showed that tonal noise of the blade passing frequency (BPF) and its harmonic frequencies is occurred by the interaction between a rotating rotor and a stationary structure through a vortex method based on Lagrangian frame. As shown in figure 1-13, Jang et al. [39-42] studied experimentally and numerically the influence of the tip leakage vortex generated by the tip clearance in an axial flow fan. They showed that reverse flow region was occurred repeatedly by periodic movement of the tip leakage vortex and the tip clearance near the reverse flow region caused the discrete frequency noise. Carlous et al. [43] studied on the noise prediction method for broadband noise of the low-pressure axial flow fan based on Semi-empirical noise prediction model (SEM) and LES models. The authors especially focused on the prediction of the interaction noise by ingested turbulence. As shown in figure 1-14, the method using SEM was easy to apply to the noise prediction; however, it was confirmed that it was not able to describe details in fan shapes and flow phenomenon such as separation. The method of the numerical analysis using LES model was good at predicting the noise influenced by the shape, the effect of the ingested turbulence on the sound sources, and fan noise; however, differences was found in broadband noise. Ballesteros-Tajadura et al. [44] conducted a numerical analysis for the unsteady flow to predict the noise from a radial flow fan and then predicted an acoustic field around the fan by using the FW-H equation and the surface pressure fluctuations on rotor and volute tongue obtained from the flow field. Finally, they measured sound pressure level (SPL) in experiment and compared it with the results obtained from the simulation in figure 1-15. They presented differences in prediction of the broadband noise and tonal noise, respectively. Scheita et al. [45] showed in figure 1-16 that wrap angle in a small radial fan was clearly related to aerodynamics and flow noise. They also reported that an isolated impeller could improve the aerodynamic efficiency but did not generate the flow-induced noise radiation.

For more accurate noise prediction, consideration on the interaction between the sound

and the structures including scattering and diffraction was known to be required. To do this, the wave equation in which the structures are considered with the aid of FED and BEM should be solved. However, the two analysis methods require additional preprocess including appropriate surface grids and space grids for aeroacoustic noise analysis. Getting more accurate result for the noise field is important; however, predicting noise in a free field by utilizing the hybrid method was determined to be sufficient for application of the numerical method to the noise reduction in the turbomachinery. Hence, the noise field was predicted by using the hybrid method rather than the direct method with high load for aeroacoustic noise prediction and aeroacoustic analogy in a free field was used.

The aeroacoustic analogy analyzes the acoustic field by using the analytical solution for all of monopole, dipole, and quadrupole noise sources. However, most fans excluding the fans used in field of aviation are operated in supersonic domain with small Mach number (*M*). Neise reported the dipole noise source as the major noise source of the turbomachinery that are operated in supersonic domain and described the understanding on the noise source of a fan as shown in figure 1-3 [8]. And it was not easy to apply the FW-H equation to practical problems; hence, an easier calculation method using Lowson equation was proposed by Jeon and Lee [46]. The static wall pressure fluctuations of a body obtained after simulating the unsteady flow field are used for CAA calculation by this method [47-54]. Jeon [48], Jeon and Lee [49], and Jeon et al. [50] predicted the noise of centrifugal fan by using the two-dimensional discrete vortex method. In those studies, BPF tone noise was well agreed whereas there was somewhat large difference found in broadband noise. As shown in figure 1-17, the disagreement in broadband noise was determined to be caused by the difference between the complicated actual flow in three-dimensional shape and the two-dimensional flow analysis. Lim et al. [51, 52] predicted the noise of the turbomachinery by taking account of the three-dimensional shape and compared the prediction with the experimental value. In addition, the authors described the flow characteristics related on noise sources by analysing the locations of the noise sources. Lim et al. [53, 54] adopted the numerical analysis method for noise reduction in the turbomachinery by analysing the locations of the noise sources.

1.3 Methodology

This study was conducted with the focus on the application of the numerical analysis on the acoustic field for noise reduction in the turbomachinery. With this purpose, the acoustic field produced by the turbomachinery was predicted in a free space by using Lowson equation that predicts the acoustic field occurring by the moving point force based on the research result that the dipole is dominant in the acoustic field. The process of the numerical analysis on the unsteady flow field for application of Lowson equation was conducted in following sequence: steady state fluid analysis that minimizes the calculation time by creating the sketchy flow field that is produced by the turbomachinery in the semi-anechoic room, the unsteady state flow analysis for full development of the unsteadiness caused by the turbomachinery, and the unsteady flow field analysis to obtain the surface pressure fluctuation in the rotating part and fixed part by time during several rotations of the rotor. At the moment, the fluid properties were checked at arbitrary locations in order to fully develop the unsteadiness of the flow field. For three-dimensional simulation of the flow field, the turbulence models used in steady state and unsteady state were SST k–ω that can predict the adverse pressure gradient on the surface of the blade and LES model that is excellent in modeling of the turbulence intensity, respectively.

The surface pressure fluctuations by time obtained from the flow field analysis and the noise spectrum predicted by aeroacoustic analogy were verified after comparing with the noise spectrum measured in the semi-anechoic room for each model. Through the comparison between the noise spectrums, good agreement in the tonal noise of the 1st BPF and its harmonic frequencies and in the broadband noise was shown at a low frequency range; however, difference was found from the broadband noise at high frequency. Such disagreement was determined to be caused by the random broadband noise. In general, random broadband noise is caused by various phenomena such as turbulent boundary layer, vortex shedding, flow separation, and tip vortex. However, the scattering influence by the turbulent boundary layer which was occurred from the trailing edge of blades was not considered in this study. As a result, such disagreement of prediction at high frequency range was caused by consideration of only the dipole.

Meanwhile, the location of the noise sources was described in validated result of the noise prediction by defining Aeroacoustic source strength (A_{st}) that can predict the

location of the noise source and the unsteady state flow producing the noise based on the location of the noise source was confirmed. Prior to this study, the feasibility of the prediction of the noise source location was verified through the comparison between the location measured by using an acoustic camera with beamforming technology and the location predicted by the numerical analysis.

In addition, the correlation between the sound pressure predicted from the microphone located 1 *m* apart from the turbomachinery and the surface pressure fluctuation by time obtained from each of the two points (bell mouth and strut) in the unsteady flow field were confirmed by conducting coherence analysis. It was able to confirm the difference in the flow field between the two points from the coherence analysis on the frequency.

The numerical analysis method was applied for the comparison of the numerically predicted value and the measured value of the flow noise in the turbomachinery, for understanding and analysis of unsteady state flow producing the noise based on the location of the noise source, for identification of the shape reducing the unsteady state flow causing the noise, and for the reduction of the flow noise in the turbomachinery.

1.4 Objectives of this study and outline

In Chapter 1, the motive, background, and purpose of the research were stated and literature review and method and range of the research were described.

In Chapter 2, the numerical analysis method for simulation of the flow field and that for prediction of the noise produced by the turbomachinery in a free space was described. The noise of the turbomachinery in a free space was calculated by using Lowson equation under the assumption that it is produced from the rotating parts (impeller and rotor) and fixed parts (shroud). However, the numerical analysis on surface pressure fluctuation acting on the rotating parts should be done first in order to calculate aeroacoustic noise. Therefore, the unsteady flow field was numerically analyzed as a preceding study for noise analysis and the method to obtain the information on the flow field was described. For prediction of the location of the noise source, the possibility of the prediction was confirmed in advance by comparing with the location of the noise source measured by the acoustic camera.

In Chapter 3, the experimental setup measuring the flow noise and the numerical setup for prediction of the flow noise were introduced. Details including the size of semi-

anechoic room for measuring the noise of the turbomachinery, the rotating speed, the location of the microphone, the conditions of the computational domain and boundary, the grid information, the convergence condition, and the time step were described.

In Chapter 4, the flow noise predicted was compared with that measured from the axial flow fan with cylindrical shroud and the unsteady state flow causing the noise was confirmed. In order to reduce the unsteady state flow causing the noise, the flow noise was reduced by correcting the shape of the shroud inlet. Degree of the noise reduction was compared by using specific noise level among all other indexes representing the changes in fan performance owing to the changes in the shape of the shroud inlet in this study.

Chapter 5 handles the prediction of the characteristics of the noise produced by a small axial flow fan for cooling. In particular, the tonal noise due to the shape of the square-type shroud and the locations of the related noise sources were predicted. In addition, the correlation between the flow field and the noise was confirmed by conducting coherence analysis on the surface static pressure fluctuation obtained from each of bell mouth and strut, the two points on the shroud, and sound pressure fluctuation that was predicted from the microphone location.

In Chapter 6, the flow characteristics and noise of the centrifugal fan that has been used for cooling in portable home electronics including small laptops and ultrabooks were predicted. For this, the centrifugal fan that is installed between the two thin square flat boards was studied in order to give the condition that is analogous to the fan operated inside a product. Based on the result of the numerical analysis, the blade tip of the impeller was corrected to reduce the unsteady flow related to the flow noise and the aeroacoustic noise in corrected impeller shape was predicted. In addition, the specific noise level was used to compare the noise reduction of the centrifugal fan considering the fan performance.

Chapter 7 described the summary of the results obtained in this study.

1.5 Summary

The sound is divided as unpleasant noise and pleasant one. Though the noise is also classified by structure borne and airborne depending on the transmission medium of the sound waves, aeroacoustics was only considered in this study. The flow-induced noise is

generated by the turbulent flow, aerodynamic force interacting between surfaces, the periodically vary flow, and so on. Especially, the flow noise defined by Ffowcs Williams [9] is known as the term used to describe the pressure fluctuations associated with unsteady flow, particularly turbulent flow. Therefore, understanding and analyzing the unsteady flow field in detail have been being required obligatorily to predict and reduce the flow noise. In other words, the flow noise is related closely to the fluid dynamics and the acoustics.

Meanwhile, as fans have been used in wide range of the industrial field, the fan performance and the noise generated from fans have been taken attention. Looking at the study by Neise [8] and fan noise mechanism to explain the noise type, the noise of fans used in the industrial field except the aviation part is known that dipole is the dominant noise source. Numerous studies using experimental methods have been conducted to reduce the noise. But due to miniaturization of a product, the numerical analysis has been asked to figure out the unsteady flow field in the inside of the product in detail and to predict the sound source. It means that finding the relationship between the unsteady flow field and the sound source is important. Therefore, the objective in this study is to apply and use the numerical method in order to find the relationship between unsteady flow field and the sound source and conduct the noise reduction.

The detailed contents for accomplishing the purpose of this study are as follows. In this chapter, the background, literature reviews about the flow-induce noise, methodology, objectives and outlines of this study were reviewed for introduction of turbomachines. Chapter 2 mentioned the numerical method for simulation, and Chapter 3 described the setup about experiment and simulation, respectively. By considering fans installed in the electronic products, three different type fans were used for applying the numerical analysis to noise reduction. Chapter 4, 5 and 6 showed validation of predicted results obtained from CAA, and then low noise models about an axial flow fan and a centrifugal fan were suggested and provided the noise reduction through numerical analysis. In Chapter 7, the results obtained in this study were summarized.

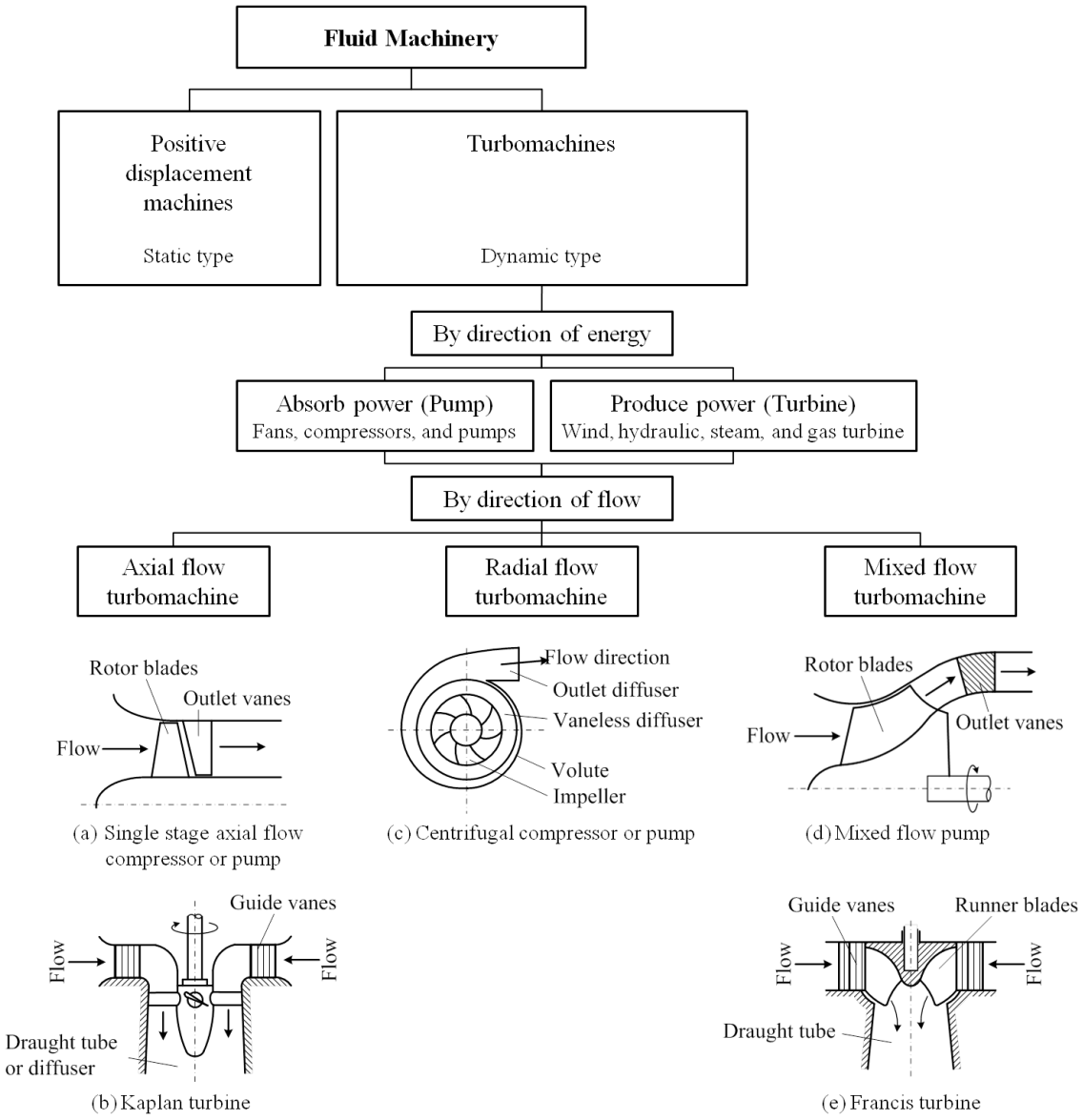

Fig. 1-1 Classification of fluid machinery and examples of turbomachines [1]

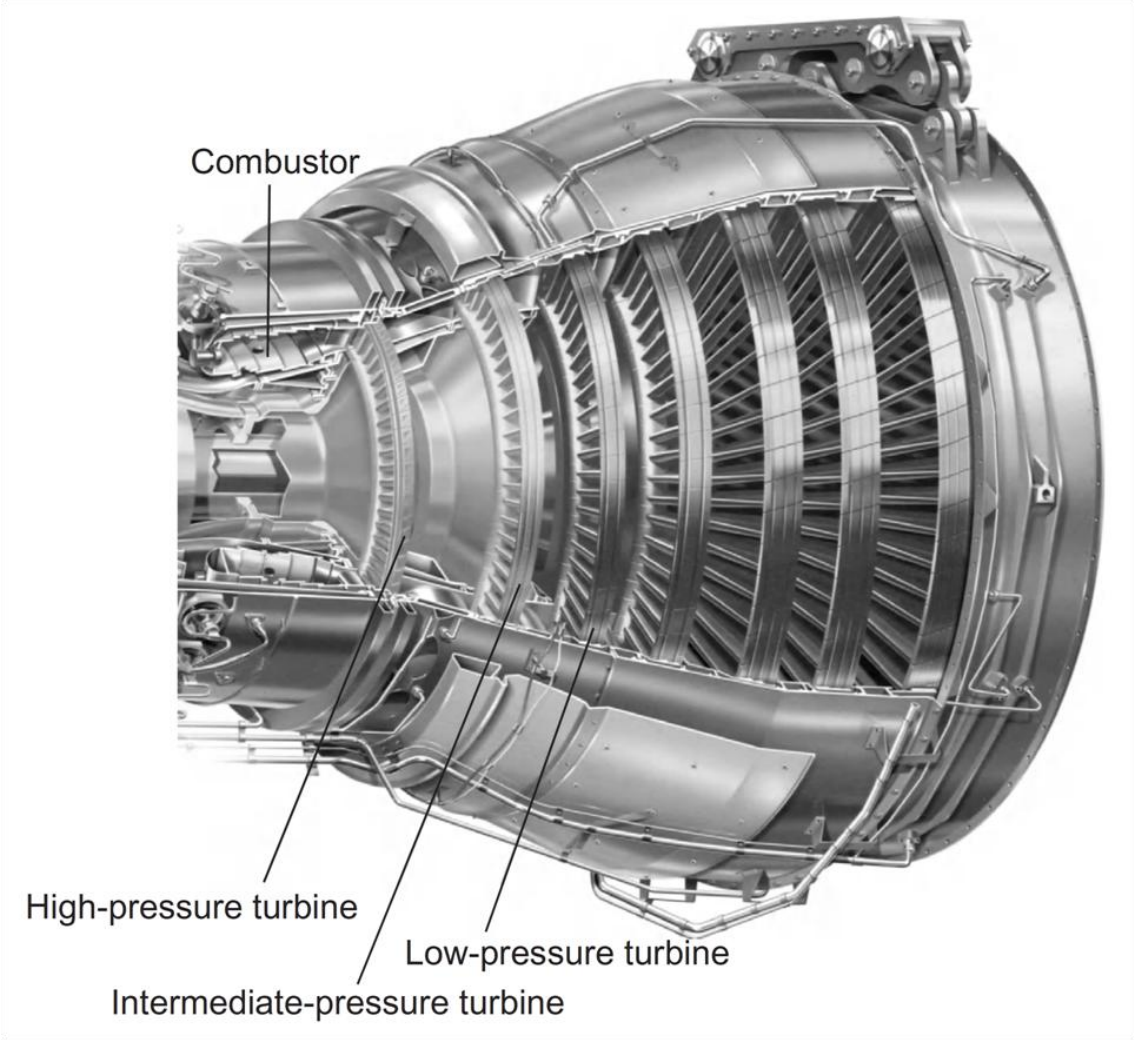

Fig. 1-2 Turbine module of a modern turbofan jet engine [1]

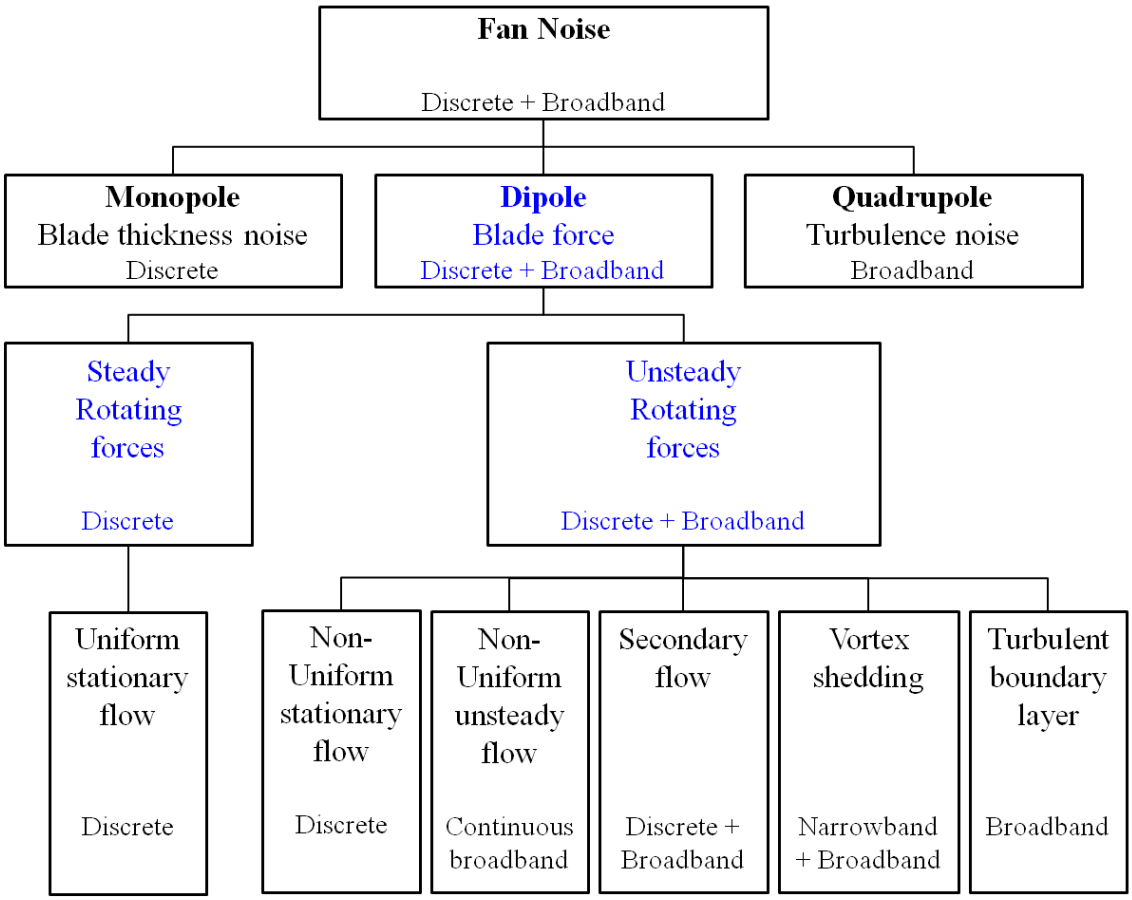

Fig. 1-3 Various noise sources generated from fan

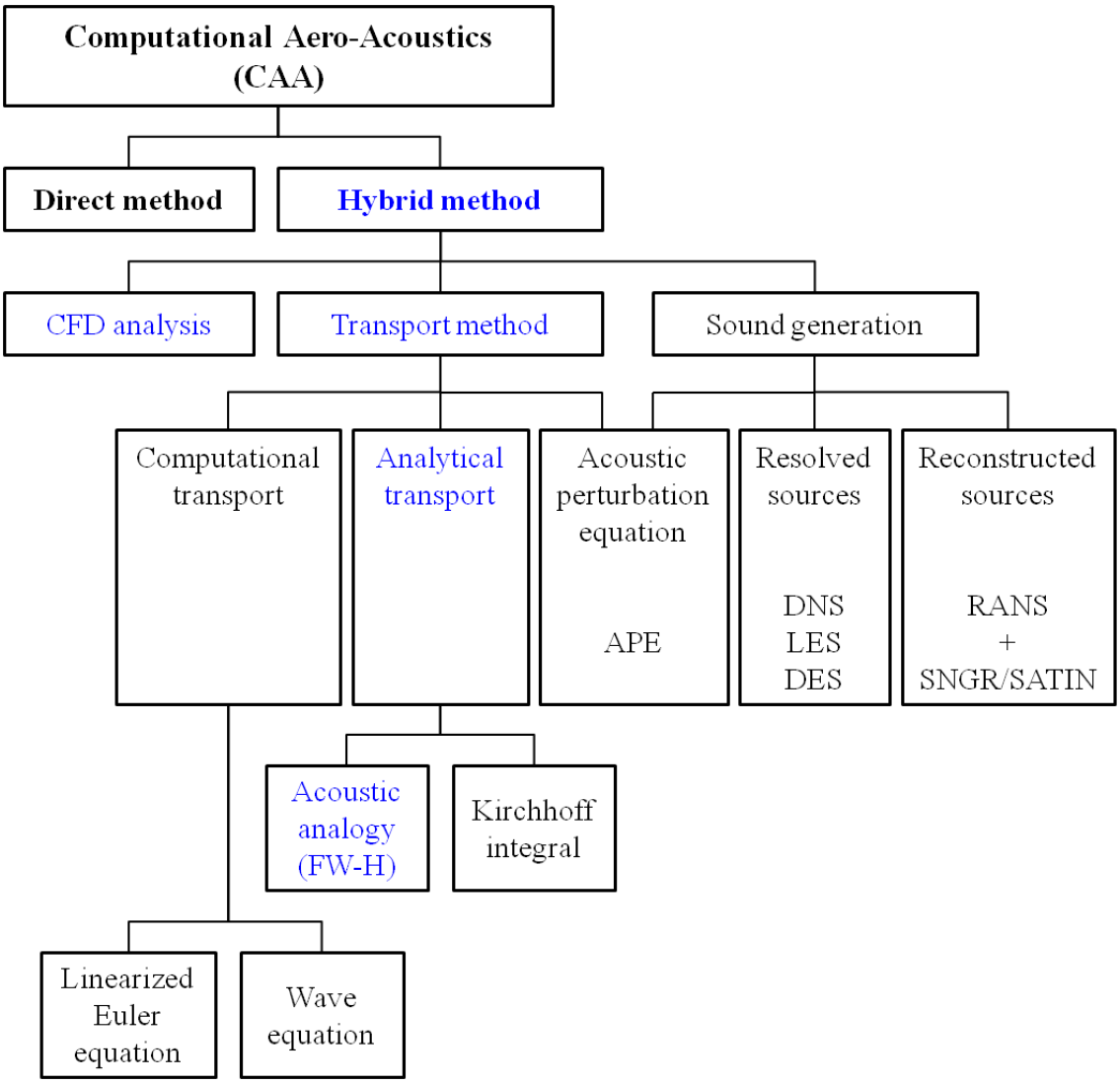

Fig. 1-4 Computational Aeroacoustics(CAA) methodology

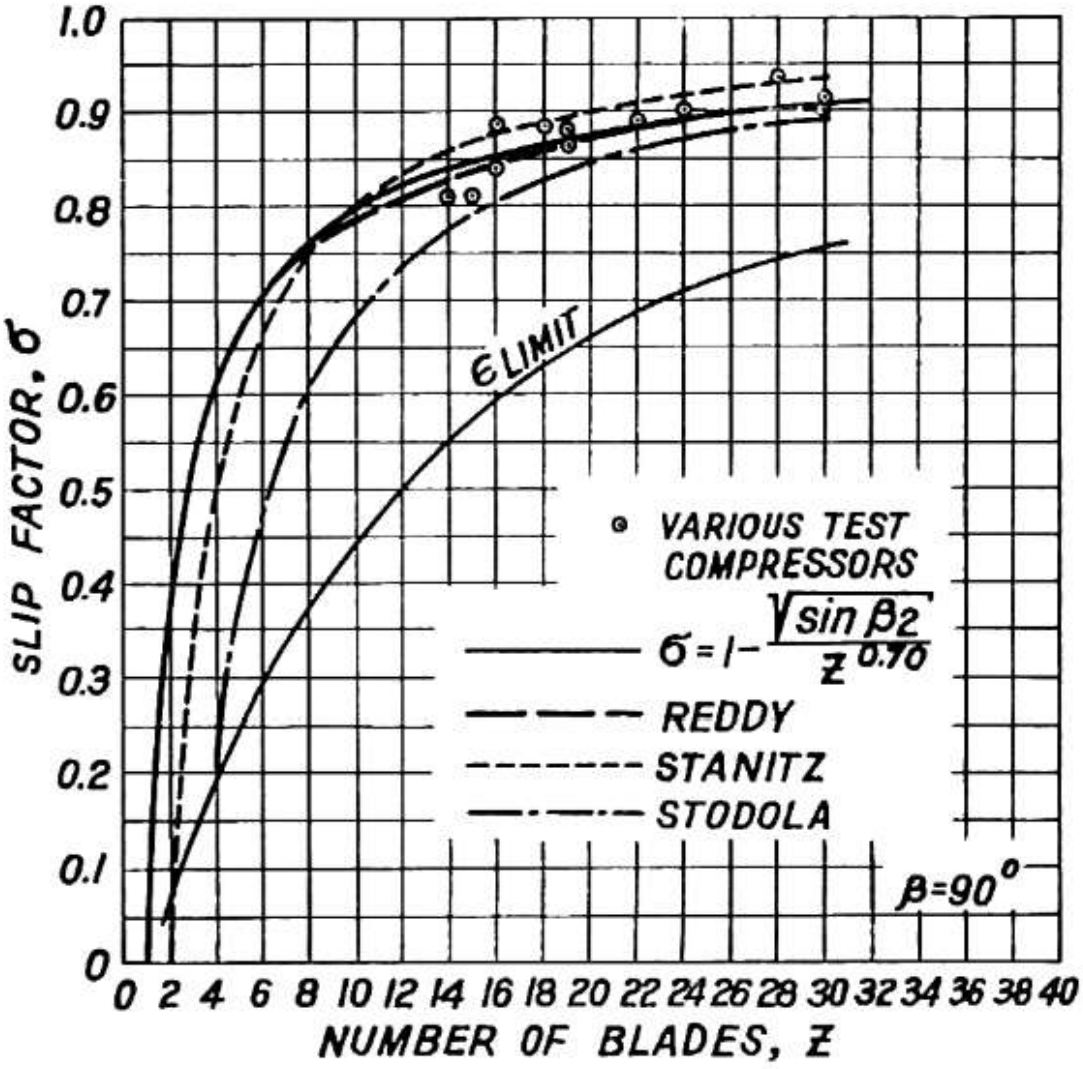

Fig. 1-5 Comparison of slip factors with some test results for radial bladed impellers [15]

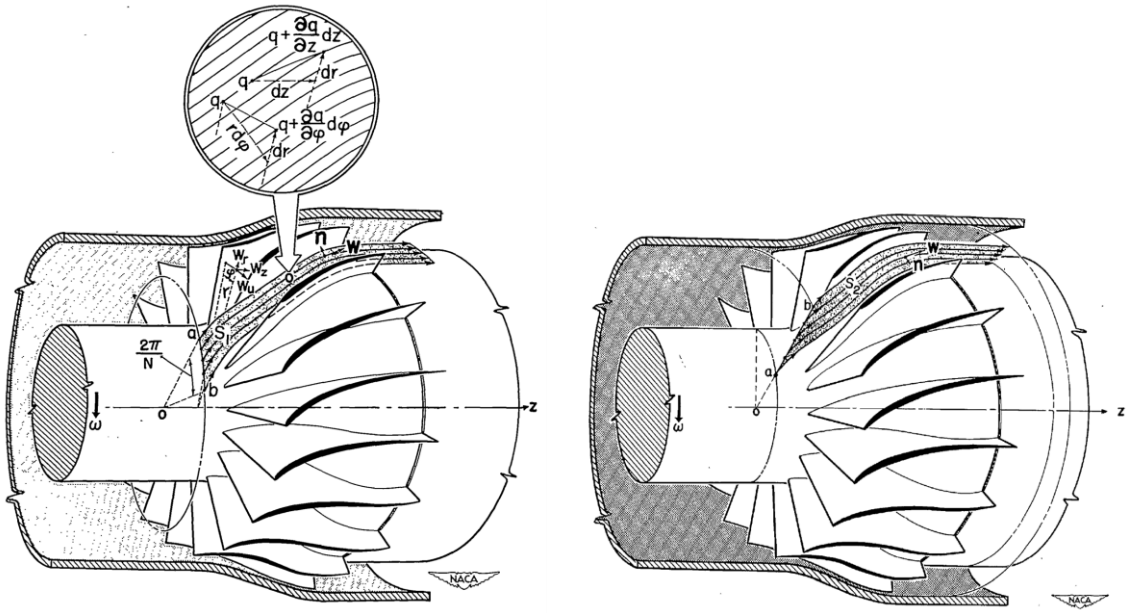

(a) Relative stream surface S_1 and S_2

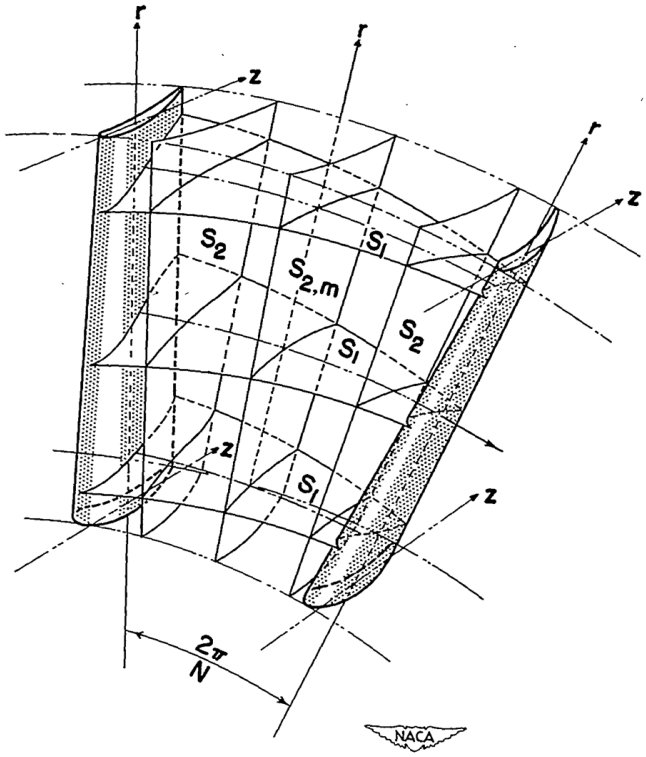

(b) Intersecting S_1 and S_2 in a blade row

Fig. 1-6 Relative stream surfaces and intersecting S_1 and S_2 surfaces in a blade row [19]

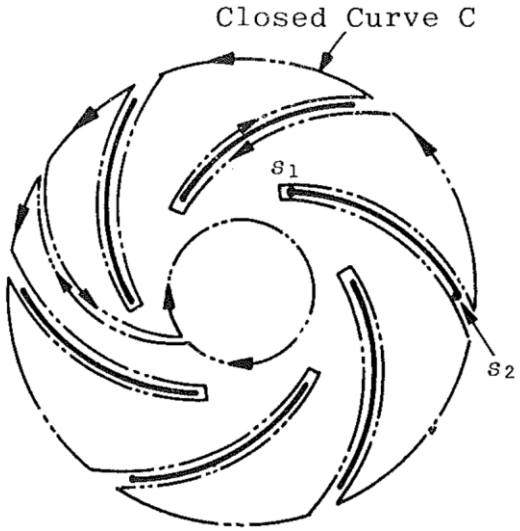

(a) Control surface for considering pressure rise through cascade

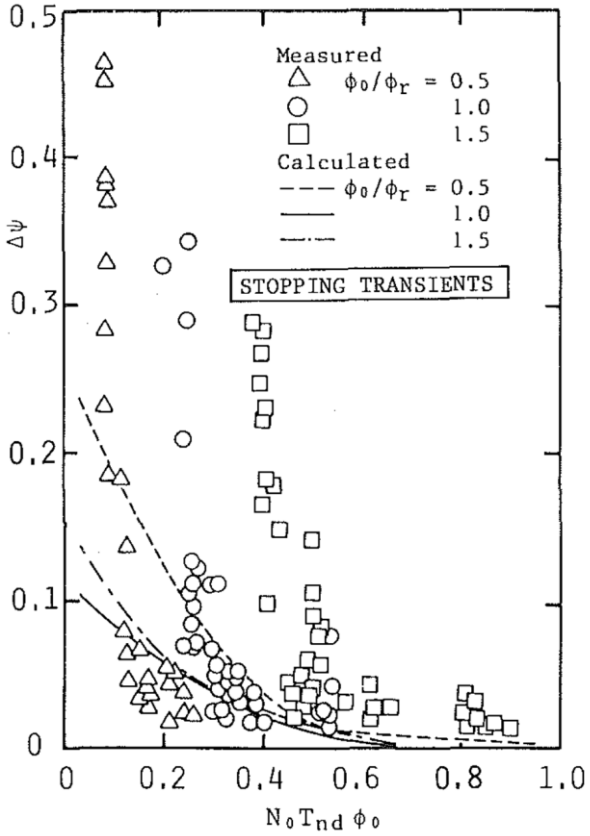

(b) Deviation of dynamic characteristics from quasi-steady ones during stopping period

Fig. 1-7 Control surface and deviation of dynamic characteristics [23]

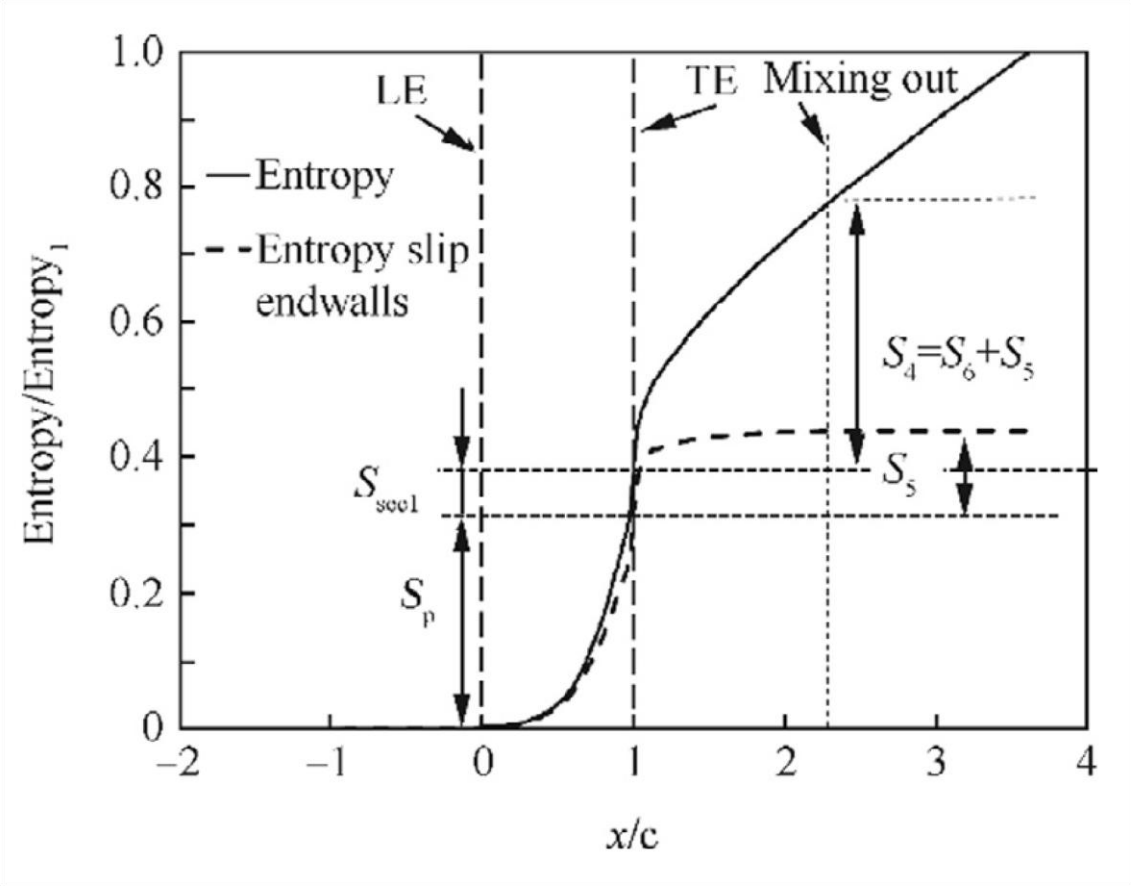

Fig. 1-8 Axial distributions of mass-flow-averaged entropy and entropy generation rate for datum nozzle guide vane (NGV) design [27]

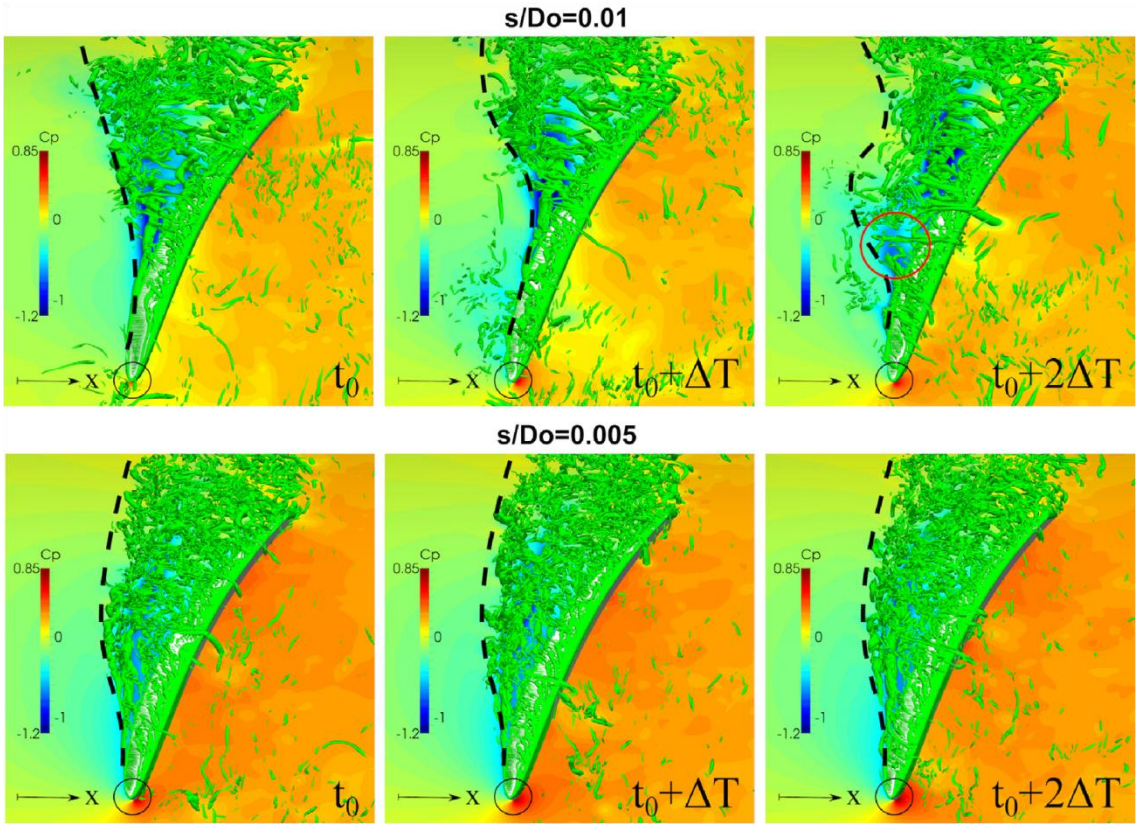

Fig. 1-9 Temporal variation of the flow field for s/D_0 = 0.01 and s/D_0 = 0.005 at three time steps [28]

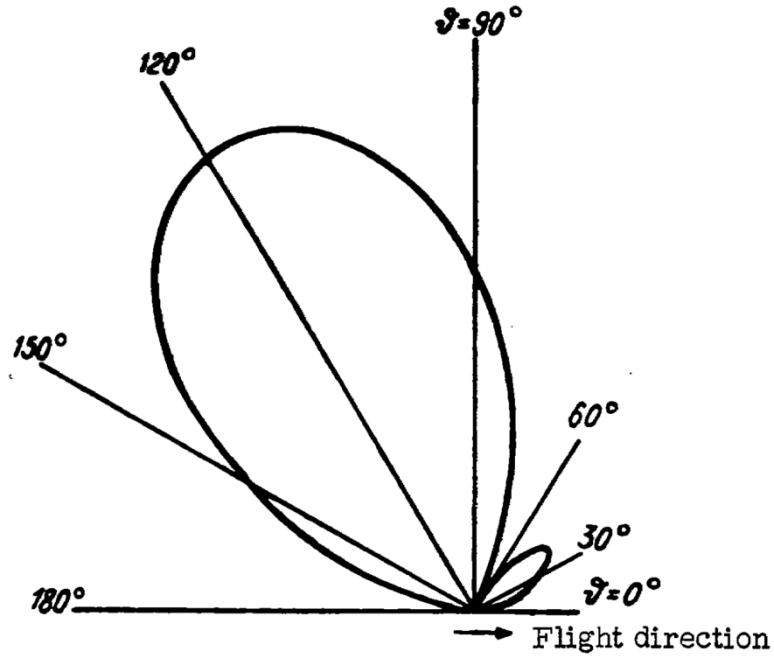

(a) R = 0.7 R_0

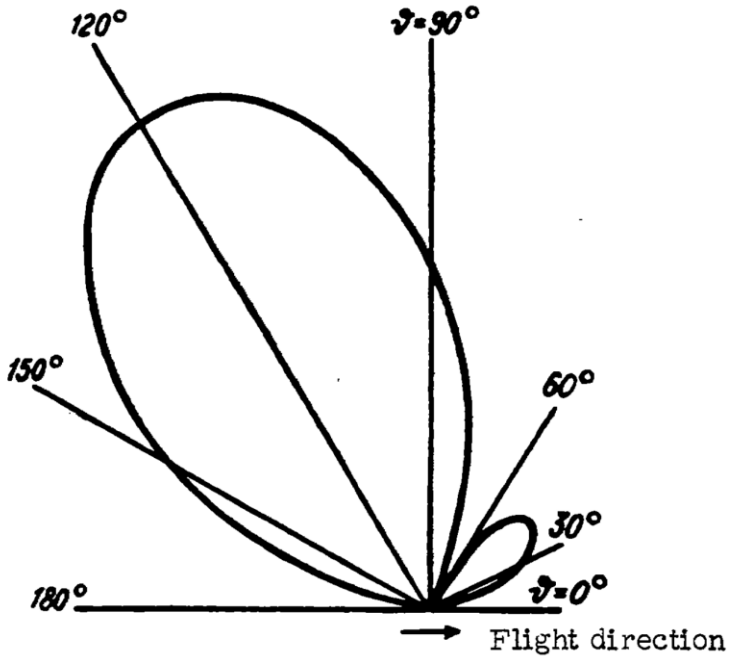

(b) R = 0.75 R_0

Fig. 1-10 Calculated directional characteristic for the fundamental tone [30]

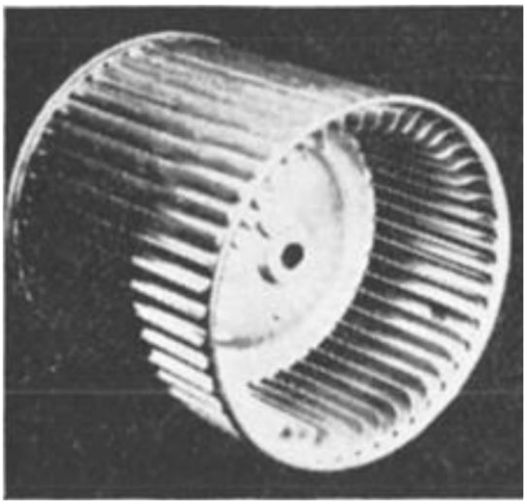

(a) Standard impeller

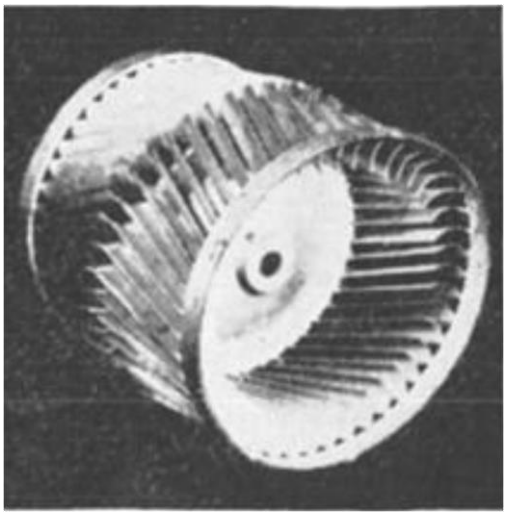

(b) Modified impeller (blades sloping : 20°)

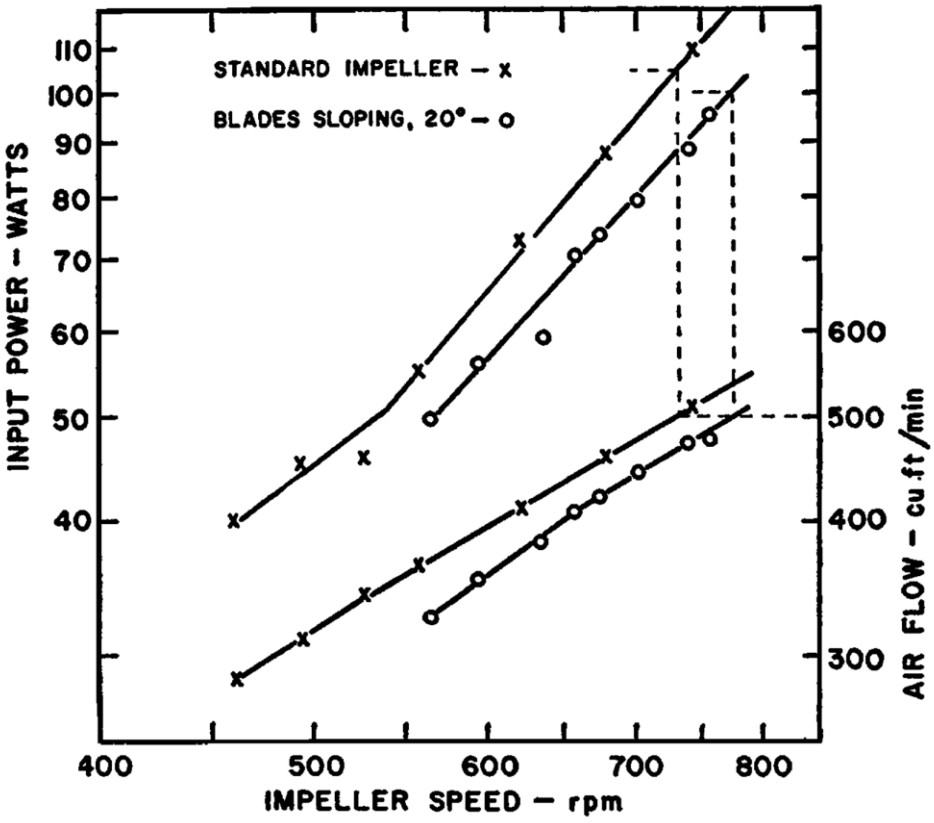

(c) Experimental results

Fig. 1-11 Effect of impeller with sloping blades [32]

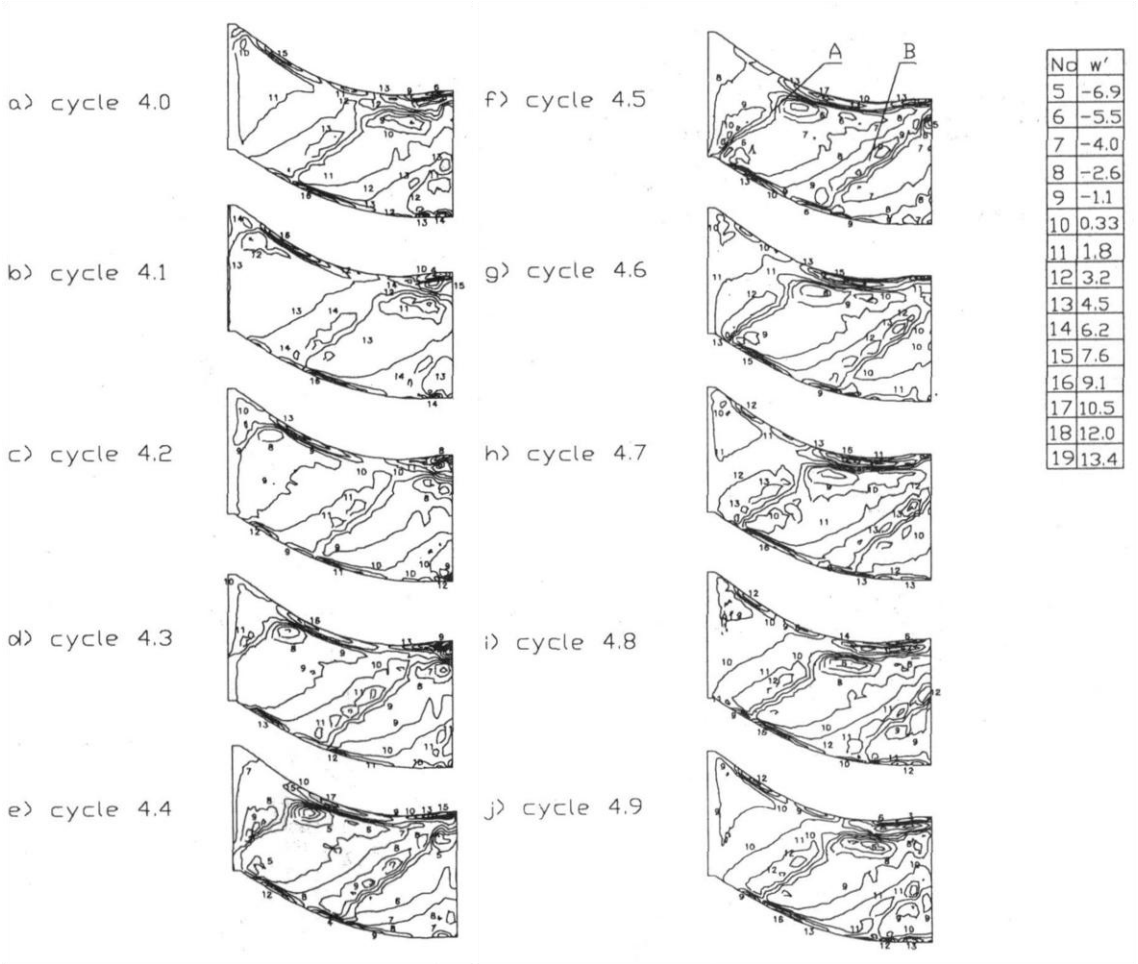

Fig. 1-12 Disturbance vorticity contours at different instants in one period [38]

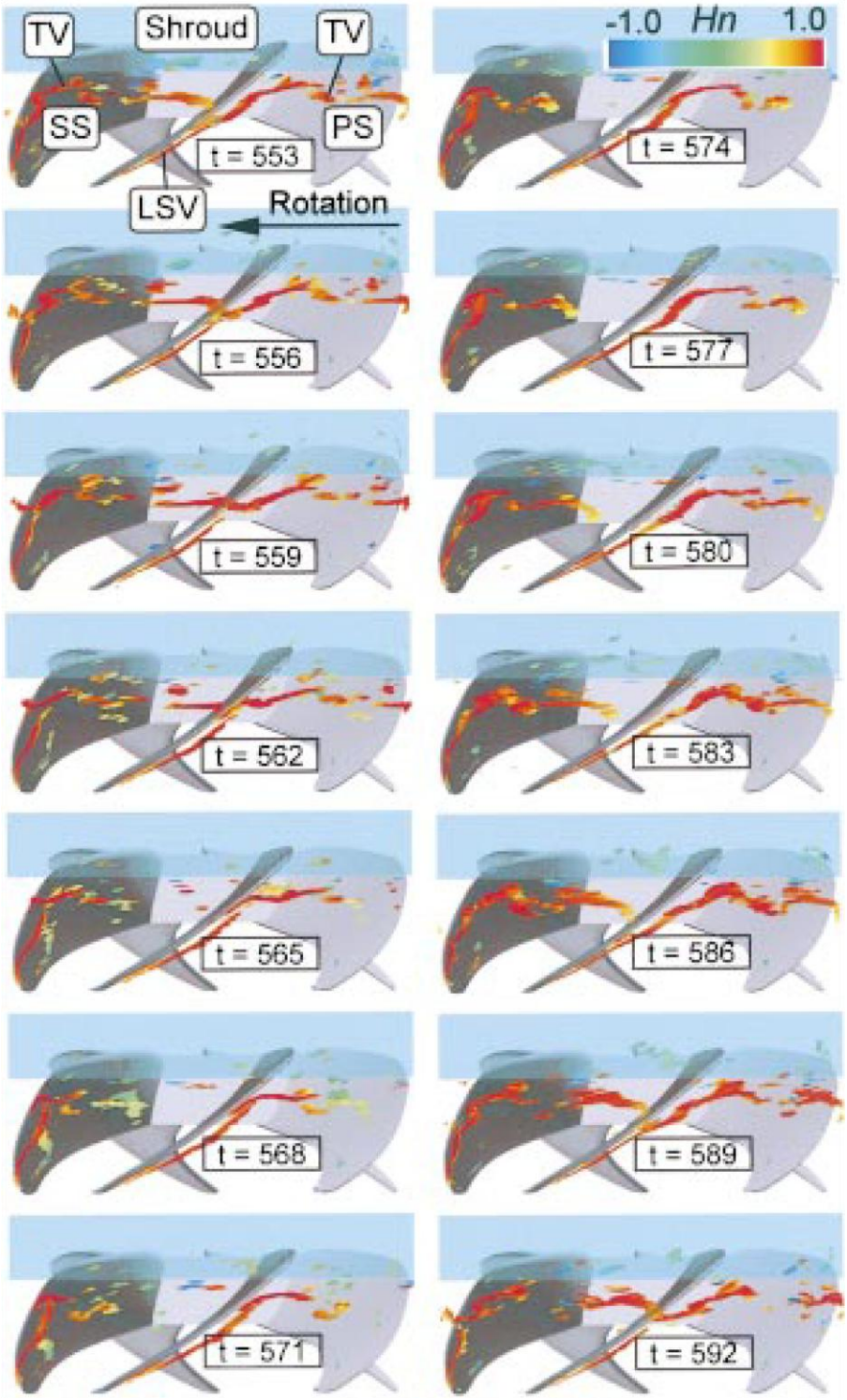

Fig. 1-13 Unsteady behavior of vortex core structures colored with normalized helicity [40]

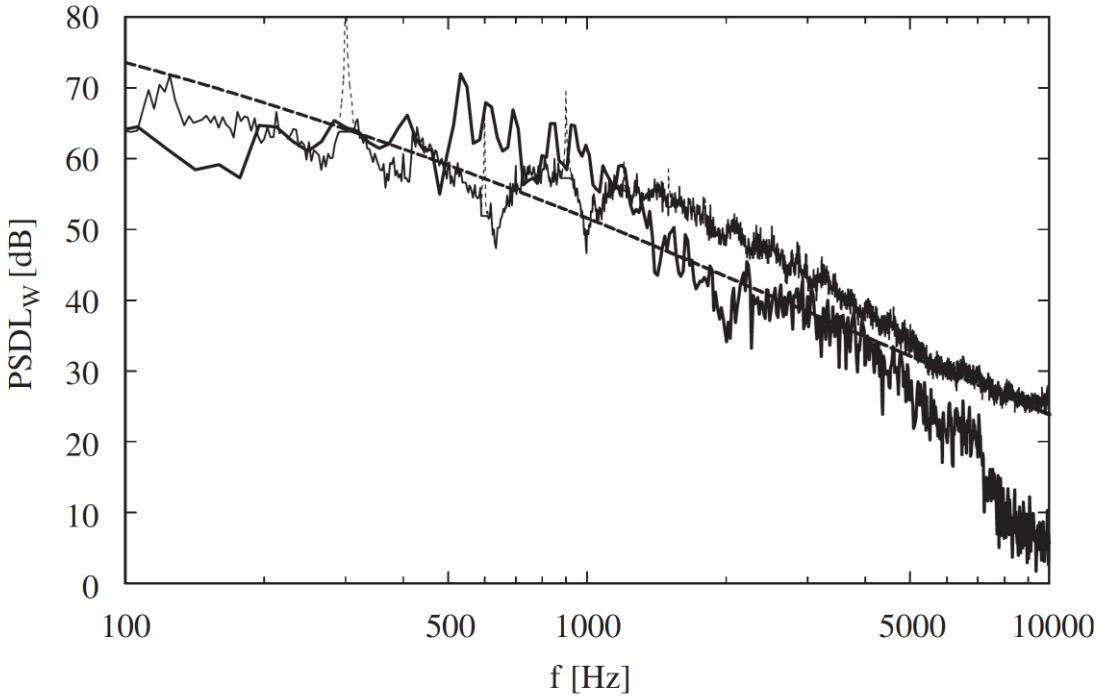

Fig. 1-14 Fan sound power spectra; measured (——), SEM (------) and LES(——) [43]

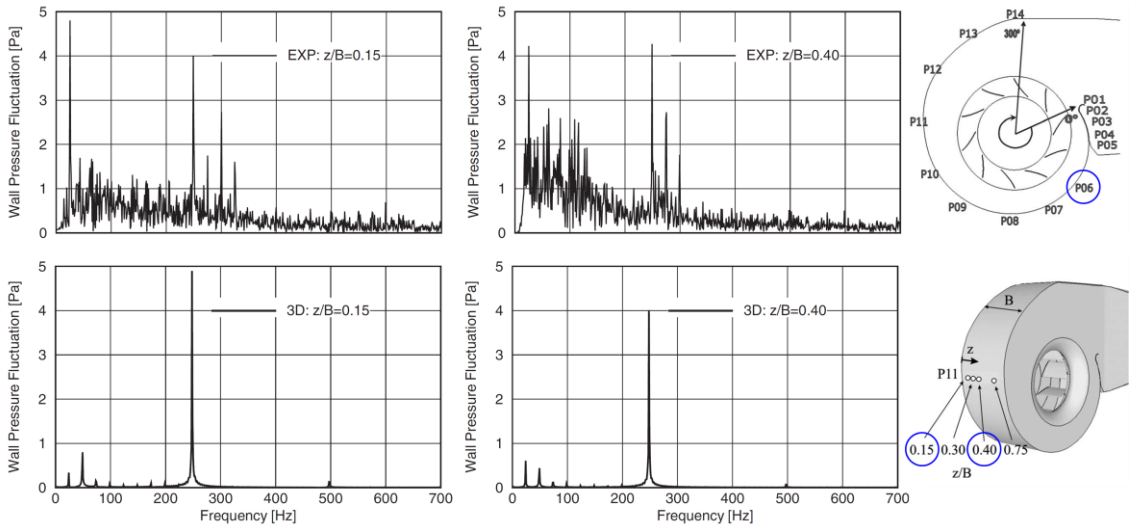

(a) At Point P06

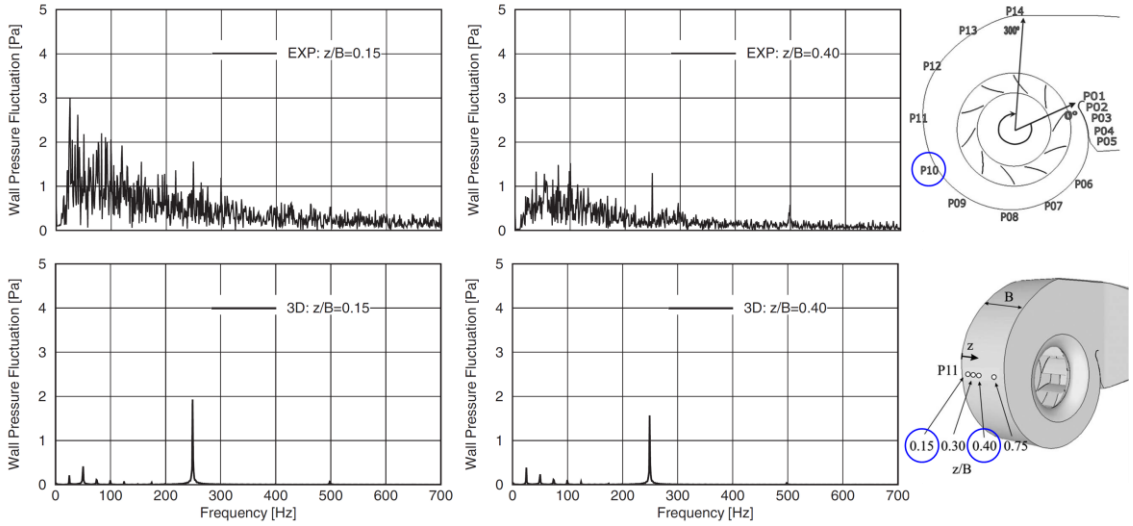

(b) At Point P10

Fig. 1-15 Power spectra of volute pressure fluctuations in pascals (experiment, upper side; 3D-numerical simulation, bottom side) [44]

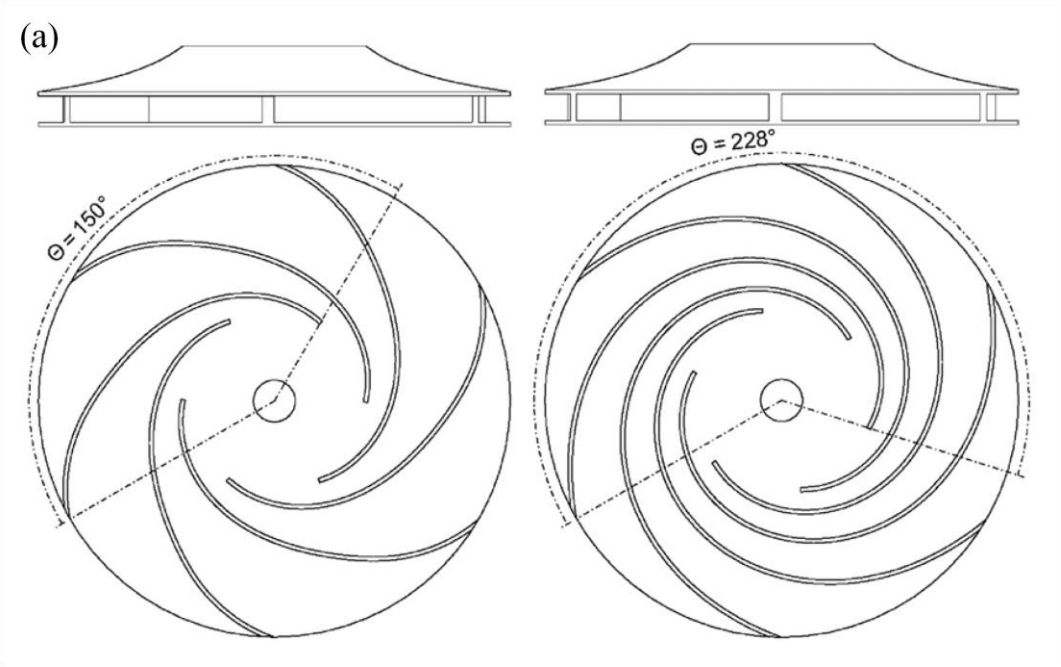

(a) Prototypes with wrap angle θ = 150° and θ = 228°

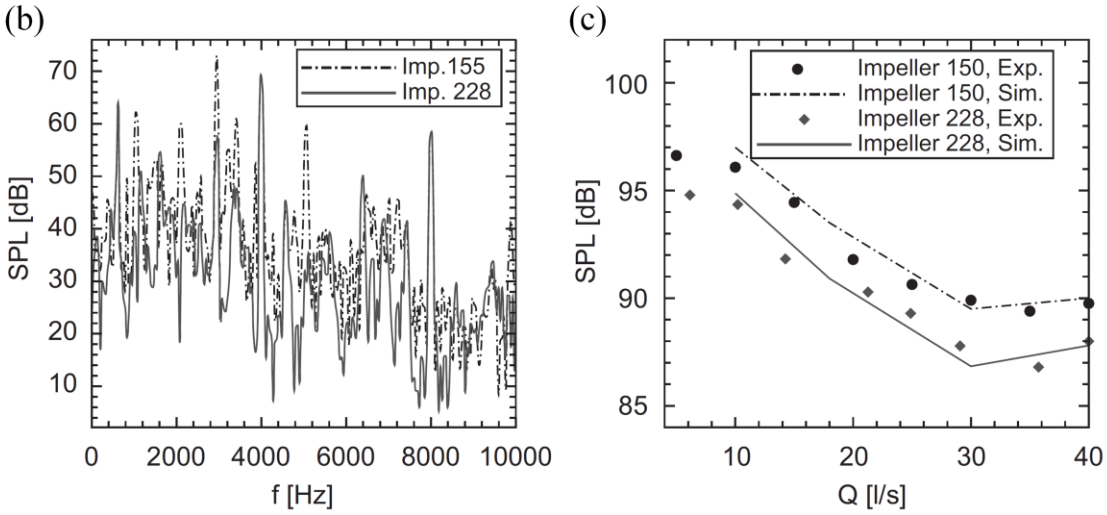

(b) Simulated SPL with different wrap angle (c) Overall SPL vs. mass flow rate

Fig. 1-16 Schematic diagram of wrap angle, simulated SPL, and comparison of the simulated and measured overall SPLs [45]

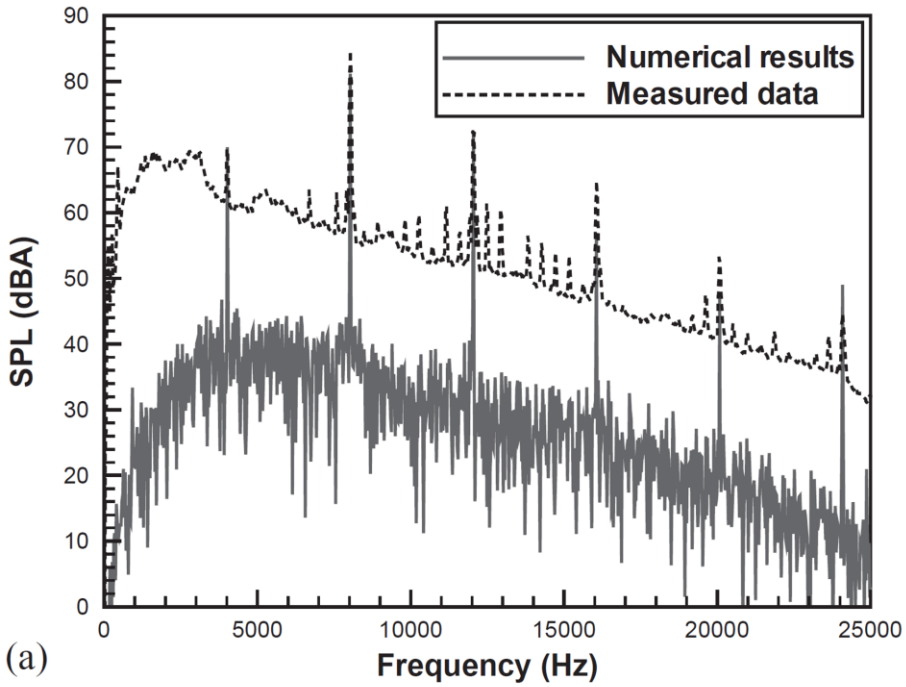

(a) Rotation speed : 26760 rpm

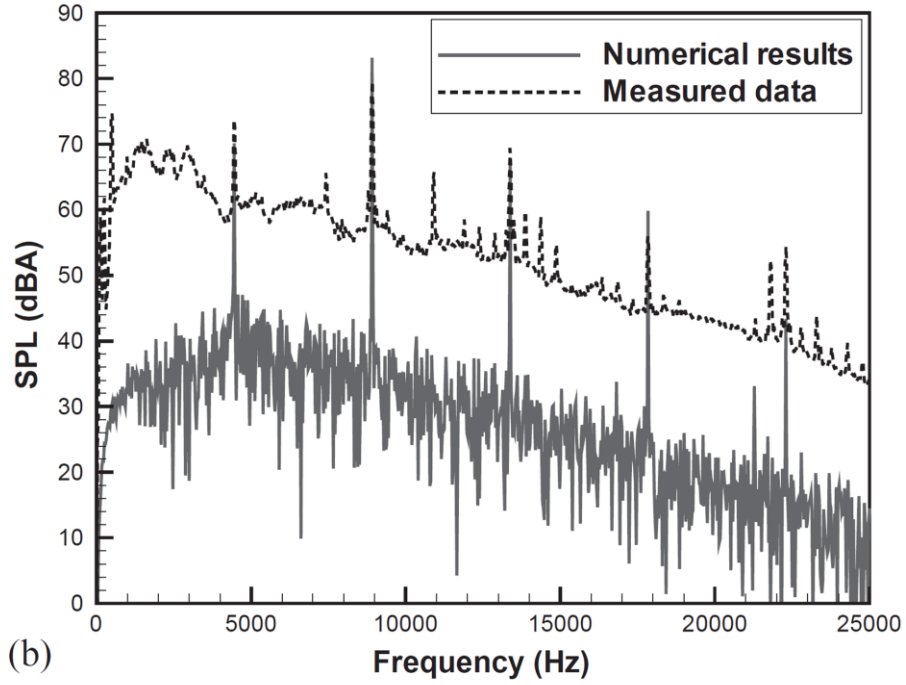

(b) Rotation speed : 29930 rpm

Fig. 1-17 Comparison of the predicted and measured sound pressure levels [50]

Chapter 2. Numerical analysis

2.1 Computational Fluid Dynamics (CFD)

2.1.1 Fundamental equations

When dealing with thermal flow phenomenon of the fluid, equilibrium equations of the flow properties are used and these equations are usually presented as the differential equations. The differential equations can be expressed in general transport equation as below when setting the dependent variable as ϕ and using a tensor [55].

$$\frac{\partial}{\partial t}(\rho\phi) + \frac{\partial}{\partial x_j}(\rho u_j \phi) = \frac{\partial}{\partial x_j}\left(\Gamma \frac{\partial \phi}{\partial x_j}\right) + S_\phi \tag{2-1}$$

Equation (2-1) is composed of an unsteady term, a convection term, a diffusion term, and a source term. Here, ρ is the fluid density. Γ, the diffusion coefficient, and S_ϕ, a source term, do not always have actual physical meaning. These can be interpreted as dependent variables including pressure, temperature, and velocity. Therefore, continuity equation can be obtained by assuming the dependent variable ϕ as 1, and Γ and S_ϕ as 0 in equation (2-1), the general transport equation. Meanwhile, a momentum equation in Cartesian coordinate system in which the gravity is not considered is obtained by substituting u_i that is the velocity component and u_{Sj} that is the velocity of the volume with moving boundary into ϕ, the dependent variable, and τ that is the shear stress and $-\partial p/\partial x$ that is the pressure gradient into Γ, the diffusion coefficient, and S_ϕ, the source term, respectively, in general transport equation [56, 57].

$$\frac{\partial}{\partial t}(\rho u_i) + \frac{\partial}{\partial x_j}\left(\rho u_i (u_j - u_{Sj}\right) = \frac{\partial \tau_{ij}}{\partial x_j} - \frac{\partial p}{\partial x_i} \tag{2-2}$$

In order to analyze the continuity equation and the flow around the moving object used in this study, Navier-Strokes equations can be presented into a simple tensor notation shown in below.

$$\frac{\partial \rho}{\partial t} + \frac{\partial}{\partial x_i}(\rho u_i) = 0 \tag{2-3}$$

$$\frac{\partial}{\partial t}(\rho u_i) + \frac{\partial}{\partial x_j}\left[\rho u_i(u_j - u_{sj})\right] = -\frac{\partial p}{\partial x_i} + \mu\frac{\partial^2 u_i}{\partial x_j \partial x_j} \quad (2\text{-}4)$$

The i(i = 1, 2, 3), the subscripts in above equation, corresponds to the (x, y, z); hence, (u_1, u_2, u_3) indicates (u, v, w) that is the notation according to three-dimensional Cartesian coordinate system of velocity and (x_1, x_2, x_3) indicates (x, y, z).

2.1.2 Discretization method

After choosing the mathematical model predicting the flow field, discretization of the differentials equation should be performed as matching the grid point and the algebraic equations for ϕ, the dependent variable, in the chosen grid point are called discretized equations. The discretization method for differential equation is classified into Finite Difference Method (FDM), Finite Element Method (FEM), and Finite Volume Method (FVM). In FDM, the derivative term in the differential equation is expressed by using Taylor-series expansion. On structured grids, FDM is a very simple and effective method. In particular, it is easy to obtain a higher-order scheme in regular grids with the method. The disadvantages of FDM are the difficulties in maintaining the conservation and applying to complicate flow. FEM expresses the unknown as an approximation function of the required accuracy and determines the size of the coefficient for each small region by using weighted residual method. Finite element methods are relatively easy to analyze mathematically and can provide optimality properties for equations of certain types. The principal disadvantage, which is occurred by methods to uses unstructured grids, is that the matrices of the linearized equations are not as well structured as those for structured grids. As a result, it makes more difficult to find efficient solution methods [55, 56]. FVM is the discretizing method of differentiating the properties that are coming in and out across the surfaces composing the volume of the polyhedron after assuming that the physical quantity including velocity and pressure can be predicted at the center of the polyhedron. The FVM can accommodate any type of grid, so it is suitable for complex geometries. The grid defines only the control volume boundaries and need not be related to a coordinate system. The method is conservative by construction, so long as surface integrals, which represent convective and diffusive fluxes, are the same for the control volumes sharing the boundary. The

FVM approach is perhaps the simplest to understand and to program. All terms that need be approximated have physical meaning. The disadvantage of FVMs compared to FDMs is that methods of order higher than second are more difficult to develop in 3D [55, 56].

The fundamental discretizing method for the space in the solver used for numerical analysis of thermal flow in this study is the vertex-based FVM. Therefore, the discretization in this study is limited to that by FVM.

Figure 2-1 shows the vertex-based scheme used in this study and the cell-based scheme, respectively [58]. The vertex-based FVM used in CFD solver is the discretizing method by re-dividing the space with the vertex as the center rather than discretizing the properties by using the center of the space; hence, the method can differ by the way of composition of the control volume. In general, the median method in which the control volume is composited by connecting the center of the cell, the center of the surface, and the center of the edge is widely used [57]. In particular, a cell-centered scheme can be expected to result in a much larger number of unknowns while generating relatively simple stencils of fixed size. The vertex-based scheme, on the other hand, will result in a smaller number of unknowns with larger variable-size stencils. Because of the larger number of unknowns, cell-centered schemes generally incur larger overheads than vertex-based schemes on equivalent grids [59]. However, vertex-based scheme has been known that the convergency of the solution can be influenced when the quality of the imaginary plane created between the two nodes is not fair [60].

2.1.3 Pressure-correction method

Solution of the Navier-Stokes equations is complicated by the lack of an independent equation for the pressure, whose gradient contributes to each of the three momentum equations. Furthermore, the continuity equation does not have a dominant variable in incompressible flows. Mass conservation is a kinematic constraint on the velocity field rather than a dynamic equation. One way out of this difficulty is to construct the pressure field so as to guarantee satisfaction of the continuity equation [56]. In other words, the velocity that is composed of three vectors in the momentum equation occupies three unknowns while the pressure term that is a scalar occupies one unknown, resulting four unknowns in total. In order to obtain solutions for the four unknowns,

discretization is conducted once after matching the number of unknowns and the equations by combining the three momentum equations and continuity equations for each vector component. However, the pressure is discretized by estimating and adjusting the pressure since continuity equations do not contain relationship with the pressure.

The two problems related to the non-linearity of the equation and pressure-velocity linkage can be resolved by adopting repetitive analysis method such as SIMPLE (Semi-Implicit Method for Pressure-Linked Equations) algorithm that was originally proposed by Patankar and Spalding [61]. In this algorithm, F, the convection flux per unit mass passing through the grid surface, is calculated from the velocity components that were guessed. Furthermore, momentum equations are calculated by using the estimated pressure field. Then the pressure-correction equation that was induced from the continuity equations is solved. Then, the velocity field and pressure field are updated by using the corrected pressure field. The method is to result convergence of the velocity field and pressure field through such procedure of repetitive correction. Figure 2-2 is the schematization of SIMPLE algorithm on two-dimensional viscous flow equation [62]. SIMPLE algorithm is relatively simple and clear, and has been successfully used in CFD method. However, the pressure correction p' was satisfied for velocity correction whereas it was not good enough for pressure correction. Therefore, a similar algorithm with improvement has been used.

In this study, SIMPLEC (SIMPLE-Consistent) method with further reinforced connectivity in between space and better convergency of solution compared to SIMPLE method was used [60]. SIMPLEC algorithm proposed by Van Doormal and Raithby [63] has same steps with SIMPLE algorithm; however, the difference is that the term that was omitted in SIMPLE is taken into account in velocity-correction equation of SIMPLEC. Namely, it is different that $d_{i,J} = A_{i,J}/(a_{i,J} - \sum a_{nb})$ and $d_{I,j} = A_{I,j}/(a_{I,j} - \sum a_{nb})$ are considered instead of $d_{i,J} = A_{i,J}/a_{i,J}$ and $d_{I,j} = A_{I,j}/a_{I,}$ that are used in STEP 3 of figure 2-2, respectively [62].

2.1.4 Convective term discretized method

Equation 2-1 is a transport equation in which continuity equation and momentum equation are expressed in dependent variable ϕ. In other words, the left-hand side is

composed of the rate of change term and convection term whereas the right-hand side is composed of the diffusion term (Γ = diffusion coefficient) and source term S_ϕ. The challenge in discretization of the convection term which is the second term on the left-hand side is to calculate the physical property ϕ that is the subject of transport on the surface of the control volume and the convection flux passing through the boundary surface. Theoretically, the analysis result is difficult to be distinguished from the exact solution of the transport equation when infinitely many grids exist, regardless of the kind of the scheme used. However, the analysis result and convergence speed are greatly dependent on the discretizing method for convection term, and the convection term is greatly influenced by the flow velocity since finite number of grids are used.

In this study, pressure fluctuations on the surfaces of the object in unsteady flow field were required to conduct numerical analysis of aeroacoustic noise. In order to reduce calculation time consumed for analysis of unsteady state, analysis process composed of three steps was conducted. The entire flow field was constructed roughly by analyzing steady state flow. Afterwards, unsteady state flow was analyzed to fully develop the unsteadiness of the flow due to the rotation of the rotor in the fluid machinery. In addition, the flow properties were reviewed based on the number of each rotation of the rotor to determine the level of unsteadiness development. Finally, fully-developed unsteadiness of the flow was confirmed and data required for numerical analysis of aeroacoustic noise were obtained by simulating the unsteady state flow during several numbers of rotation.

Meanwhile, QUICK (Quadratic Upstream Interpolation for Convective Kinetics) scheme was used as the second order upwind differencing scheme that is a higher order differencing scheme for discretization of convection term in steady state flow analysis at the first step among those three steps of analysis process mentioned above. Although the error due to the false diffusion can be minimized; however, it may reduce the stability in terms of calculation. The risk of undershooting and overshooting that may occur when the gradient of dependent variable ϕ is large was minimized through the use of limiter. The differencing scheme for discretization of the convection term used while analyzing unsteady state flow in the second and third step was the second order central differencing scheme. The large number of grids with small size was used to get rid of the vibration solution such as wiggles [62].

2.1.5 Turbulence model

In turbulent flow, complicated vortex motion occurs and the size of such vortex motion varies from a large scale to a very small scale. Despite of the rapid improvement of computer performance, it is still challenging to secure the number of grids that is sufficient for resolution of a small-scale vortex motion composing the turbulent flow. Hence, turbulence model is required to be introduced for numerical analysis of turbulent flow using Navier-Stokes equations. Prior to the introduction of the turbulence model, physical characteristics of the turbulence presented by the two-dimensional turbulent shear flow that is parallel to *x*-axis and has the gradient of average velocity toward *y*-direction within the control volume should be understood as shown in figure 2-3 [62]. The random flow due to the eddy near the control volume transports the fluid across the boundary of the control volume. This is the momentum exchange owing to the convective transport by the eddy and is called Reynolds stress. In other words, observation on the influence of the turbulence fluctuation on the mean flow by applying the Reynolds decomposition to velocity components (*u*, *v*, *w*) and taking time average to them results in additional production of three normal stresses and three shear stresses. Here, the Reynolds decomposition defines that the velocity ($u(t)$) of the turbulent flow is divided into the steady mean value (U) and its fluctuating components ($u'(t)$). The six additional turbulence stresses in consequence of the multiplication of fluctuation velocities due to convective momentum transport by the turbulence eddy are called Reynolds stress and these are as follows.

$$\tau_{xx} = -\rho\overline{u'^2}, \tau_{yy} = -\rho\overline{v'^2}, \tau_{zz} = -\rho\overline{w'^2} \tag{2-5a}$$

$$\tau_{xy} = \tau_{yx} = -\rho\overline{u'v'}, \tau_{xz} = \tau_{zx} = -\rho\overline{u'w'}, \tau_{yz} = \tau_{zy} = -\rho\overline{v'w'} \tag{2-5b}$$

Hence, a turbulence model that predicts additional Reynolds stress is required in order to calculate the turbulence by using Reynolds-Averaged Navier-Stokes (RANS) equations. On this occasion, RANS turbulence model is classified by the number of additional equation.

Meanwhile, Boussinesq model (1877) in which the size of the Reynolds stress is

assumed to be proportional to the rate of change (velocity slope) of the average velocity in the same context of the shear stress occurring by the molecular viscosity has been widely used. The turbulence mode adopting such assumption is called turbulent viscosity model; and the Reynolds stress with the assumption is as below.

$$\tau_{ij} = -\rho\overline{u_i'u_j'} = \mu_t\left(\frac{\partial U_i}{\partial x_j} + \frac{\partial U_j}{\partial x_i}\right) - \frac{2}{3}\rho k\delta_{ij} \quad (2\text{-}6a)$$

$$k = \frac{(\overline{u'^2} + \overline{v'^2} + \overline{w'^2})}{2} \quad (2\text{-}6b)$$

Here, k is turbulence energy per unit mass, μ_t is turbulent viscosity coefficient, and δ_{ij} is Kronecker delta.

On the other hand, a model type in which Reynolds stress equation is established without making the assumption about the turbulence viscosity is called Reynolds stress equation model. In this study, numerical analysis on the flow field was done by using the turbulence viscosity model.

In order to obtain the information on the pressure fluctuations on the surfaces of the object for analysis of aeroacoustic noise as mentioned above, the numerical analysis was conducted for steady state and unsteady state. For steady state analysis, SST(Shear-Stress Transport) k–ω model that was proposed by Menter [64, 65] and Menter et al. [66] was used as the turbulence model. This turbulence model is the combination of k–ω model proposed by Wilcox [67-69] in 1988 and k–ε model proposed by Launder et al. [70] in 1974, carrying the advantages of the two models. Namely, this is the model in which k–ω is applied to the region near the wall surface whereas k–ε model is applied to the region of fully developed free flow distant to the wall surface. In this model, the model equations on turbulence momentum energy k and the turbulence frequency ω are in flowing forms, respectively [57]. In other words, the formula for Reynolds stress and k–equation are the same as the original k–ω model proposed by Wilcox; however, ε–equation is converted into ω–equation through substitution of $\varepsilon = C_\mu k\omega$. For numerical analysis of the flow due to a moving object such as a fan, ALE (Arbitrary Lagrangian Eulerian) method proposed by Donea et al. [71] in 2004 was used. Transport equations of SST k–ω in fixed coordinates are as follows [58, 64, and 70].

$$\frac{\partial}{\partial t}(\rho k) + \frac{\partial}{\partial x_j}\left[\rho k\left(u_j - v_j\right)\right] = G_s - \rho\beta^*\omega k + \frac{\partial}{\partial x_j}\left[\left(\mu + \frac{\mu_t}{\sigma_k}\right)\frac{\partial k}{\partial x_j}\right] \tag{2-7}$$

$$\frac{\partial}{\partial t}(\rho\omega) + \frac{\partial}{\partial x_j}\left[\rho\omega\left(u_j - v_j\right)\right] = \frac{\gamma}{\nu_t}G_s - \beta\rho\omega^2 + \frac{\partial}{\partial x_j}\left[\left(\mu + \frac{\mu_t}{\sigma_\omega}\right)\frac{\partial\omega}{\partial x_j}\right] + 2(1 - F_1)\rho\frac{\sigma_{\omega 2}}{\omega}\frac{\partial k}{\partial x_j}\frac{\partial\omega}{\partial x_j} \tag{2-8}$$

where,

$$G_s = P = \tau_{ij}\frac{\partial u_i}{\partial x_j} \tag{2-9a}$$

$$\tau_{ij} = \mu_t\left(2S_{ij} - \frac{2}{3}\frac{\partial u_k}{\partial x_j}\delta_{ij}\right) - \frac{2}{3}\rho k\delta_{ij} \tag{2-9b}$$

$$S_{ij} = \frac{1}{2}\left(\frac{\partial u_i}{\partial x_j} + \frac{\partial u_j}{\partial x_i}\right) \tag{2-9c}$$

$$F_1 = tanh(arg_1^4) \tag{2-9d}$$

$$arg_1 = min\left[max\left(\frac{\sqrt{k}}{\beta^*\omega y}, \frac{500\nu}{y^2\omega}\right), \frac{4\rho\sigma_{\omega 2}k}{CD_{k\omega}d^2}\right] \tag{2-9e}$$

$$CD_{k\omega} = max\left(2\rho\sigma_{\omega 2}\frac{1}{\omega}\frac{\partial k}{\partial x_j}\frac{\partial\omega}{\partial x_j}, 10^{-20}\right) \tag{2-9f}$$

$$F_2 = tanh(arg_2^2) \tag{2-9g}$$

$$arg_2 = max\left(2\frac{\sqrt{k}}{\beta^*\omega y}, \frac{500\nu}{y^2\omega}\right) \tag{2-9h}$$

Numerical instabilities may be caused by differences in the computed values of the eddy viscosity with the standard k–ε model in the far field and the transformed k–ε model near the wall. Blending functions are used to achieve a smooth transition between the two models. Blending functions are introduced in the equation to modify the cross-diffusion term and are also used for model constants that take value C_1 for the original k–ω model and value C_2 in Menter's transformed k–ε model [62]:

$$C = F_1 C_1 + (1 - F_1)C_2 \tag{2-10}$$

Typically, a blending function $F_1 = F_1(l_t/y, Re_y)$ is a function of the ratio of turbulence $l_t = k^{0.5}/\omega$ and distance y to the wall and of a turbulence Reynolds number $Re_y = y^2\omega/\nu$. The functional form of F_1 is chosen so that it (i) is zero at the wall, (ii) tends to unity in

the far field and (iii) produces a smooth transition around a distance half way between the wall and the edge of the boundary layer. This way the method now combines the good near-wall behavior of the *k*–*ω* model with the robustness of the *k*–*ε* model in the far field in a numerically stable way. The eddy viscosity is limited to give improved performance in flows with adverse pressure gradients and wake regions, and the turbulent kinetic energy production is limited to prevent the build-up of turbulence in stagnation regions. The limiters are as follows [62]:

$$\mu_t = \frac{a_1 \rho k}{max(a_1 \omega, SF_2)} \tag{2-11}$$

where, $S = (2S_{ij}S_{ij})^{0.5}$, $a_1 = 0.31$ and F_2 is a blending function. The subscripts 1 and 2 indicate the SST-inner and the SST-outer, respectively [64].

$$C_\mu = \beta^* = 0.09,\ \ \gamma = \gamma_1 = \gamma_2 = \frac{\beta}{C_\mu} - \frac{\kappa^2}{\sigma_\omega \sqrt{C_\mu}},\ \ \kappa = 0.41 \tag{2-12a}$$

$$\sigma_{k1} = 0.8500,\ \ \sigma_{\omega 1} = 0.5000,\ \ \beta_1 = 0.0750 \tag{2-12b}$$

$$\sigma_{k2} = 1.0000,\ \ \sigma_{\omega 2} = 0.8560,\ \ \beta_2 = 0.0828 \tag{2-12b}$$

In this study, LES model was used to simulate the unsteady flow field. The larger eddies, which interact with and extract energy from the mean flow, are more anisotropic and their behavior is dictated by the geometry of the computational domain, the boundary conditions and body forces. On the other hand, the smaller eddies are nearly isotropic and have a universal behavior, for turbulent flows at sufficiently high Reynolds numbers at least. With considering the characteristics of turbulent flows, the larger eddies need to be computed with a time-dependent simulation and the universal behavior of the smaller eddies, on the other hand, should hopefully be easier to capture with a compact model like Sub-Grid Scale(SGS) model. This is the key point of the LES approach to the numerical treatment of turbulence [62].

LES model uses a spatial filtering operation to separate the larger and smaller eddies for the time-dependent flow equations. The operation of filtering is performed along with the following definition [58, 72]:

$$\bar{u}(x,t) = \int_{-\infty}^{+\infty} G\,(x-\xi)u(\xi,t)d\xi \tag{2-13}$$

$$\overline{u+u} = \bar{u} + \bar{u} \tag{2-14a}$$

$$\overline{\frac{\partial u}{\partial s}} = \frac{\partial \bar{u}}{\partial s} \tag{2-14b}$$

$$s = x, t \tag{2-14c}$$

where a filter function *G* denotes the convolution kernel characterizing the filter used and the overbar of u indicates the resolved part filtered by *G*. If the Navier-Stokes equations are filtered by equation (2-13) and by the following conditions equation (2-14), we can easily obtain the following equation [58]:

$$\frac{\partial}{\partial t}(\rho\overline{u_\iota}) + \frac{\partial}{\partial x_j}\left[\rho\overline{u_\iota}\left(\overline{u_J} - \overline{u_{SJ}}\right)\right] = -\frac{\partial \bar{p}}{\partial x_i} + \frac{\partial}{\partial x_j}\left[\mu\left(\frac{\partial \overline{u_i}}{\partial x_j} + \frac{\partial \overline{u_j}}{\partial x_i}\right)\right] - \frac{\partial}{\partial x_j}\rho\left(\overline{u_\iota u_J} - \overline{u_\iota}\,\overline{u_j}\right) \tag{2-15}$$

Equation (2-15) above presents LES momentum equation. The terms except the last term on the right-hand side mean the properties after filtering. The last terms are caused by the filtering operation, just like the Reynolds stresses in the RANS momentum equations that arose as a consequence of time averaging. They can be considered as a divergence of a set of stresses(τ_{ij}) [62]. In recognition of the fact that a substantial portion of τ_{ij} is attributable to convective momentum transport due to interactions between the unresolved or SGS eddies, these stresses are commonly termed the sub-grid-scale stresses [62]. Based on the relationship mentioned by Leonard decomposition [73], SGS stresses can be calculated as below.

$$\tau_{ij} = \rho\overline{u_\iota u_J} - \rho\overline{u_\iota}\,\overline{u_J} = \left(\rho\overline{\overline{u_\iota}\,\overline{u_J}} - \rho\overline{u_\iota}\,\overline{u_j}\right) + \rho\overline{\overline{u_\iota}u_J'} + \rho\overline{u_\iota'\overline{u_J}} + \rho\overline{u_\iota' u_J'} \tag{2-16}$$

where Leonard stresses L_{ij}, cross-stresses C_{ij} and LES Reynolds stresses R_{ij} is contained in equation (2-16), respectively.

$$L_{ij} = \rho\overline{\overline{u_\iota}\,\overline{u_J}} - \rho\overline{u_\iota}\,\overline{u_J}, \tag{2-17a}$$

$$C_{ij} = \rho\overline{\bar{u}_i u_j'} + \rho\overline{u_i'\bar{u}_j}, \tag{2-17b}$$

$$R_{ij} = \rho\overline{u_i' u_j'} \tag{2-17c}$$

If the filter is a Reynolds operator, then the tensors C_{ij} and L_{ij} are identically zero and the two decompositions are then equivalent [72]. The LES Reynolds stresses R_{ij} are caused by convective momentum transfer due to interactions of SGS eddies. Therefore, only Reynolds stress R_{ij} in the last term is modeled with the SGS turbulence model. Various types of SGS model have been proposed by numerous researchers. Smagorinsky model [72, 74] that is the simplest and widely used among SGS models was used in this study. In his studies, since the smallest turbulent eddies are almost isotropic, the Boussinesq hypothesis can provide a good description of the effects of the unresolved eddies on the resolved flow [62]. The SGS model of Smagorinsky is defined as follows:

$$\tau_{ij} = \rho\overline{u_i u_j} - \rho\bar{u}_i\bar{u}_j = R_{ij} = -2\mu_{SGS}\bar{S}_{ij} = -\mu_{SGS}\left(\frac{\partial\bar{u}_i}{\partial x_j} + \frac{\partial\bar{u}_j}{\partial x_i}\right) \tag{2-18}$$

$$\mu_{SGS} = \rho(C_s\Delta)^2|\bar{S}| = \rho(C_s\Delta)^2\sqrt{2\bar{S}_{ij}\bar{S}_{ij}} \tag{2-19}$$

where C_s and Δ denote a Smagorinsky model constant and filter size, respectively. The Smagorinsky constant C_s = 0.15 is recommended for the external flows around bluff bodies and flows in turbomachines [58].

In summary, the fundamental equation used in LES is as follows:

$$\frac{\partial}{\partial t}(\rho\bar{u}_i) + \frac{\partial}{\partial x_j}\left[\rho\bar{u}_i\left(\bar{u}_j - \overline{u_{Sj}}\right)\right] = -\frac{\partial\bar{p}}{\partial x_i} + \frac{\partial}{\partial x_j}\left[(\mu + \mu_{SGS})\left(\frac{\partial\bar{u}_i}{\partial x_j} + \frac{\partial\bar{u}_j}{\partial x_i}\right)\right] \tag{2-20}$$

Since unsteady Navier-Stokes equations are to be solved, appropriate boundary condition is required. For the regions where the thickness of the first boundary layer as $y^+ \leq 1$, in particular, minute grids are required [75]. However, practical utilization is challenging yet since calculation time is delayed exponentially in case of considering

grids that satisfies the condition of $y^+ \leq 1$ in all wall surface for complicated and rotating shapes adopted in this study. Therefore, the condition was adjusted not to go beyond $y^+ \leq 10$ in maximum for the thickness of the first boundary layer and $y^+ \leq 5$ in maximum for most regions. And sub-iteration for each iteration with double precision of solver was performed, in order to obtain accurate solutions. In addition, a convergence condition, that each residual for velocity and pressure was set to 0.000001 or below and 0.00001 or below, was used for each iteration, thus the next iteration was conducted after achieving convergence.

2.2 Computational Aeroacoustics (CAA)

2.2.1 Fundamental theory of aeroacoustic noise

The noise produced by aerodynamic fluctuation occurring while flow induced by rotation of the fluid machinery flows brushing past the blade or the casing is called aeroacoustic noise. Since the characteristics of such noise get differ not only by the blade shape of the fluid machinery but also by the operation condition and the state of the flow brushing past the blade, it is known that the prediction and/or handling of such noise is difficult. Meanwhile, understanding on the occurrence of aerodynamic noise including fan noise is based on acoustic analogy that was developed by Lighthill [10], Curle [11], and Ffowcs Williams and Hawkings [13]. Despite that the noise occurring device in fluid machinery such as axial flow fan and centrifugal fan is similar, various and detailed researches have been conducted as an axial flow fan was used in field of aircraft. The following is a brief review on acoustic analogy.

(a) Lighthill analogy

The theory that enables mathematical and physical understanding on how sound is produced by the flow is firstly introduced by Lighthill in 1952. He induced acoustic wave propagation equation (Lighthill equation) having sound source term $g(y)$ in free flow field without boundary from the governing equation of the flow.

$$\frac{\partial^2 \rho'}{\partial t^2} - a_0^2 \frac{\partial^2 \rho'}{\partial x_i^2} = \frac{\partial^2 T_{ij}}{\partial x_i \partial x_j} = g(y) \tag{2-21}$$

where a_0 is the speed of sound, T_{ij} is Lighthill's stress tensor and is defined as follows.

$$T_{ij} = \rho u_i u_j + p_{ij} - a_0^2 \rho \delta_{ij} \tag{2-22}$$

In equation (2-21), the left-hand side is in forms of wave equation and the rest terms are all transpositioned to the right-hand side with Lighthill's stress tensor; and this was defined as acoustic source. However, the density that is the dependent variable in this equation is also on the right-hand side; hence, the solution is not able to be calculated. Through dimensional analysis on general jet flow under the assumption of compact, characteristics and trend of monopole, dipole, and quadrupole were studied. Lighthill's similarity theory tells governing equation on flow noise in free flow field and allows initial mathematical understanding on flow noise.

(b) Curle's solution

Lighthill equation has limitation since it is applicable only for the cases without solid boundaries. Afterwards, Curle applied generalized theory to Lighthill equation and proposed general solution for cases with objects as follows.

$$\begin{aligned} \rho(\vec{x}, t) = & \frac{1}{4\pi a_0^2} \frac{\partial^2}{\partial x_i \partial x_j} \int_V \left[\frac{T_{ij}}{r}\right] dV && \text{: quadrupole} \\ & - \frac{1}{4\pi a_0^2} \frac{\partial}{\partial x_i} \int_S n_j \left[\frac{\rho u_i u_j + p_{ij}}{r}\right] dS && \text{: dipole} \\ & + \frac{1}{4\pi a_0^2} \frac{\partial}{\partial t} \int_S \left[\frac{\rho u_i n_i}{r}\right] dS && \text{: monopole} \end{aligned} \tag{2-23}$$

Here, square brackets mean the amount at acoustic source time *t*.

The acoustic source in above formula is independently acting and forms acoustic field by superposition; hence, each acoustic source can be studied individually. However, the method using the solution above requires both information on the surface obtained from the analysis on flow field and disturbed velocity value due to turbulent flow field. Acoustic analysis using Curle solution is also not an easy method as well since accurate analysis on the flow field must be possible. Because turbulent flow must be accurately simulated in order to predict acoustic field based on this equation.

(c) Ffowcs Williams and Hawkings equation

Although Curle's result can be applied to the cases with boundaries, it cannot be applied to the cases with moving objects that is moving acoustic source in other words. Ffowcs Williams and Hawkings expanded the equation so that it enables application to the cases with moving acoustic sources.

$$\begin{aligned}\rho(\vec{x},t) = {} & \frac{1}{4\pi a_0^2}\frac{\partial^2}{\partial x_i \partial x_j}\int_V \left[\frac{T_{ij}}{r|1-M_r|}\right] dV(\vec{y}) && \text{: quadrupole} \\ & -\frac{1}{4\pi a_0^2}\frac{\partial}{\partial x_i}\int_S \left[\frac{p_{ij}n_j}{r|1-M_r|}\right] dS(\vec{y}) && \text{: dipole} \\ & +\frac{1}{4\pi a_0^2}\frac{\partial}{\partial t}\int_S \left[\frac{\rho u_i n_i}{r|1-M_r|}\right] dS(\vec{y}) && \text{: monopole}\end{aligned} \tag{2-24}$$

The first term contributes as same as the distribution of the moving point quadrupole and the noise due to turbulent shear stress is called quadrupole noise. Such acoustic source was well described by Morfey [4] in literatures studied on noise occurring through the interaction between the disturbance of the inflow and the flow around the blades; and the term was revealed to be significant only when the Mach number at the tip is 0.8 or greater. The second term presents the noise radiation due to unsteady force and can be considered to be the distribution of the moving point force. Here, $p_{ij}n_j$ denotes the force per unit area acting from the surface onto the fluid. The last term means the noise radiation caused by the volume displacement effect due to a moving object. Such noise is often called thickness noise.

Monopole and quadrupole sources are sometimes important; however, Neise [8] insisted the dipole that is the disturbance of unsteady force occurring in blades and vane as the major cause of the fan noise. Hence, fan noise was predicted by using the method predicting acoustic field due to dipole under the assumption that dipole is dominant cause of fan noise in this study.

(d) Lowson equation

In Ffowcs-Williams and Hawkings equation, the differential for observer's location or time has to be done after performing the integral for acoustic source time; hence, its

practical application is very difficult. Therefore, this study adopted Lowson equation that is easy for numerical application. In 1967, Lowson induced the equation predicting acoustic field generated by moving point force. In this study, acoustic field of rotating fluid machinery was able to be predicted by considering the moving distributed point forces by using this equation. To induce the equation, mass conservation and momentum conservation can be rewritten in terms of tensor as follows.

$$\frac{\partial \rho}{\partial t} + \frac{\partial}{\partial x_i}(\rho u_i) = Q = 0 \tag{2-25}$$

$$\frac{\partial}{\partial t}(\rho u_i) + \frac{\partial}{\partial x_j}\left(\rho u_i u_j\right) + \frac{\partial P_{ij}}{\partial x_i} = F_j \tag{2-26}$$

Here, *F* means external force acting on fluid.

Equation (2-26) can be rewritten as follows.

$$\frac{\partial}{\partial t}(\rho u_i) + a_0^2 \frac{\partial \rho}{\partial x_j} = -\frac{\partial (T_{ij})}{\partial x_i} + F_j \tag{2-27}$$

$$T_{ij} = \rho u_i u_j + p_{ij} - a_0^2 \rho \delta_{ij} \tag{2-22}$$

When ρu_i is eliminated in equation (2-25) and (2-27) above,

$$\frac{\partial^2 \rho}{\partial t^2} - a_0^2 \frac{\partial^2 \rho}{\partial x_j^2} = \frac{\partial^2 T_{ij}}{\partial x_i \partial x_j} - \frac{\partial F_i}{\partial x_j} + \frac{\partial Q}{\partial t} \tag{2-28}$$

The terms on the left-hand side in equation (2-28) is the acoustic wave transport equation in stationary medium and the terms on the right-hand side means numerous acoustic sources in fluid. The first term on the right presents the influence of quadrupole, the second term presents that of dipole, and the last term presents that of monopole. In cases with the dominance of dipole like what in this study, the influence of monopole and quadrupole can be ignored. Therefore, only the terms of the most dominant force among the noise sources of the general fan are considered.

If the acoustic source term of equation (2-28) is $g(y)$, then, the solution is as follows.

$$\rho - \rho_0 = \frac{1}{4\pi a_0^2} \int_v \left[\frac{g}{r}\right] dv(\vec{y}) \tag{2-29}$$

The square bracket [ ] in above equation means $\tau = t - r/a_0$, the value in retarded time, and, t and $r = | x_i - y_i |$ present observation time and the distance from the acoustic source to the observation location, respectively. By using the equation above, not only the acoustic field when the point force is moving but also the acoustic field due to distributed forces can be expressed as follows by defining the acoustic source term $g(y)$ in terms of force change in equation (2-29).

$$g(y) = -\frac{\partial F_i}{\partial y_i} \tag{2-30}$$

Therefore, the acoustic field can be expressed as follows.

$$\rho - \rho_0 = \rho' = -\frac{1}{4\pi a_0^2} \int_v \left[\frac{1}{r}\frac{\partial F_i}{\partial y_i}\right] dv(y) \tag{2-31}$$

To express the point force changing by time in random space, three-dimensional Dirac delta function δ, is used. In other words, F_i is considered as a function of time only by changing F_i to $F_i\delta$; and Dirac delta function δ, is regarded as a function for space (y_i) and time ($y_{0i}(\tau)$). It is as follows when Dirac delta function is substituted into equation (2-31).

$$\rho - \rho_0 = -\frac{1}{4\pi a_0^2} \int_v \left[\frac{1}{r}\frac{\partial\{F_i(\tau)\delta(y_i - y_{0i}(\tau))\}}{\partial y_i}\right] dv(y) \tag{2-32a}$$

$$\delta = \delta(\vec{y} - \vec{y}_0),\ F : \text{function of time only} \tag{2-32a}$$

When chain rule is applied to an arbitrary function $f(y, \tau(y))$, it is as follows, and the variables related to this equation are presented in figure 2-4. r is the vector from a source to an observer, V is the angular velocity vector of a rotating force and $M = V \times y / a_0$, x and y are the position vectors of an observer and a source, respectively.

$$\frac{\partial[f]}{\partial y_i} = \frac{\partial f}{\partial y_i}\Big|_{y,\tau=t-r/a_0} + \frac{\partial \tau}{\partial y_i}\frac{\partial f}{\partial \tau}\Big|_{y,\tau=t-r/a_0} = \left[\frac{\partial f}{\partial y_i}\right] + \left[\frac{\partial \tau}{\partial y_i}\frac{\partial f}{\partial \tau}\right] \tag{2-33}$$

In above equation, $\partial\tau/\partial y_i$ is induced as follows.

$$\begin{aligned}\left[\frac{\partial \tau}{\partial y_i}\right] &= \frac{\partial \tau}{\partial y_i}\Big|_{y,\tau=t-r/a_0} = \frac{\partial}{\partial y_i}\left(t - \frac{|x_i - y_i(\tau)|}{a_0}\right) \\ &= -\left[\frac{\partial}{\partial y_1}\left(\frac{\sqrt{(x_1-y_1)^2+(x_2-y_2)^2+(x_3-y_3)^2}}{a_0}\right)i + \frac{\partial}{\partial y_2}\left(\frac{\sqrt{(x_1-y_1)^2+(x_2-y_2)^2+(x_3-y_3)^2}}{a_0}\right)j + \right. \\ &\quad \left. \frac{\partial}{\partial y_3}\left(\frac{\sqrt{(x_1-y_1)^2+(x_2-y_2)^2+(x_3-y_3)^2}}{a_0}\right)k\right] \\ &= -\left[\frac{1}{a_0}\frac{-2(x_1-y_1)}{2\sqrt{(x_1-y_1)^2+(x_2-y_2)^2+(x_3-y_3)^2}}i + \frac{1}{a_0}\frac{-2(x_2-y_2)}{2\sqrt{(x_1-y_1)^2+(x_2-y_2)^2+(x_3-y_3)^2}}j + \right. \\ &\quad \left. \frac{1}{a_0}\frac{-2(x_3-y_3)}{2\sqrt{(x_1-y_1)^2+(x_2-y_2)^2+(x_3-y_3)^2}}k\right]\end{aligned}$$

$$\left[\frac{\partial \tau}{\partial y_i}\right] = \left[\frac{x_i - y_i}{a_0|x_i - y_i|}\right] = \left[\frac{x_i - y_i}{a_0 r}\right] \tag{2-34}$$

Finally, if the chain rule is applied, it is as follows.

$$\frac{\partial[f]}{\partial y_i} = \left[\frac{\partial f}{\partial y_i} + \frac{x_i - y_i}{a_0 r}\frac{\partial f}{\partial \tau}\right] \tag{2-35}$$

The differential for an arbitrary function $f(y, \tau(y))$ in acoustic source time can be written as follows by fixing other variables and performing partial differential for τ.

$$\frac{\partial[f(y,\tau(y))]}{\partial \tau} = \frac{\partial}{\partial \tau}f(y,\tau)\Big|_{y,\tau=t-r/a_0} = \left[\frac{\partial}{\partial \tau}f\big(y,\tau(y)\big)\right] \tag{2-36}$$

Therefore, the differential equation for acoustic source time (τ) of an arbitrary function $f(y, \tau(y))$ is as follows.

$$\frac{\partial[f]}{\partial \tau} = \left[\frac{\partial f}{\partial \tau}\right] \tag{2-37}$$

Meanwhile, the differential for acoustic source time (τ) of an arbitrary function $\delta(y_i - y_{0i}(\tau))$ can be expanded as follows when induced by substituting $q = y_i - y_{0i}(\tau)$.

$$\frac{\partial \delta(q)}{\partial \tau} = \frac{\partial q}{\partial \tau}\frac{\partial \delta}{\partial q} = -\frac{\partial y_{0i}}{\partial \tau}\frac{\partial \delta}{\partial q} = -\frac{\partial y_{0i}}{\partial \tau}\frac{\partial \delta}{\partial y_i}\frac{\partial y_i}{\partial q} \tag{2-38}$$

Here, $\partial y_i/\partial q = 1$; hence, the differential for time of the delta function is the equation below.

$$\frac{\partial}{\partial \tau}\delta\big(y_i - y_{0i}(\tau)\big) = -\frac{\partial y_{0i}}{\partial \tau}\frac{\partial \delta}{\partial y_i} \tag{2-39}$$

In order to identify the relationship between the differential for acoustic source time and the differential for space in delta function, substitute the delta function into f in Equation (2-35), then it is as follow.

$$\frac{\partial [\delta]}{\partial y_i} = \left[\frac{\partial \delta}{\partial y_i} + \frac{x_i - y_i}{a_0 r}\frac{\partial \delta}{\partial \tau}\right] \tag{2-40}$$

Substitute equation (2-39) into the differential term for time of the delta function, it is as follow.

$$\frac{\partial [\delta]}{\partial y_i} = \left[\frac{\partial \delta}{\partial y_i}\right] - \left[\frac{(x_i - y_i)}{a_0 r}\frac{\partial y_{0i}}{\partial \tau}\frac{\partial \delta}{\partial y_i}\right] \tag{2-41}$$

The differential of time for y_{0i} is the velocity of moving acoustic source; hence, the relationship is as follows.

$$\frac{\partial y_{0i}}{\partial \tau} = aM_i$$

Therefore, it can be rewritten as

$$\frac{\partial [\delta]}{\partial y_i} = \left[\frac{\partial \delta}{\partial y_i}\right] - \left[\frac{(x_i - y_i)}{r} M_i \frac{\partial \delta}{\partial y_i}\right] = [1 - M_r]\left[\frac{\partial \delta}{\partial y_i}\right] \tag{2-42}$$

and M_r has following relationship.

$$M_r = \frac{(x_i - y_i)}{r} M_i \tag{2-43}$$

To express equation (2-39) as the equation in retarded time, it is as follows when equation (2-39) is put into the square bracket

$$\left[\frac{\partial \delta}{\partial \tau}\right] = -\left[\frac{\partial y_{0i}}{\partial \tau}\frac{\partial \delta}{\partial y_i}\right] = -\left[a_0 M_i \frac{\partial \delta}{\partial y_i}\right] \tag{2-44}$$

By eliminating $[\partial\delta/\partial y_i]$ with using equation (2-42) and (2-44), the value of the time differential for the delta function in acoustic source can be expressed with the value of the differential for space as follows.

$$\left[\frac{\partial \delta}{\partial \tau}\right] = \left[-\frac{a_0 M_i}{1 - M_r}\right]\frac{\partial [\delta]}{\partial y_i} \tag{2-45}$$

To make equation (2-32) easier for the integral using the equations obtained above, the equation can be expanded as follows. The space differential value for $F_i\delta$ in equation (2-32) is modified by using chain rule in equation (2-35) as follows.

$$\begin{aligned}\left[\frac{\partial (F_i \delta)}{\partial y_i}\right] &= \frac{\partial}{\partial y_i}[F_i \delta] - \left[\frac{(x_i - y_i)}{a_0 r}\frac{\partial (F_i \delta)}{\partial \tau}\right] \\ &= \frac{\partial}{\partial y_i}[F_i \delta] - \left[\frac{(x_i - y_i)}{a_0 r}\frac{\partial F_i}{\partial \tau}\right][\delta] - \left[\frac{(x_i - y_i)}{a_0 r} F_i \frac{\partial \delta}{\partial \tau}\right]\end{aligned} \tag{2-46}$$

The following is that equation (2-46) is rewritten by substituting equation (2-45) that is the differential equation for time of the delta function.

$$\left[\frac{\partial (F_i \delta)}{\partial y_i}\right] = \frac{\partial}{\partial y_i}[F_i \delta] - \left[\frac{(x_i - y_i)}{a_0 r}\frac{\partial F_i}{\partial \tau}\right][\delta] + \left[\frac{(x_i - y_i)}{r}\frac{F_i M_j}{1 - M_r}\right]\frac{\partial [\delta]}{\partial y_j} \tag{2-47}$$

Equation below is obtained by substituting equation (2-47) into equation (2-31) that is the equation for general solution of acoustic field.

$$\rho - \rho_0 = -\frac{1}{4\pi a_0^2}\int_v \left\{\left[\frac{1}{r}\right]\frac{\partial[F_i\delta]}{\partial y_i} - \left[\frac{(x_i-y_i)}{a_0 r^2}\frac{\partial F_i}{\partial \tau}\right][\delta] + \left[\frac{(x_i-y_i)}{r^2}\frac{F_i M_j}{1-M_r}\right]\frac{\partial[\delta]}{\partial y_j}\right\} dv \quad (2\text{-}48)$$

In the meantime, surface integral is not able to contain acoustic source that is a singular in Green's identity that is expressed with equation (2-49); hence, it becomes "0" by the delta function and the term is transposed to the left-hand side as below.

$$\int_s UV_i n_i ds = \int_v \left\{\frac{\partial U}{\partial x_i}V_i + U\frac{\partial V_i}{\partial x_i}\right\} dv \quad (2\text{-}49)$$

$$\int_v \left\{U\frac{\partial V_i}{\partial x_i}\right\} dv = -\int_v \left\{\frac{\partial U}{\partial x_i}V_i\right\} dv \quad (2\text{-}50)$$

The obtained equation (2-48) can be rewritten by applying Green's identity to the first and the third term as follows.

$$\rho - \rho_0 = \frac{1}{4\pi a_0^2}\int_v \left\{[F_i]\frac{\partial}{\partial y_i}\left[\frac{1}{r}\right] + \left[\frac{(x_i-y_i)}{a_0 r^2}\frac{\partial F_i}{\partial \tau}\right] + \frac{\partial}{\partial y_j}\left[\frac{(x_i-y_i)}{r^2}\frac{F_i M_j}{1-M_r}\right]\right\}[\delta] dv \quad (2\text{-}51)$$

Here, the delta function with square bracket is $[\delta] = \delta\{y_i - y_{0i}(t - r/a)\}$. For the integral, the variable y is substituted by η and Jacobian for the integral is calculated as below.

$$\eta = y - y_0\left(t - \frac{r}{a_0}\right)$$
$$dv(\eta) = (1 - M_r)dv(y) \quad (2\text{-}52)$$

In order to eliminate time component for sound source coordinate system by using the characteristic of the delta function and equation (2-52), equation (2-51) is integrated for the points satisfying $y_{0i}(\tau) = y_i$ as follows.

$$\rho - \rho_0 = \frac{1}{4\pi a_0^2[1-M_r]}\left\{[F_i]\frac{\partial}{\partial y_i}\left[\frac{1}{r}\right] + \left[\frac{(x_i-y_i)}{a_0 r^2}\frac{\partial F_i}{\partial \tau}\right] + \frac{\partial}{\partial y_j}\left[\frac{(x_i-y_i)}{r^2}\frac{F_i M_j}{1-M_r}\right]\right\} \quad (2\text{-}53)$$

By expanding the equation (2-53) from the first term, r can be regarded as the function

for space in partial differential of the first term; hence, the differential can be done in such a simple way as follows.

$$[F_i]\frac{\partial}{\partial y_i}\left[\frac{1}{r}\right] = [F_i]\frac{1}{r^2}\frac{\partial r}{\partial y_i} \tag{2-54}$$

Here, the differential for r can be obtained by equation (2-34); and the first term is as follows.

$$[F_i]\frac{\partial}{\partial y_i}\left[\frac{1}{r}\right] = \left[F_i\frac{1}{r^2}\frac{x_i-y_i}{r}\right] = \left[F_i\frac{1}{r^2}\hat{r}_i\right] = \left[\frac{F_r}{r^2}\right] \tag{2-55}$$

The second term of equation (2-53) can be briefly expressed as follows.

$$\left[\frac{(x_i-y_i)}{a_0 r^2}\frac{\partial F_i}{\partial \tau}\right] = \left[\frac{1}{a_0 r}\frac{\partial F_r}{\partial \tau}\right] \tag{2-56}$$

The third term of equation (2-53) is expanded by using equation (2-35) as following.

$$\frac{\partial}{\partial y_j}\left[\frac{(x_i-y_i)}{r^2}\frac{F_i M_j}{1-M_r}\right] = \left[\frac{\partial}{\partial y_j}\left\{\frac{(x_i-y_i)}{r^2}\frac{F_i M_j}{1-M_r}\right\} + \frac{(x_i-y_i)}{a_0 r}\frac{\partial}{\partial \tau}\left\{\frac{(x_i-y_i)}{r^2}\frac{F_i M_j}{1-M_r}\right\}\right] \tag{2-57}$$

Let's take a look on the differential for space first; then F_i and M_j can be considered to be the function for time only. They can be simplified as follows.

$$\frac{\partial}{\partial y_j}\left\{\frac{(x_i-y_i)}{r^2}\frac{F_i M_j}{(1-M_r)}\right\} = F_i M_j\frac{\partial}{\partial y_j}\left\{\frac{(x_i-y_i)}{r^2(1-M_r)}\right\} \tag{2-58}$$

Equation (2-58) is differentiated for space as follows.

$$F_i M_j\frac{\partial}{\partial y_j}\left\{\frac{(x_i-y_i)}{r^2(1-M_r)}\right\} = F_i M_j\left\{\frac{r^2(1-M_r)\frac{\partial(x_i-y_i)}{\partial y_j} - (x_i-y_i)\frac{\partial\{r^2(1-M_r)\}}{\partial y_j}}{r^4(1-M_r)^2}\right\} \tag{2-59}$$

If Kronecker delta, δ_{ij} is introduced, then it is expressed as $\partial(x_i - y_i)/\partial y_i = -\delta_{ij}$.

$$F_i M_j \left\{ \frac{r^2(1-M_r)\frac{\partial(x_i-y_i)}{\partial y_j} - (x_i-y_i)\frac{\partial\{r^2(1-M_r)\}}{\partial y_j}}{r^4(1-M_r)^2} \right\}$$
$$= F_i M_j \left\{ -\frac{\delta_{ij}}{r^2(1-M_r)} - \frac{(x_i-y_i)}{r^4(1-M_r)^2}\frac{\partial\{r^2(1-M_r)\}}{\partial y_j} \right\}$$
$$= F_i M_j \left\{ -\frac{\delta_{ij}}{r^2(1-M_r)} - \frac{(x_i-y_i)}{r^4(1-M_r)^2}\left((1-M_r)\frac{\partial r^2}{\partial y_j} - r^2\frac{\partial M_r}{\partial y_j} \right) \right\} \quad (2\text{-}60)$$

The equation above can be rewritten follows.

$$F_i M_j \frac{\partial}{\partial y_j}\left\{ \frac{(x_i-y_i)}{r^2(1-M_r)} \right\}$$
$$= F_i M_j \left\{ -\frac{\delta_{ij}}{r^2(1-M_r)} - \frac{(x_i-y_i)}{r^4(1-M_r)^2}\left((1-M_r)\frac{2r(x_i-y_i)}{r} - r^2\frac{\partial M_r}{\partial y_j} \right) \right\} \quad (2\text{-}61)$$

Here, the differential of space for M_r can be obtained by expanding the equation as follows.

$$\frac{\partial M_r}{\partial y_j} = \frac{\partial}{\partial y_j}\left(\frac{(x_k-y_k)}{r} M_k \right) = M_k \frac{\partial}{\partial y_j}\left(\frac{x_k-y_k}{r} \right)$$
$$= M_k \frac{-\delta_{jk} r - (x_k-y_k)\frac{\partial r}{\partial y_j}}{r^2} = M_k \left(-\frac{\delta_{jk}}{r} + \frac{r_j r_k}{r^3} \right) \quad (2\text{-}62)$$

The result obtained from above calculation was substituted into equation (2-61), which is expanded for the space differential-related part of the third term in equation (2-53); then it is simplified as follows.

$$F_i M_j \frac{\partial}{\partial y_j}\left\{ \frac{(x_i-y_i)}{r^2(1-M_r)} \right\} = -\frac{F_i M_i}{r^2(1-M_r)} + \frac{2F_r M_r}{r^2(1-M_r)} - \frac{F_r M^2}{r^2(1-M_r)^2} + \frac{F_r M_r^2}{r^2(1-M_r)^2} \quad (2\text{-}63)$$

The part for the time differential in the third term of equation (2-53) becomes the function for space only, since the term for time was eliminated from the coordinate system (y_i, r) of moving sound source in the integral of function δ; and it can be written

as follows.

$$\begin{aligned}&\frac{(x_i-y_i)}{a_0 r}\frac{\partial}{\partial\tau}\left\{\frac{(x_i-y_i)}{r^2}\frac{F_i M_j}{1-M_r}\right\}\\&=\frac{(x_i-y_i)(x_j-y_j)}{a_0 r^3}\frac{\partial}{\partial\tau}\left\{\frac{F_i M_j}{1-M_r}\right\}\\&=\frac{(x_i-y_i)(x_j-y_j)}{a_0 r^3}\frac{1}{(1-M_r)^2}\left\{(1-M_r)M_j\frac{\partial F_i}{\partial\tau}+(1-M_r)F_i\frac{\partial M_j}{\partial\tau}+F_i M_j\frac{\partial M_r}{\partial\tau}\right\}\end{aligned}\quad (2\text{-}64)$$

It can be simplified as follows.

$$\frac{(x_i-y_i)}{a_0 r}\frac{\partial}{\partial\tau}\left\{\frac{(x_i-y_i)}{r^2}\frac{F_i M_j}{1-M_r}\right\}=\frac{1}{a_0 r}\left\{\frac{M_r}{(1-M_r)}\frac{\partial F_r}{\partial\tau}+\frac{F_r}{(1-M_r)}\frac{\partial M_r}{\partial\tau}+\frac{F_r M_r}{(1-M_r)^2}\frac{\partial M_r}{\partial\tau}\right\}\quad (2\text{-}65)$$

The equation can be rewritten as follows by combining all of equation (2-55), (2-56), (2-63), and (2-65) that were derived.

$$\begin{aligned}\rho-\rho_0&=\frac{1}{4\pi a_0^2[1-M_r]}\left\{[F_i]\frac{\partial}{\partial y_i}\left[\frac{1}{r}\right]+\left[\frac{(x_i-y_i)}{a_0 r^2}\frac{\partial F_i}{\partial\tau}\right]+\frac{\partial}{\partial y_j}\left[\frac{(x_i-y_i)}{r^2}\frac{F_i M_j}{1-M_r}\right]\right\}\\&=\frac{1}{4\pi a_0^2[1-M_r]}\left[\frac{F_r}{r^2}\right]+\frac{1}{4\pi a_0^2[1-M_r]}\left[\frac{1}{a_0 r}\frac{\partial F_r}{\partial\tau}\right]\\&\quad+\frac{1}{4\pi a_0^2[1-M_r]}\left[-\frac{F_i M_i}{r^2(1-M_r)}+\frac{2F_r M_r}{r^2(1-M_r)}-\frac{F_r M^2}{r^2(1-M_r)^2}+\frac{F_r M_r^2}{r^2(1-M_r)^2}\right]\\&\quad+\frac{1}{4\pi a_0^2[1-M_r]}\left[\frac{1}{a_0 r}\left\{\frac{M_r}{(1-M_r)}\frac{\partial F_r}{\partial\tau}+\frac{F_r}{(1-M_r)}\frac{\partial M_r}{\partial\tau}+\frac{F_r M_r}{(1-M_r)^2}\frac{\partial M_r}{\partial\tau}\right\}\right]\end{aligned}\quad (2\text{-}66)$$

Exact solution as below is obtained when equation (2-66) is simplified through reduction to common denominator.

$$\rho'=\frac{1}{4\pi a_0^2[1-M_r]}\left[\frac{(x_i-y_i)}{a_0 r^2(1-M_r)}\left\{\frac{\partial F_i}{\partial\tau}+\frac{F_i}{1-M_r}\frac{\partial M_r}{\partial\tau}\right\}+\frac{1}{r^2(1-M_r)}\left(F_r\frac{(1-M^2)}{(1-M_r)}-F_i M_i\right)\right]\quad (2\text{-}67)$$

In this equation, the first term inside the square bracket on the right-hand side is the value of the time differential for force and the second term is the acceleration term. Although the force is steady on time, noise is produced since the value of the second term exists if it is rotating. Also, it can be written as follows by using the relationship

between density and aeroacoustic pressure ($p' = a^2\rho'$).

$$p' = \frac{1}{4\pi[1-M_r]}\left[\frac{1}{a_0 r(1-M_r)}\left\{\frac{\partial F_r}{\partial \tau} + \frac{F_r}{1-M_r}\frac{\partial M_r}{\partial \tau}\right\} + \frac{1}{r^2(1-M_r)}\left(F_r\frac{(1-M^2)}{(1-M_r)} - F_i M_i\right)\right] \quad (2\text{-}68)$$

Equation (2-68) above is recognized to be composed of the far field term that is decreased by the multiple of $1/r$ and the near field term that is decreased by the multiple of $1/r^2$, depending on the distance. The pressure above is calculated from the time region and fast Fourier transform should be done to identify the characteristics of the frequency. In addition, log scale is convenient for expressing pressure; hence, the equation is rewritten in decibel scale based on formula below.

$$SPL = 10log\left(\frac{p}{p_{ref}}\right)^2, \text{ where } p_{ref} = 2 \times 10^{-5}\ (N / m^2) \quad (2\text{-}69)$$

2.2.2 Sound source analysis

Equation (2-67) is aeroacoustic field in cases of one-point source that is moving. In this study, the region of interest in fluid machinery was divided into small elements and the force in each element was calculated as a point force. Therefore, aeroacoustic filed due to rotation of the fluid machinery can be calculated by merging equation (2-67) for overall impeller elements. The grid system used to predict aeroacoustic field in this study was the surface grid as is that was used in CFD shown in figure 2-5. Hence, all of the moving point force for three-dimensional shapes can be considered and more accurate result can be achieved for flow noise. However, only the radiation of the noise source in free space was considered in this equation; and reflection, diffraction, refraction, and scattering were not considered.

Methods predicting flow noise are classified into two primary types.

First is the method in which unsteady flow analysis and noise analysis are conducted simultaneously; and this method yields the most accurate noise analysis since it considers radiated noise and quadrupole. But this method requires high order schemes in order to capture the broad range of time and length scales associated with the physics

of aerodynamically-generated sound, and specific boundary treatment in order to deal with the radiation of sound waves [76]. Resultingly, the disadvantage is excessive retardation of time for analysis.

Another is the method predicting flow noise by linking CFD and CAA together. In the method, a flow property by time is calculated through unsteady flow field analysis and flow noise is predicted by setting the calculated value of a flow property as the input value for noise analysis. This method has advantage of saving time required for analysis since higher order terms are not considered; however, it also has disadvantage that the result of noise analysis may be influenced by the result of flow field. In case of analysis region with complicated shape and large number of grids, the latter severely limits the choice of turbulence model with great influence of hardware (H/W) due to calculation time, data capacity for flow field analysis, memory for data handling; and previous studies mostly adopted URANS (Unsteady Reynolds Averaged Navier-Stokes) turbulence model. However, rapid development of hardware with high performance and development of CFD software have enabled the use of LES model that replicates vortex in detail even in Sub-Grid Scale (SGS); hence, the disadvantage is gradually offset. The flow noise prediction method used in this study is the hybrid method in which CFD and CAA are linked, and figure 2-6 is presenting the process. During the process, surface pressure fluctuation for time in surface grids used for unsteady state flow analysis and surface grid points in region of interest is obtained. Noise spectrum and the location of the noise source are predicted by performing FFT (fast Fourier transform) on surface pressure fluctuation for each grid point.

Meanwhile, the numerical algorithms are concerned with the numerical process and the needed approximations to offer a discrete result from the formulation. Numerical algorithms can be varied significantly by different formulation types, even though obtaining ultimately the same physical and mathematical solution.

After the change of variables to integrate the Dirac delta functions $\delta(f)$ and $\delta(g)$, integral representation of the solution by using the free-space Green's function for the surface source term in the FW-H equation can be expressed as the retarded-time formulation [77].

$$4\pi\phi(\vec{x},t) = \int_{f=0}\left[\frac{Q(y,\tau)}{r|1-M_r|}\right]_{ret} dS \tag{2-70}$$

In above formulation, Q is the known source strength which is a function of the source position and time (y, τ), subscript "*ret*" means that quantity is evaluated at the retarded time, $\tau^* = t - r/a_0$. In acoustic predictions, ϕ is described normally as the acoustic pressure $p' = p - p_0$. Brentner [77] noted that the formulation requires that the observer location x and the observer time t are fixed during the evaluation of the integral. As a result, he mentioned that numerical implementations of this formula have proven to be very robust and efficient; hence, most acoustic-analogy-based rotor noise predictions from other studies utilize retarded-time formulations.

In this study, source-time-dominant algorithm was used as one of the retarded-time algorithms. This is the method determining the time point when the signal reaches observer by selecting source time rather than selecting observer time in advance if the source time is regarded to be dominant. Time history interpolation is required in order to provide the contribution from all noise sources at time of the desired observer. So, time interpolation is necessary to add together the contribution from all source elements at the same observer times and at observer location that is apart certain distance. This algorithm can be expressed with symbols as follows.

$$4\pi\phi(\vec{x},t) \approx \sum_{i=1}^{N} I(K_i(t), t^*) \tag{2-71}$$

where $I(K_i(t), t^*)$ is an interpolation operator and t^* is the time of desired observer. The approximation of the integral over the element K is defined as follows.

$$K_i(t) = \frac{Q(y_i,\tau)}{r_i|1-M_r|_i}\Delta S_i \tag{2-72}$$

The t^* value is determined by the choice of y_i and τ from above equation. In other words, regardless of that the source time is regular, rearrangement with the new observer time t^* is required since time delay that takes for the signal arisen in each element to reach observer location occurs. This algorithm has been known for its advantage that it does not require calculation of retarded time and interpolation of

discrete time-dependent input data. Such characteristic is considered to be useful for the use of CFD result as input data [77].

2.2.3 Aeroacoustic source strength and visualization (presented method)

As noted early, the sound is generated by the unsteady flow fluctuation and is significantly associated with the fluid dynamics and the acoustics. Inferring from this definition, the simulation of the unsteady flow field is very closer related with prediction and validation of flow noise using hybrid method. If understanding the unsteady flow field based on positions of sound sources, low noise model can be suggested and designed to reduce the noise. Especially, because the dipole is dominant at the noise in cases considering only fans operated at the range of subsonic, the location of sound source can be predicted by using fluctuating static wall pressures depending on the time from CFD. As a result, a property to describe the locations of sound sources was needed and defined.

Meanwhile, equation (2-68) is known to predict the acoustic field generated by moving point force.

$$p' = \frac{1}{4\pi[1-M_r]}\left[\frac{1}{a_0 r(1-M_r)}\left\{\frac{\partial F_r}{\partial \tau} + \frac{F_r}{1-M_r}\frac{\partial M_r}{\partial \tau}\right\} + \frac{1}{r^2(1-M_r)}\left(F_r\frac{(1-M^2)}{(1-M_r)} - F_i M_i\right)\right] \quad (2\text{-}68)$$

If the second term in a square bracket of the right-hand side is neglected by considering the acoustical compactness of region containing aeroacoustic sources, equation (2-68) is simplified as follows.

$$p' = \frac{x_i - y_i}{4\pi a_0 r^2(1-M_r)^2}\left\{\frac{\partial F_i}{\partial \tau} + \frac{F_i}{1-M_r}\frac{\partial M_r}{\partial \tau}\right\} \quad (2\text{-}73)$$

Here, if considering that *F* is the aerodynamic force acting on the area of an element, *F* can be rewritten as the static wall pressure(p_{fluid}) acting on an element and the integrated area of an element; and the below is the result of considering equation (2-73) as sound pressure for an element area.

$$p' = \frac{1}{4\pi a_0}\int_S \left[\frac{x_i - y_i}{r^2(1-M_r)^2}\left(\frac{\partial}{\partial\tau}\{n_i \cdot p_{fluid}(y_i,\tau)\} + \frac{n_i \cdot p_{fluid}(y_i,\tau)}{1-M_r}\frac{\partial M_r}{\partial\tau}\right)\right] d\sigma \quad (2\text{-}74)$$

In order to predict the location of noise source through aeroacoustic noise analysis, "Aeroacoustic source strength, A_{st}" was defined as below; and this was obtained by integrating p_{fluid} inside square bracket for element area in equation (2-74).

$$A_{st} = \frac{x_i - y_i}{r^2}\left(\frac{\partial}{\partial\tau}\{n_i \cdot F_{fluid}(y_i,\tau)\} + \frac{n_i \cdot F_{fluid}(y_i,\tau)}{1-M_r}\frac{\partial M_r}{\partial\tau}\right) \quad (2\text{-}75)$$

In addition, it's not easy to find other software to indicate the locations of sound source after predicting the sound field. Most of tools using hybrid method for CAA focus on the phenomenon of the noise radiation from around the sound source to the space. Recently, the locations of sound source are visualized through the measurement of equipments with adopting beamforming technology. So, prior to conducting this study, the noise source location that is predicted by numerical analysis and measured from the flow noise occurring in a ring blower were compared to identify the validity and feasibility of aeroacoustic noise analysis. The ring blower is a device that is widely used in industrial site and machineries requiring high pressure air and is also called a regenerative blower. In figure 2-7 [51], one model among air supercharging regenerative blowers offering low-flow/high-pressure is shown. For flow noise occurring while operating a blower, noise sources were measured by utilizing acoustic camera with a beamforming technology and compared with the location of noise sources obtained from aeroacoustic noise analysis.

When comparing noise source location in figure 2-7(b) and (c), accurate location cannot be compared due to external shape of the blower casing; however, both are indicating the region near the outlet of the ring blower. Hence, the prediction of noise source by aeroacoustic noise analysis was determined to be utilized to predict unsteady flow field that causes flow noise.

2.3 Summary

The fundamentals of CFD and acoustic analogy, numerical analysis methods, and a definition to indicate the locations of sound source were described in this chapter,

because a hybrid method for CAA was used. In CFD, SST k-ω and LES turbulence model was used to simulate the flow field of steady state and unsteady state, respectively. In acoustic analogy, Lowson's equation which can predict the sound field due to a moving point force was introduced to calculate the acoustic field due to dipole. The high accuracy of noise prediction in CAA was maintained by using the mesh used in CFD.

Studies conducted so far have been contributing to the establishment of concept for fan noise reduction by predicting the flow-induced noise through the development of noise prediction model, but are not connected directly with the production of the low-noise product. In addition, because it's not easy to find software to indicate the locations of sound source after predicting the sound field, the objective of this study is to provide the numerical method which can reduce the noise in the fan development or improvement. Because the flow noise is caused to the pressure fluctuation of the unsteady flow field, a property was required to find the locations of sound source and was finally defined as A_{st} in this chapter. To find the locations of sound sources means that the unsteady flow field to generate the flow noise can be controlled.

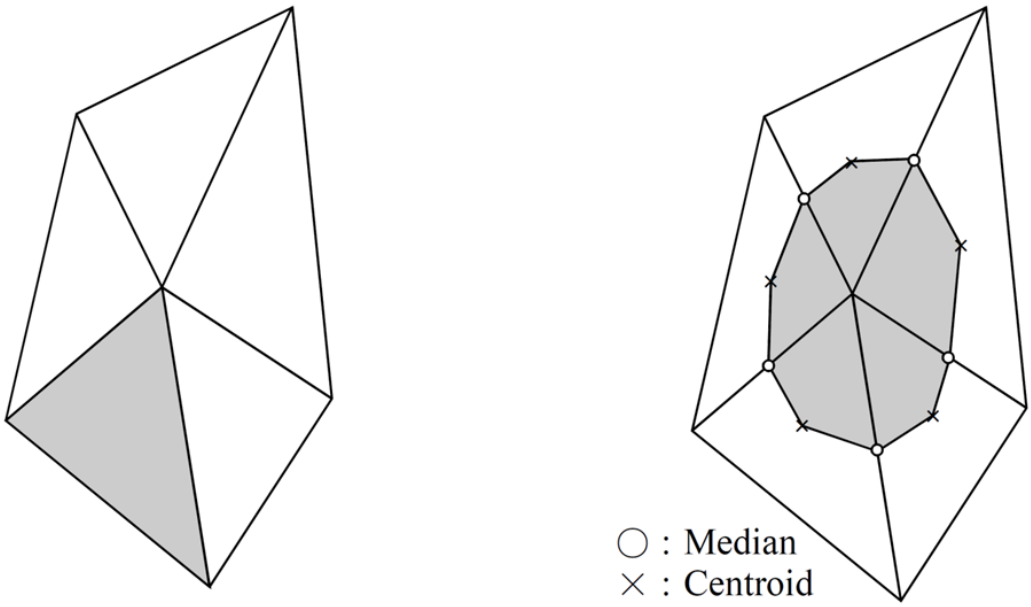

(a) Cell-based scheme (b) Vertex-base scheme

Fig. 2-1 Comparison of control volume formulations used in the finite volume method

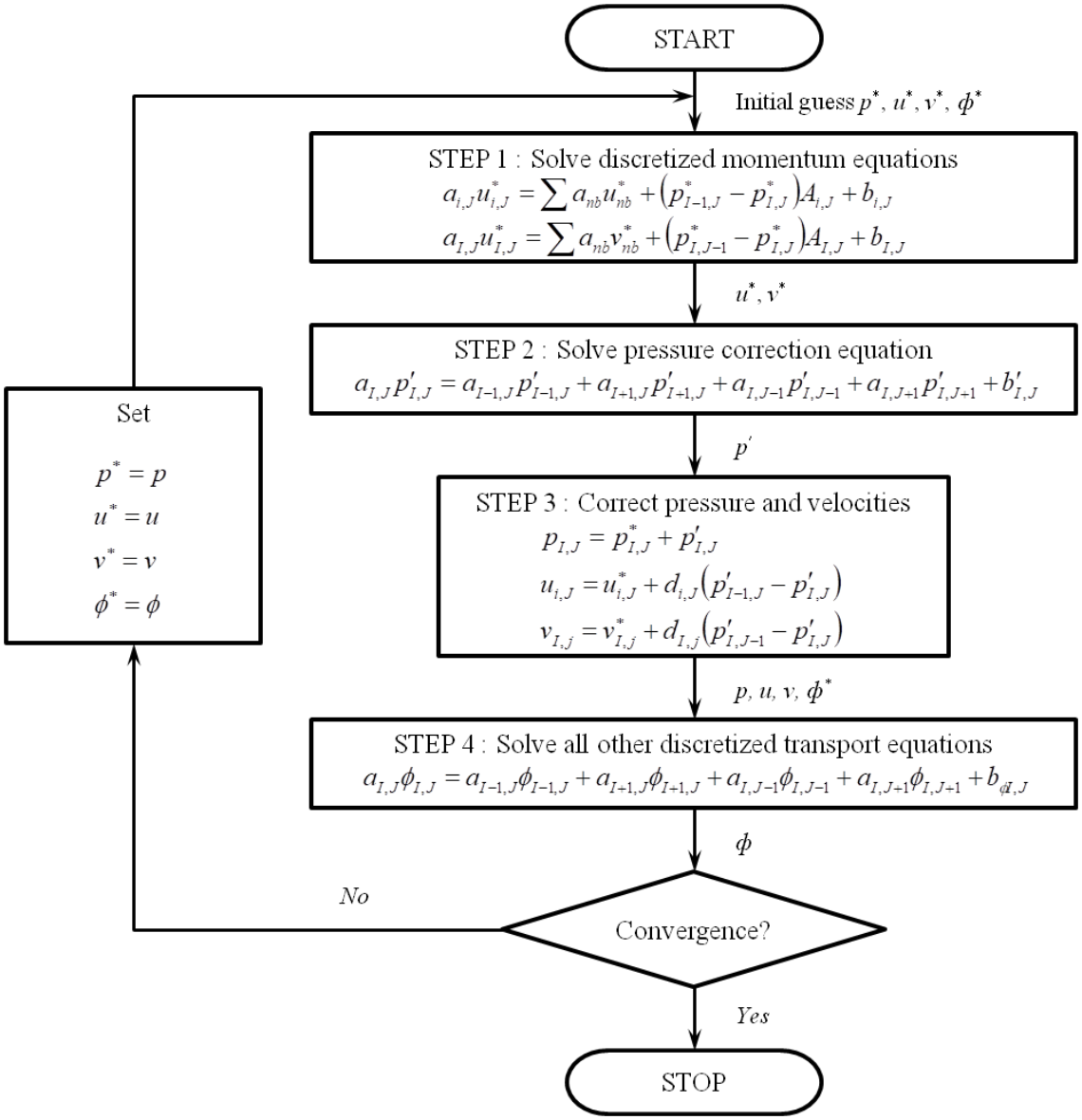

Fig. 2-2 SIMPLE algorithm

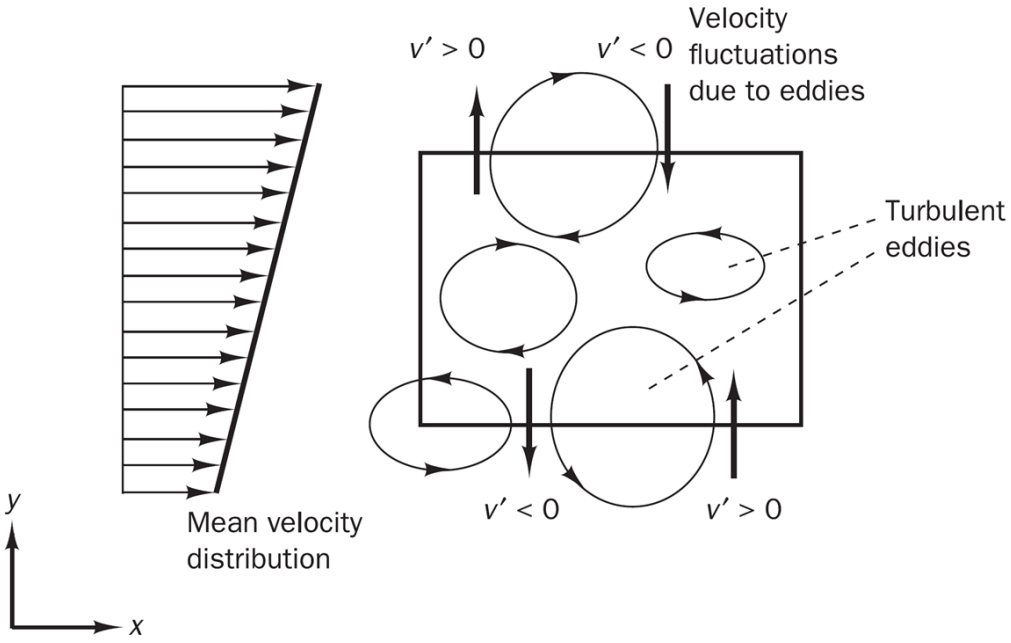

Fig. 2-3 Control volume within a two-dimensional turbulent shear flow [62]

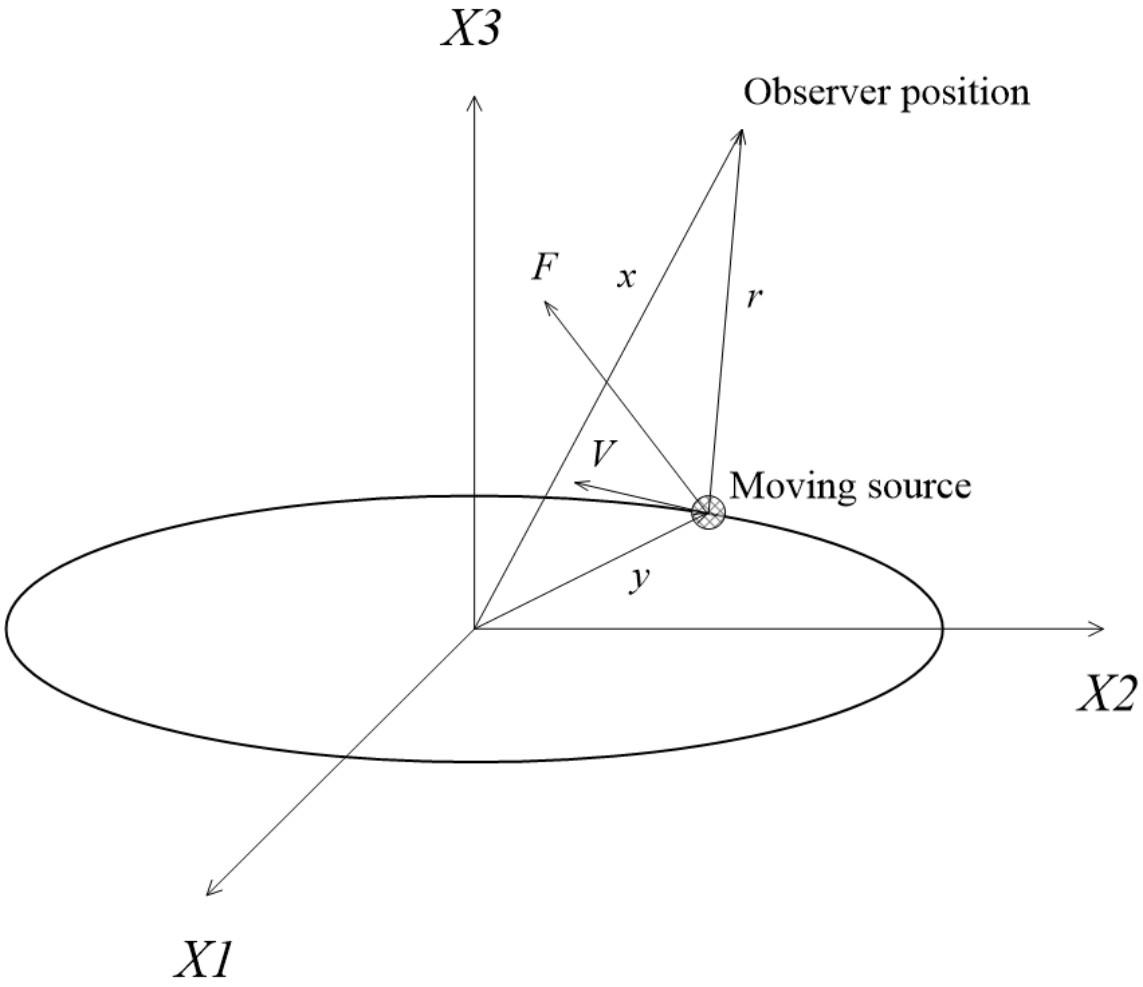

Fig. 2-4 Definitions of the variables

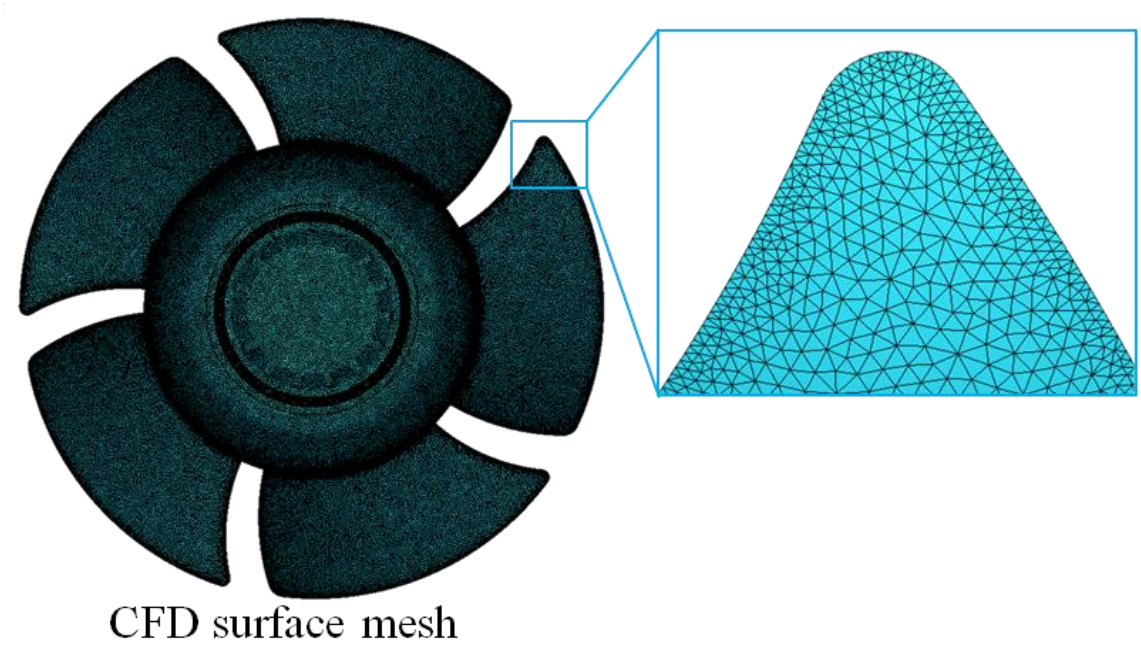

(a) CFD and CAA surface mesh used in this study

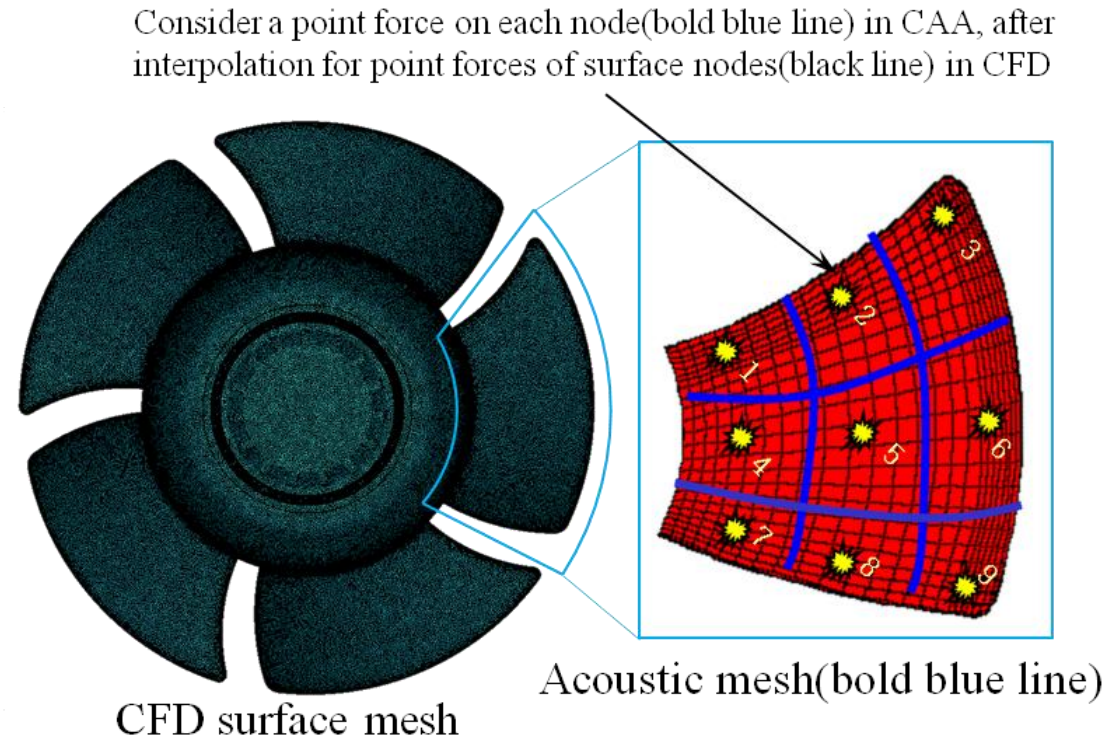

(b) CAA surface mesh used in other CAA software

Fig. 2-5 Comparison of surface meshes used for CAA

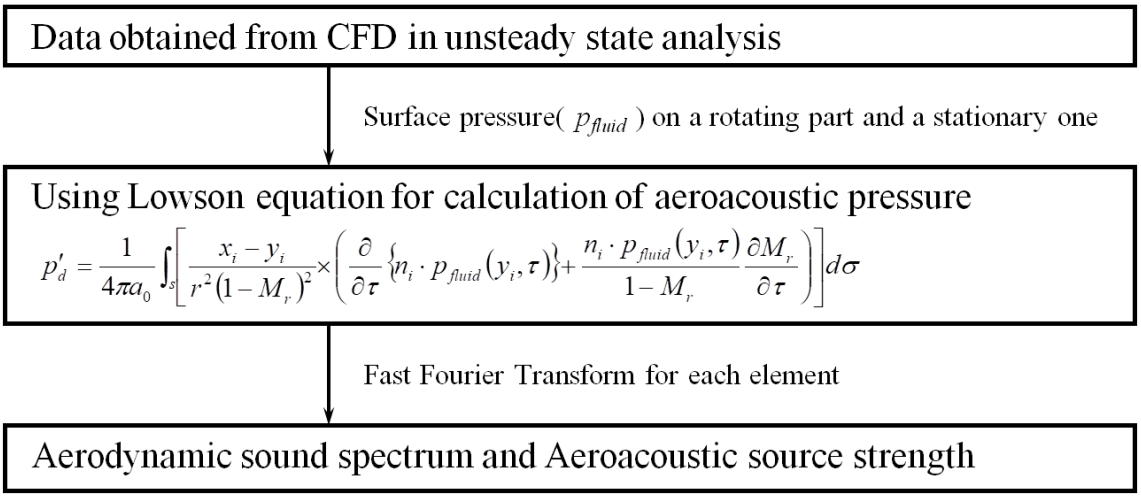

Fig. 2-6 Schematic diagram of the simulation for prediction of the noise

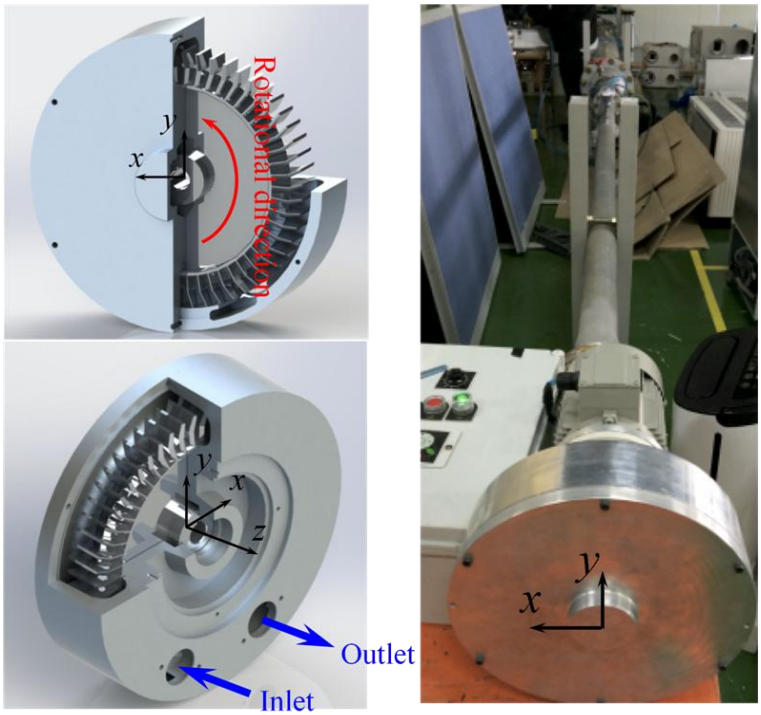

(a) Ring blower and experimental setup [51]

(b) Sound source by acoustic camera

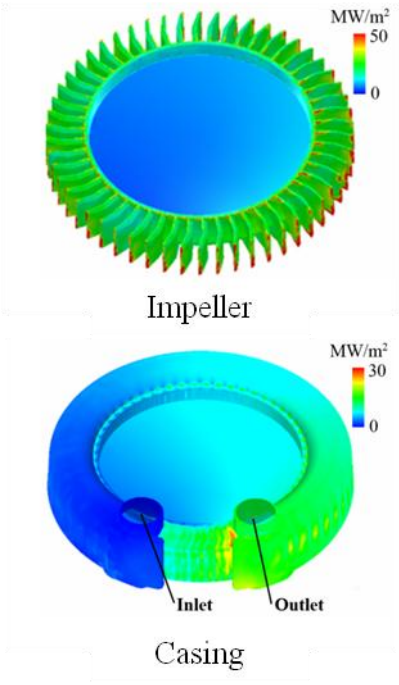

(c) Sound source by CAA [51]

Fig. 2-7 Comparison of sound sources between experiment and CAA

Chapter 3. Experimental and numerical setup

3.1 Experimental setup

The measurement of the noise generated by all three-dimensional fans used in this study was conducted in a semi-anechoic room under a condition which fan operation was not affected from the external environment. All fans were fixed by wires or mounted on the plate, in order to prevent the structure noise. The airborne noise from a fan was collected using a microphone and then was measured by a sound level meter. The signal of the noise was analyzed and converted into the components of frequency domain by using an FFT analyzer.

(a) Axial flow fan with a circular shroud

In order to obtain the characteristics of the rotating noise source, the pressure fluctuations on the strut were measure by two microphones [77]. Two small microphones were installed one by one at the surface of two struts as shown in figure 3-1. Figure 3-2 minutely shows the setup of a microphone, which is 4 *mm* in width, 6 *mm* in length and a pressure port of 1.02 *mm* in diameter. The frequency response range of the microphone is from 100 Hz to 10 kHz. The pressure port was sealed with a film to prevent that the flow from blades hits a microphone directly.

An axial flow fan (Base model) driven by AC-motor was fastened with wires to avoid structure-borne noise at a semi-anechoic room and rotated with rotational speed 2850 rpm under a condition without the influence of external environment. Figure 3-3 shows the dimensions of the axial flow fan. The diameter (D), height (H), hub's diameter (D_{hub}) and shroud's collar (L_{collar}) of an axial flow fan are 0.165 *m*, 0.035 *m*, 0.088 *m* and 0.0145 *m*, respectively. Figure 3-4 shows the experimental setup of the axial flow fan and microphone used for measuring aeroacoustic noise. And the microphone was installed to be 1.0 *m* apart from the rotation center of the rotor. Each position of a microphone for measuring the noise is shown in figure 3-5. The measuring positions were located at different longitude angle divided by 0° and 40°, but at the same height. The rotational speed in the noise measurement was at 2850 rpm and the 1st BPF was 237.5 Hz.

(b) Small axial flow fan with a square-type shroud used at a rack mount server computer

The axial flow cooling fan with square-type shroud mentioned in this study is equipped for discharging the heat generated inside a rack mount server. The reason is that the narrow space inside a server computer makes it difficult to discharge naturally the heat into the outside. Figure 3-6 shows an actual axial flow fan with square-type shroud used generally at the rear of the rack mount server and its dimensions. The dimensions of the axial flow fan are 0.076 *m* in diameter (*D*) and 0.0275 *m* in height (*H*), respectively. The axial flow fan consists of a rotor with 5 blades and a hub, and a casing with 8 struts. The casing has also a shape including partially four planes on the bell mouth, because a rack mount type fan cannot have the same clearance between a blade tip and a casing. It's caused to the shape and size of a rack mount server. Also, 8 struts connected to the casing are designed for converting the complicated flow into uniform flow.

Figure 3-7 shows the experimental setup for measuring the noise generated from an axial flow fan in a semi-anechoic room. The steel wire was used for connecting to a circular jig with each hole of the casing corner in order to fasten an axial flow fan. The microphone was placed at a upstream position 1.0 m apart from the rotation center of the fan in order to measure the fan noise. The fan noise measurement was performed under a condition which the fan rotates 7000 rpm in the free space of a semi-anechoic room. In this condition, the 1^{st} BPF was 583 Hz.

(c) Small centrifugal fan

Figure 3-8 shows the centrifugal fan shape and its dimension. In detail, the size of the fan with 17 blades in the impeller was 0.040 *m* in length (*L*), 0.040 *m* in width (*W*) and 0.003 *m* in height (*H*), respectively. Also, diameter (*D*) and thickness (*T*) of an impeller considering a hub was 0.032 *m* and 0.002 *m*, respectively. Figure 3-9 shows an experiment model including a centrifugal fan and a schematic diagram of a cross-section of a model. The lower casing of the fan was mounted on a lower plate and the upper casing having an inlet of the centrifugal fan was apart from the upper plate with a distance of 0.001 m, in order to simulate the similar flow field to an actual product. The rotational axis of the centrifugal fan was *z* axis and rotational direction was toward -*z*

direction as a right-hand screw. The impeller of centrifugal fan rotated with rotational speed of 10460 rpm for noise measurement at the free space in a semi-anechoic room. Figure 3-10 shows a microphone location measured the fan's noise installed 0.1 m apart from the rotation center. In experiment measuring the noise, the 1st BPF was 2964 Hz.

3.2 Numerical setup (CFD/CAA)

A three-dimensional flow field by the turbomachines was obtained by applying the code used to simulate the thermal-fluid flow. This code solved three-dimensional Unsteady Reynolds-averaged Navier-Stokes (URANS) equations and continuity equation simultaneously. The whole flow field in steady state analysis generated by the rotation of turbomachines was simulated roughly by SST k–ω model as the RANS turbulence model. The steady state analysis was conducted to reduce the solving time for obtaining the whole flow field. Obtaining the information for noise prediction, the unsteady state analysis was performed by using LES turbulence model which has provided the more accuracy than the URANS turbulence model in the prediction for eddy viscosity. The Sub-Grid Scale (SGS) in the LES turbulence model utilized the Smagorinsky model for predicting the eddy viscosity generated among the smaller eddies than a filter. According to recommendation in a commercial thermal-fluid solver for prediction of the flow field occurred by the turbomachines, the value of Smagorinsky constant (C_s) was 0.15 [58].

In the grid system of this study, the hybrid grid system to utilize tetrahedral, prism, pyramid and hexahedral was used. The all surfaces of the computational domain were considered as an adiabatic no-slip wall for boundary condition. The rotation effect of the rotor was simulated by using the boundary condition which was divided the rotating frame of reference containing a rotor and the stationary frame of reference except a rotor. And, the interfaces between the rotating frame and the stationary frame were considered as the surfaces of sliding mesh.

In addition, the rotor surface and the inner surface of casing in all fan of this study were imposed as the acoustic source area for analysis of aeroacoustic noise. And then, the flow properties of unsteady flow field and data for acoustic noise prediction were obtained from the unsteady state analysis after unsteadiness of the flow field grows up fully.

In this study using LES turbulence model, the simulations of all cases were conducted with double precision because the value of y^+ was not sufficiently smaller than the recommended value suggested from the previous studies.

(a) Axial flow fan with a circular shroud

For rough and quick simulation of the flow field occurring by the rotation of the axial flow fan, steady state analysis with SST k–ω model was used initially. For simulation of the unsteady flow field, LES turbulence model was selected. To develop sufficient unsteadiness, which can be generated at an axial fan with a circular shroud, the simulation of unsteady flow field was conducted continuously during 9 rotations of the rotor. The data for acoustic noise prediction were obtained from the analysis of unsteady flow field after the 9th rotation of the rotor.

Figure 3-11 shows computational domain, fan location, boundary conditions for numerical analysis, and the rotating frame including the axial flow fan, respectively. Also, the shape and size of computational domain and the fan location were similar to those of the semi-anechoic room to measure the noise. In detail, the width (w), length (l) and height (h) of the computational domain was 2.80 m, 2.35 m and 3.10 m, respectively. The location of an axial flow fan was away 1.580 m from the left wall, 0.600 m from the rear side wall and 0.695 m, from the floor of the anechoic room, respectively. For rotation effect of an axial flow fan, a sliding mesh function was used. The rotational speed of fan was 2850 rpm.

Figure 3-12 shows the computational grid system and the meshes near the surface piled up of 5 layers prism type elements. The y^+ value of the first prism element from the rotor surface except some parts of the leading edge, blade tip, and hub's edge was set as 5.5 or smaller for correct prediction of the velocity profile near the wall. The maximum value of y^+ was nearly 9.6. In detail, the size of a rotor surface mesh and the thickness of the first prism layer neighboring to the surface near the blade tip were 0.0007 m and 0.000031 m, respectively. The space except around the surface was filled up with tetrahedral and hexahedral meshes. The number of elements and nodes used in this grid system was about 17.8 million and about 6.7 million, respectively.

(b) Small axial flow fan with a square-type shroud used at a rack mount server computer

The process for numerical analysis followed the procedure mentioned in Sec. 3.1. Figure 3-13 indicates the computational domain used in this simulation and the perspective views of the axial flow fan with square-type shroud used at a rack mount server computer. The computational domain was also similar to that of the semi-anechoic room to measure the noise. The domain size was 2.0 *m* in width, length and height, respectively.

The computational grid system used in this case was shown in figure 3-14. In order to obtain $y^+ < 10$ at the first boundary layer and to predict the more accurate velocity profile near the surface, five boundary layers by prism element type were stacked up in a direction normal to the surface; and for the space excluding the boundary layers, tetrahedron, pyramid and hexahedron grids were used. The small surface meshes of 0.2 *mm* the size were located near the blade tip, the leading edge and trailing edge. The first thickness of the prism piled up normal to the surface at those regions was 0.02 *mm*. The number of elements used was about 22.0 million, and the number of nodes was about 6.3 million in this case. The rotational speed of this axial flow fan was 7000 rpm.

(c) Small centrifugal fan

The process for numerical analysis followed the procedure mentioned in Sec. 3.1. Figure 3-15 illustrates the dimensions of computational domain, the boundary conditions and the detailed centrifugal fan positioned in rotating frame used for numerical analysis, respectively. Below are the boundary conditions: (1) The pressure condition for all planes that compose the boundaries of the computational domain was imposed as the atmospheric pressure. (2) The rotational speed of the impeller was 10460 rpm.

A grid system used for this case is shown in figure 3-16. In order to obtain $y^+ < 3.6$ at the first boundary layer and to predict the more accurate velocity profile near the surface, five layers of a flat triangular prism shape were piled up in the direction normal to the surface. The tetrahedral, pyramid and hexahedral grids were filled up in the major spaces excluding boundary layers. The surface mesh size of an impeller has approximately a length of 0.0001 *m* and the first boundary layer thickness neighboring to the surface of impeller was approximately 0.000017 *m*. The number of elements and nodes used for in this case was approximately 22.9 million and 7.7 million, respectively.

3.3 Summary

Materials in this chapter were rewritten based on papers [52-54]. In experiment, the fan noise in this study was measured in a semi-anechoic room, under a condition which the external environment does not have influence on the internal environment of the semi-anechoic room during fan operation. All fans were fixed to prevent the structure noise. The fan noise was collected by a microphone and then was measured by using a sound level meter. The noise signal was analyzed and converted into the components of frequency domain by using an FFT analyzer.

In order to simulate the thermal-fluid flow, the code solved three-dimensional Unsteady Reynolds-averaged Navier-Stokes (URANS) equations and continuity equation simultaneously. After fully developing the unsteadiness, the unsteady state analysis using LES turbulence model was conducted in order to obtain the information for noise prediction. And then, the flow properties of unsteady flow field and the data for acoustic noise prediction were obtained from the unsteady state analysis after developing full unsteadiness of the unsteady flow field.

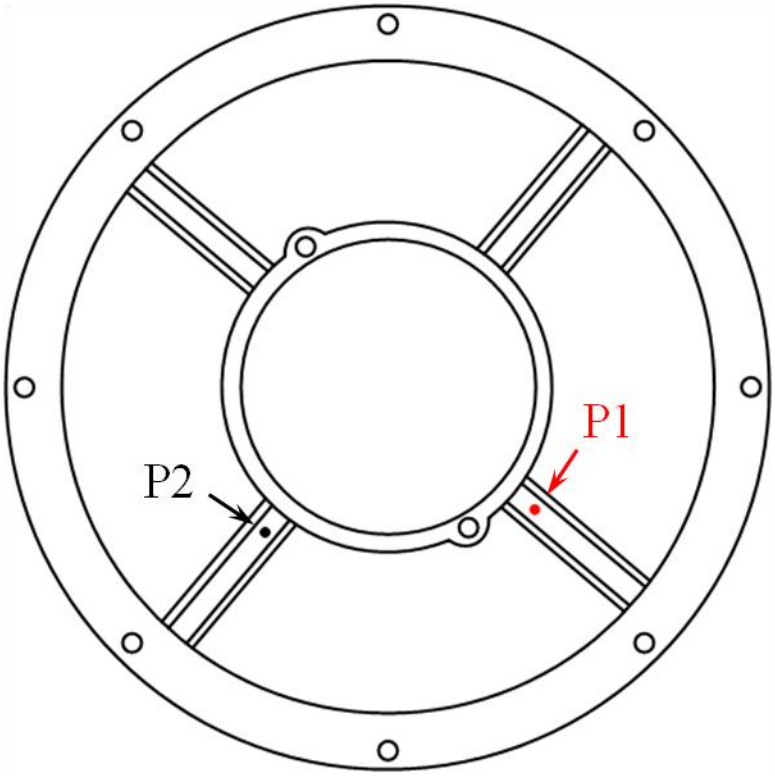

Fig. 3-1 Measuring points for pressure fluctuations

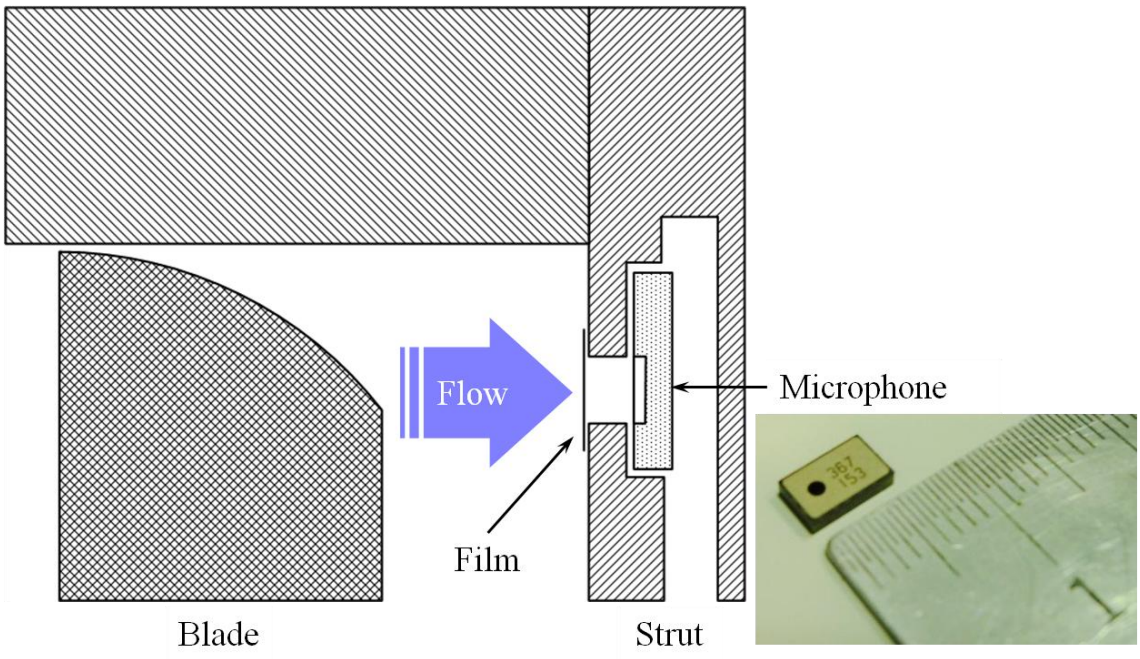

Fig. 3-2 Schematic diagram of a microphone setup

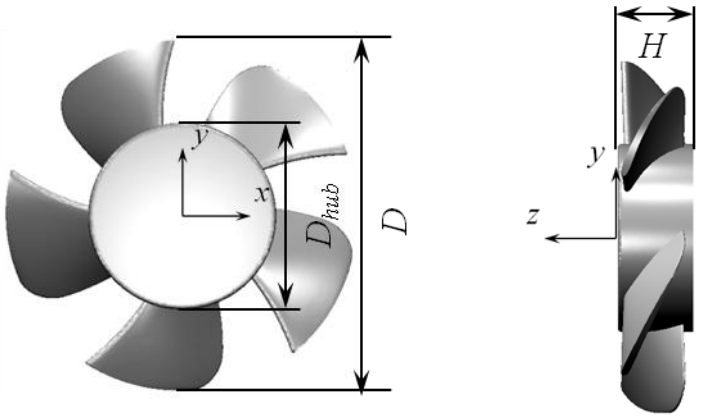

(a) Dimension and shape of rotor

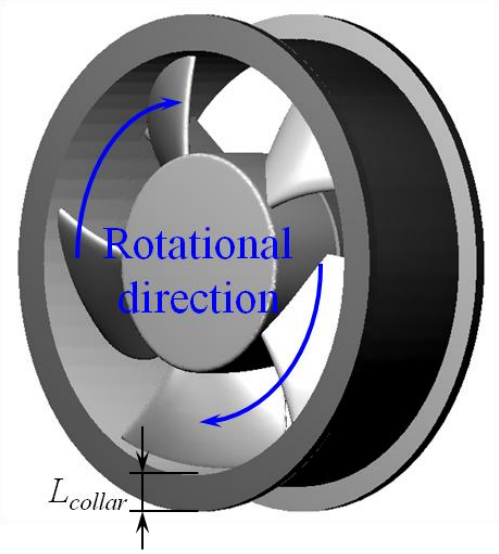

(b) Perspective view of axial flow fan with circular shroud

Fig. 3-3 Main dimensions of the axial flow fan

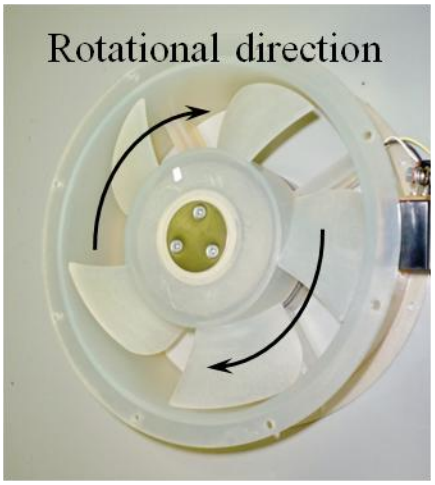

(a) Axial flow fan used in experiment

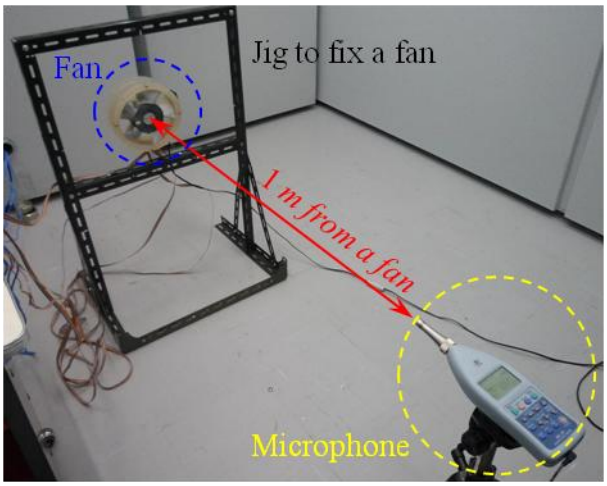

(b) Experimental setup to measure noise in a semi-anechoic room

Fig. 3-4 Experimental setup for noise measurement

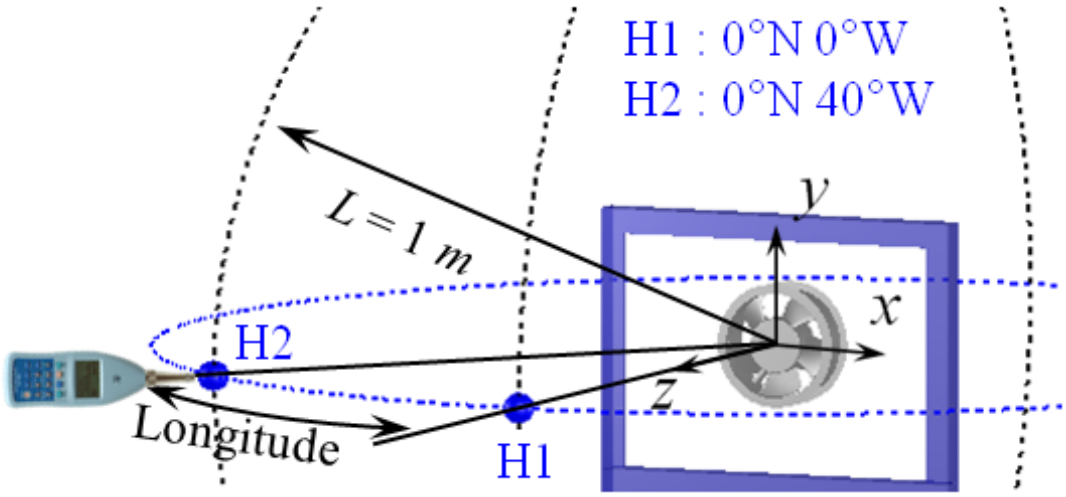

Fig. 3-5 Location of the microphone for noise measurement

(a) Axial flow fan with rectangular shroud used at a rack mount server computer

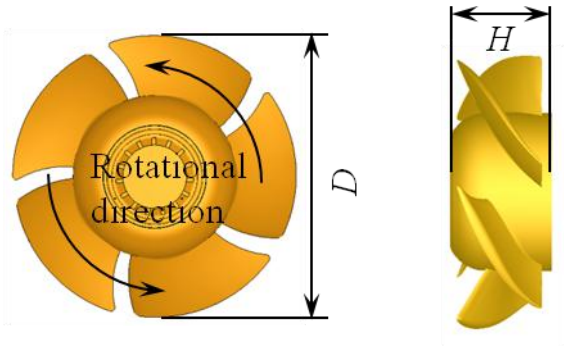

(b) Dimension of rotor

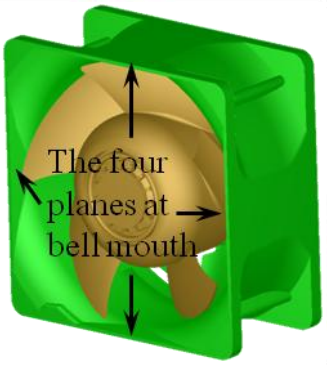

(c) Perspective view of axial flow fan with rectangular shroud for CFD

Fig. 3-6 Perspective view of fan and its shape

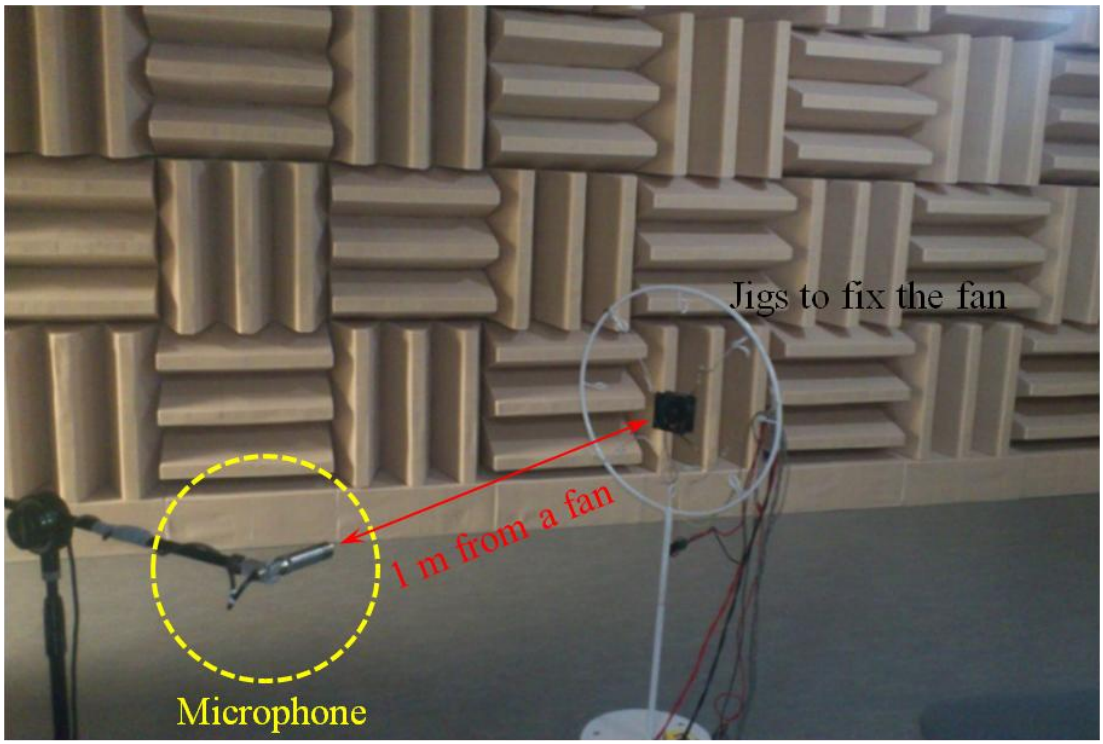

Fig. 3-7 Photo of experimental set-up to measure the noise

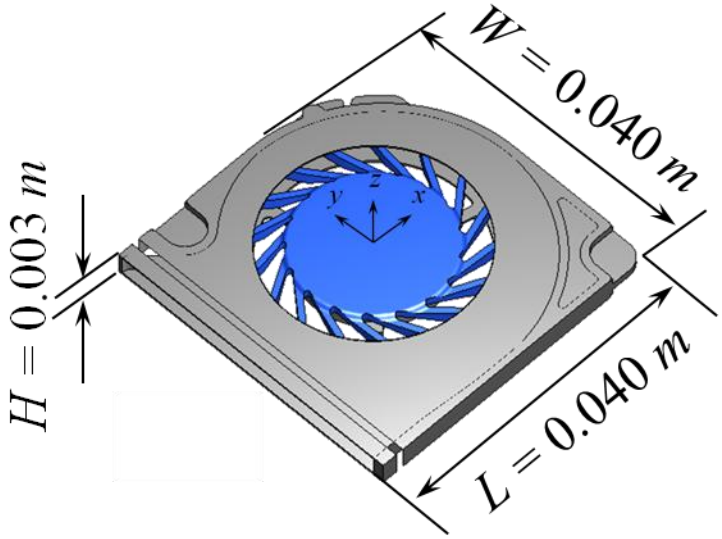

(a) Dimension of casing

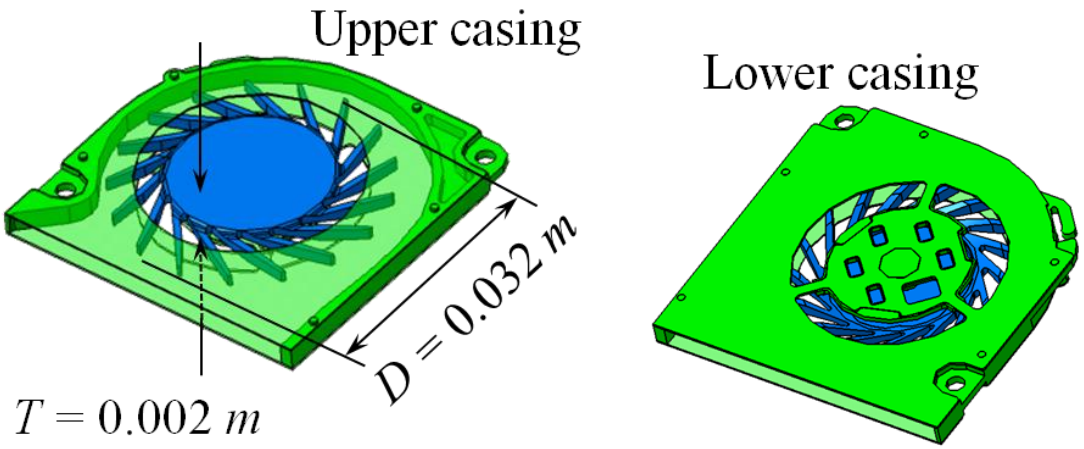

(b) CAD shape of a centrifugal fan and dimension of impeller

Fig. 3-8 Main dimensions and shape of a small centrifugal fan

(a) Outside view

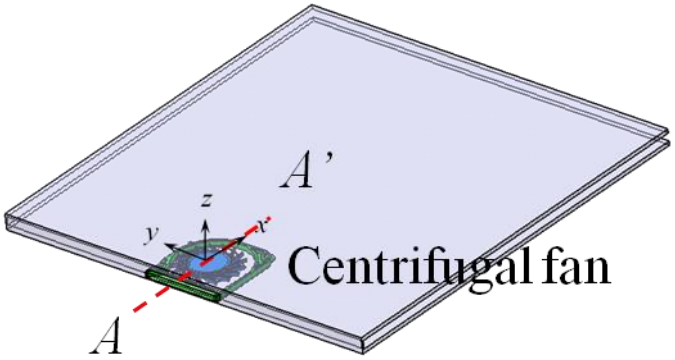

(b) CAD model

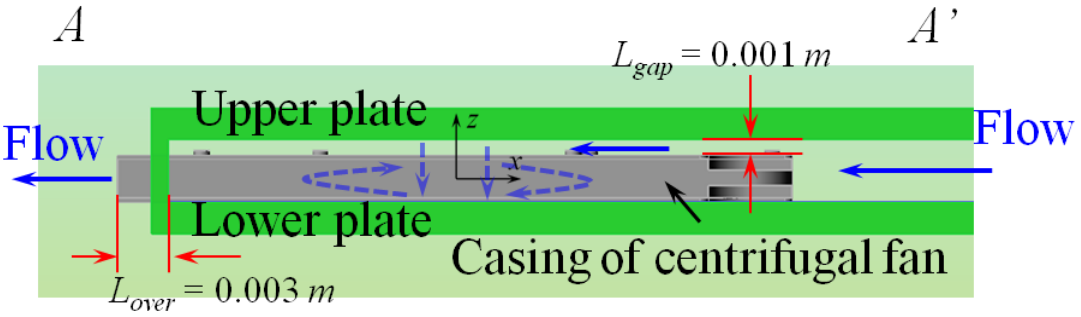

(c) Cross sectional view of flow channel

Fig. 3-9 Experimental setup and schematic diagram of flow channel and a small centrifugal fan

Fig. 3-10 Microphone location for noise measurement

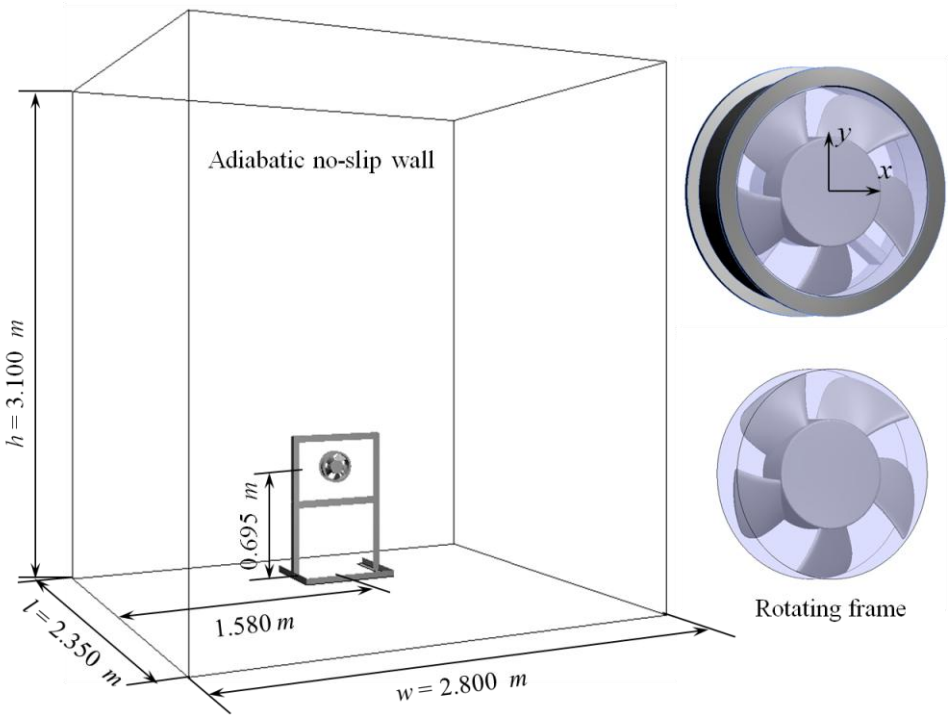

Fig. 3-11 Detailed description of computational domain, boundary conditions and rotating frame

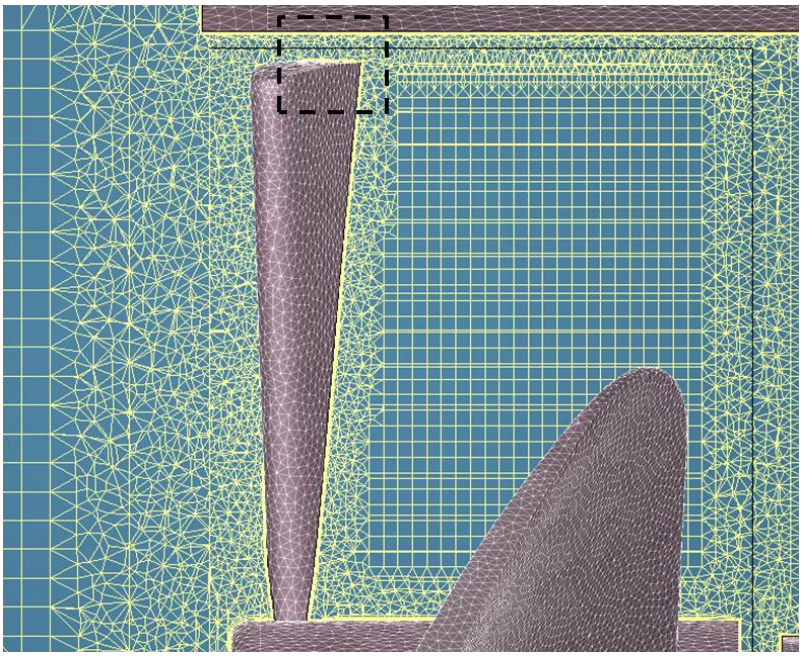

(a) Axial flow fan

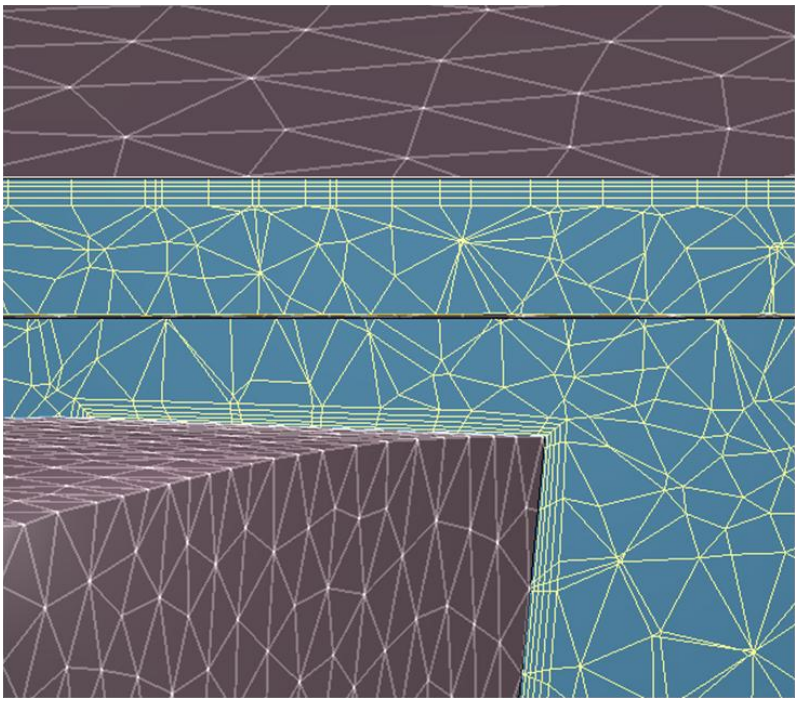

(b) Near blade tip

Fig. 3-12 Computational grids

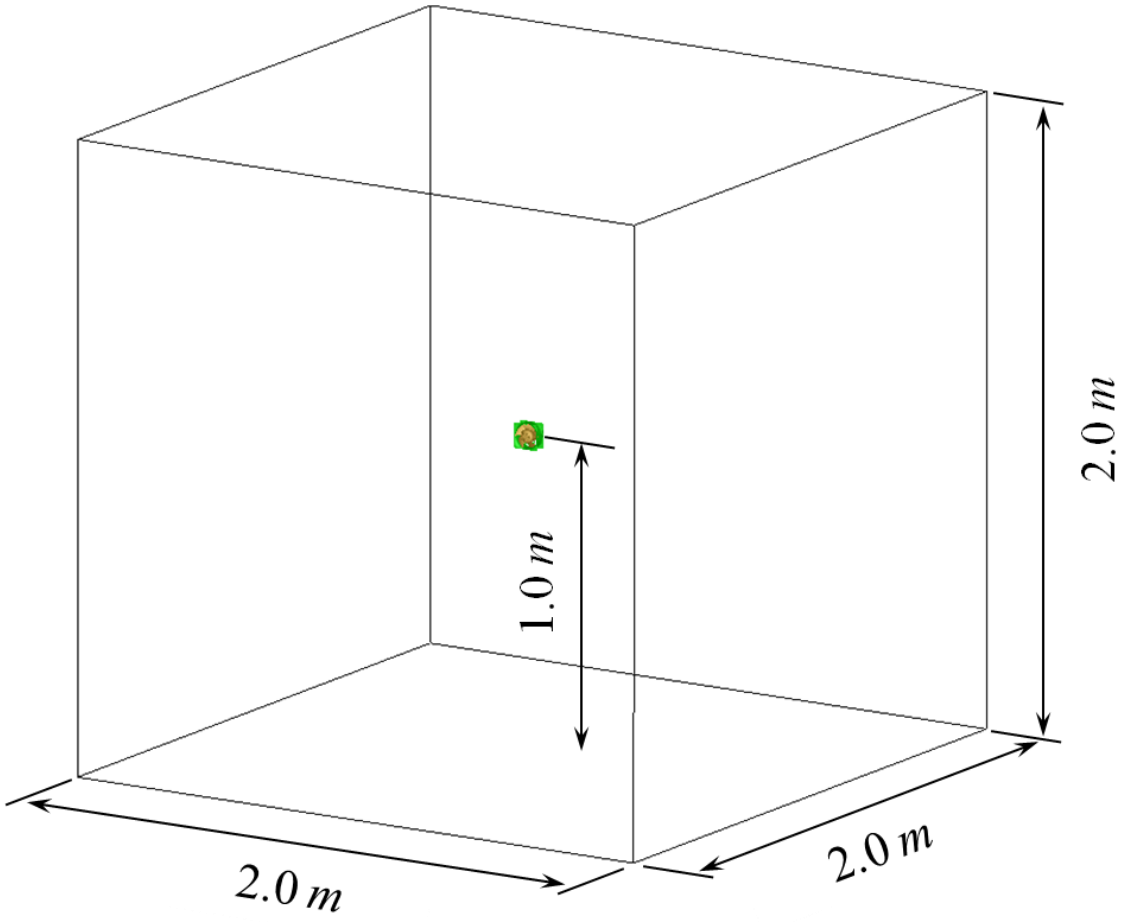

(a) Computational domain

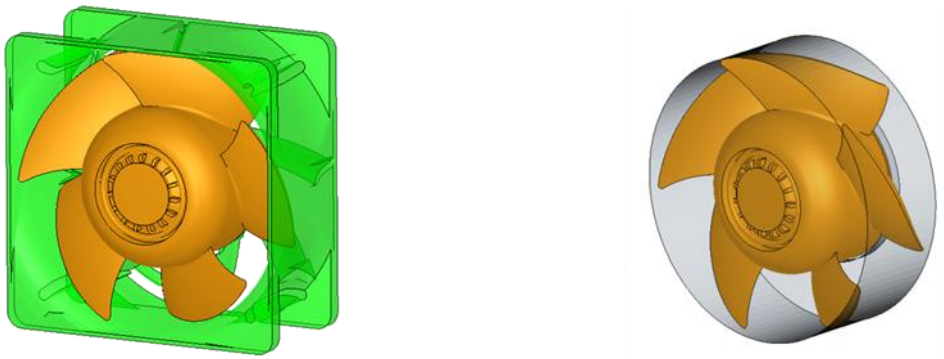

(b) Rotating frame at an axial flow fan

Fig. 3-13 Computational domain and detail view of rotating frame

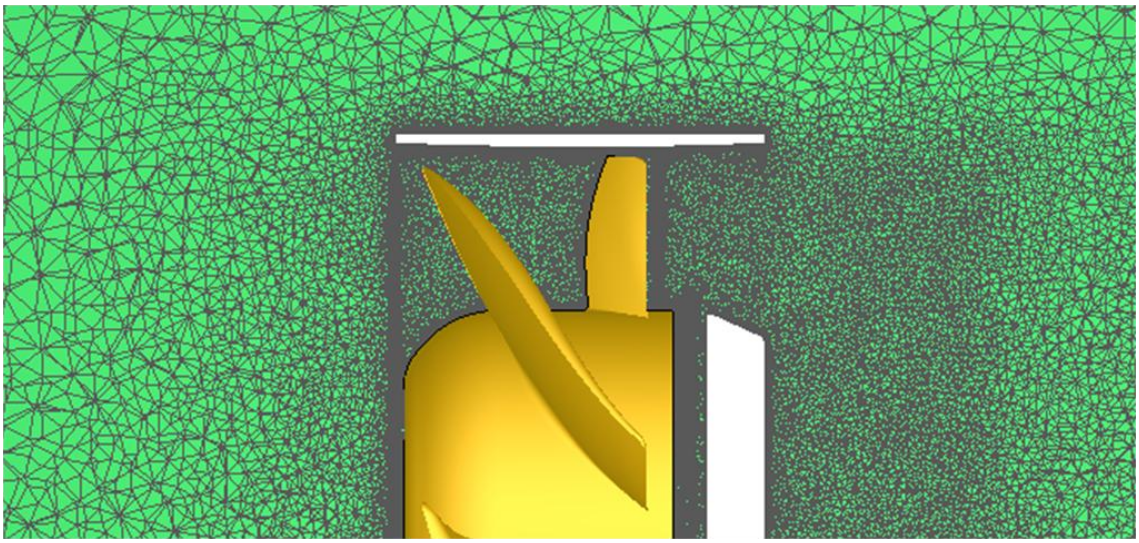

(a) Fan and casing

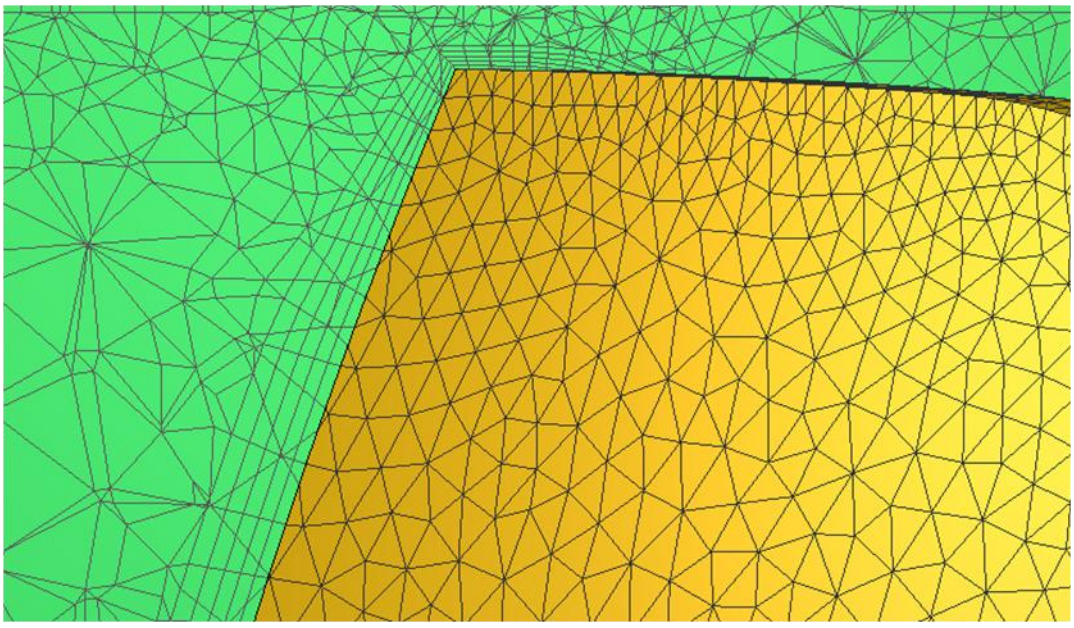

(b) Near a blade tip

Fig. 3-14 Computational grids used to simulate the flow field

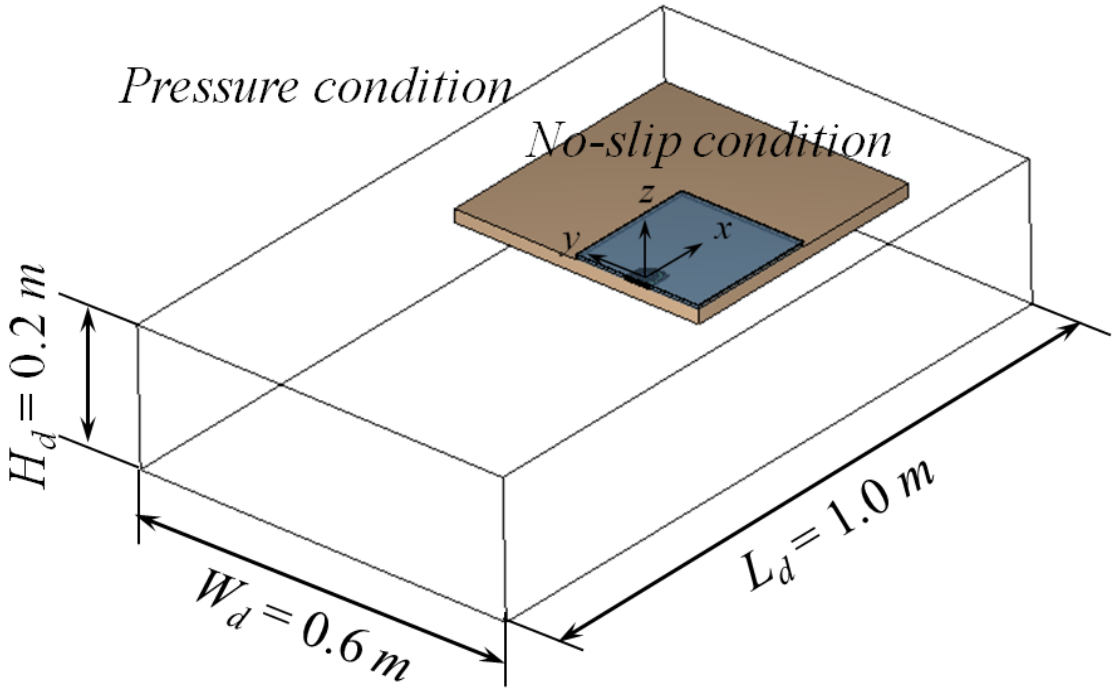

(a) Computational domain and boundary conditions

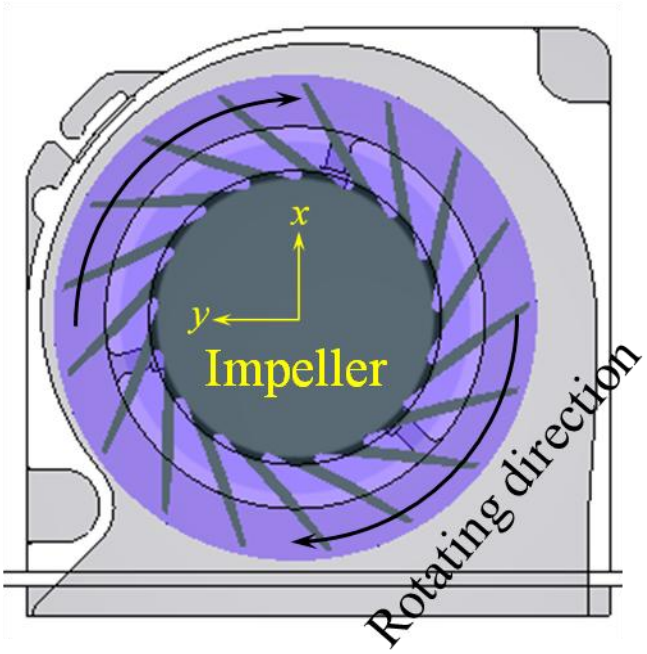

(b) Rotating frame in the fan

Fig. 3-15 Computational domain, boundary conditions and rotating frame in detail

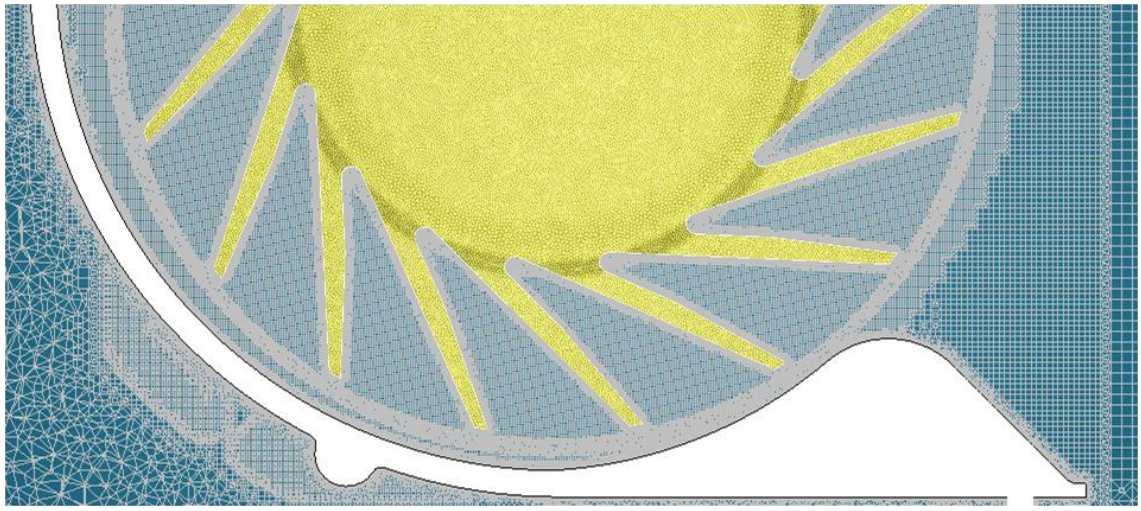

(a) Centrifugal fan and casing

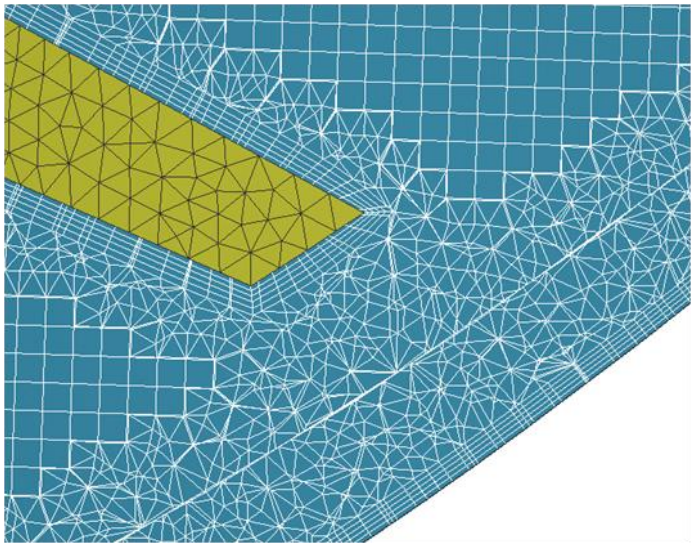

(b) Near blade tip

Fig. 3-16 Computational grids for simulation of a centrifugal fan

Chapter 4. Prediction of the flow-induced noise and noise reduction

4.1 Introduction

Cooling modules installed in automobile, electrical devices, and construction machinery heat up and need to be cooled down. For this, axial flow fans are commonly used. In order to enhance the cooling performance, an increase in the flow rate is essential because an axial flow fan supplies only low increase in pressure. High speed rotation is required for flow rate rise; and aerodynamic noise is produced. Such aerodynamic noise is the chief problem. Therefore, a fan with improved performance and reduced aeroacoustic noise was pursued; and experimental and numerical researches have been performed to develop the fan [78-82].

4.2 Characteristics of the unsteady flow field at an axial flow fan

Pressure oscillation in unsteady flow field must be calculated in order to analyze the aeroacoustic noise. Since it takes long time to obtain the fully developed unsteady flow field, the result obtained from the steady state analysis was entered for unsteady flow analysis to save time required for the calculation. Despite of the fact that the characteristics of static wall pressure oscillation produced by the unsteady flow field were found after rotating the rotor twice, the first unsteady state analysis was continued until the eighth rotation in order to fully develop the unsteadiness by keeping the time step of 29.2398 μsec per iteration. The static pressure oscillation in the second unsteady state analysis was obtained while rotating the rotor five more times. For accurate FFT analysis requires the number of 2 to the exponent of n is required for sampling data, the time step per iteration was modified to 25.6990 μsec in the second step. Each sub-iteration was done to get the accurate solution as well, the value 0.000001 was given for the residual for each velocity component and the value 0.00001 were given for the residual for pressure as the convergence condition for all iterations; then, proceeding to the next iteration was allowed after convergence.

The oscillation of static pressure at two points on the strut surface (Base model) is shown in figure 4-1. The fully developed unsteadiness in the flow field was found during 5 rotations after the ninth rotation of the rotor because of the repetitive

distributions of static pressure presenting similar amplitude at two points. On each strut of the shroud, continuous change in the static pressure fluctuation was found with the rotation. In particular, sudden increase of the static pressure oscillation due to the interaction between the strut and PS of the blade was found as the blade passed through the point on each strut.

4.3 Prediction of the flow-induced noise and validation

Figure 4-2 is showing the axial flow fan's sound spectra obtained by the numerical analysis and the experimental measurement on Base model. By solving the Ffowcs Williams and Hawkings equation, the aeroacoustic pressure was calculated. The total noise level was measured at each point by using a microphone that was 1 *m* away from the axial flow fan. Up to 1300 Hz, the sound spectrum of tonal/broadband noise was consistent between the measurement and the prediction by the numerical analysis; however, discrepancy was found in the broadband noise at higher frequency over 1300 Hz. Random broadband noise is known commonly due to numerous phenomena such as turbulent boundary layer, flow separation, vortex shedding, and tip vortex. However, the influence of the scattering of the turbulent boundary layer shed from the trailing edge of each blade was ignored in this study. Consequently, such discrepancy at higher frequency occurred since only the dipole was considered. The measured and predicted OASPL (overall sound pressure level) at H2 was 57.2 dB(A) and 60.1 dB(A), respectively. The tonal noise predicted by the numerical analysis was higher than the tonal noise measured in the experiment; hence, OASPL was presented.

Aeroacoustic source strength (A_{st}) distributed in the axial flow fan is shown in figure 4-3. Major noise sources in rotating rotor were found from the leading edge tip "*a*", the blade tip "*b*", and the blade surface "*c*". Major noise sources in the shroud were presented from the region "*d*" of each strut, the region "*e*" near each strut, and the region "*f*" adjacent to rotation path of the leading edge tip.

Figure 4-4 is showing the static pressure on the blade's surface and pressure distribution upon radial direction (r/R) in the rotating axis at t = 0.288647 sec. In figure 4-4(a), pressure change caused by the impingement between the flow and the leading edge tip is seen in the leading edge tip "*Region A*" of the blade. This is concerned with the noise source "*a*" presented in figure 4-3. In figure 4-4(b), change in pressure

difference between the PS and the SS depending on x/C_x is not big within the radius of $r/R \leq 0.90361$. On the other hand, vigorous change was observed in the pressure difference between the two surfaces depending on the radius x/C_x of $r/R \geq 0.96386$. In particular, a huge difference in static pressure between "1" at the SS and "2" at the PS was found in the range of $x/C_x = 0.2 \sim 0.4$ when the radius $r/R = 0.96386$; and this is predicted to be the source where the tip leakage vortex is produced. Subsequently, static pressure oscillation in "*Region B*" of the SS was influenced by the tip leakage vortex developing toward downstream direction and this is concerned with the noise source "*b*" presented in figure 4-3. Both the interaction between the strut and the blade and the tip leakage vortex that was produced by the preceding blade impinge against the PS surface of the approaching blade; thus, complicated distribution of static wall pressure along the rotating portion of the blade was found in "*Region C*" of the PS. This is associated with the noise source "*c*" shown in figure 4-3.

The vorticity on the iso-surface with the helicity of -0.95 depending on time change is illustrated in figure 4-5(a). The helicity was applied to describe the tip leakage vortex produced by the pressure difference between the PS and the SS of the blade. Figure 4-5(b) is presenting the static pressure distribution and streamlines on the cross-section *A-A′*. The helicity is defined as follows.

$$H_n = \frac{\vec{\omega}\cdot\vec{u}_{rel}}{|\vec{\omega}||\vec{u}_{rel}|} = \frac{\omega_i\cdot u_i+\omega_j\cdot u_j+\omega_k\cdot u_k}{\sqrt{\omega_i^2+\omega_j^2+\omega_k^2}\sqrt{u_i^2+u_j^2+u_k^2}} \tag{4-1}$$

Because of the interaction between the rotor rotating in *z*-axis and the flow, the fluid flowed downstream by the PS with time. In addition, the fluid in the upstream of the axial flow fan flowed into the SS. Here, the flow could not flow along the surface of the shroud wall because of the shroud inlet shape of the square-edged cross-section; thus, the separation of the flow occurred, and the separated flow produced vortex "*B*" shown in figure 4-5(a). The tip leakage vortex "*C*" was produced as described in figure 4-4(b). Figure 4-5(b) is showing the distribution of static pressure and streamlines by time on cross-section *A-A′*. Occurrence, movement, and dissipation of the vortices occurring due to tip leakage flow and the inlet shape of shroud depending on time were confirmed.

In figure 4-5(b), "*Related B*" that is the flow structure of the vortex is disappeared upon the impingement with the leading edge tip. By the impingement, a complicated flow field upon time was induced; this can be understood as caused by the rise in the stagnation pressure at the leading edge tip of the blade and the pressure that is relatively low and caused by the separated flow from the inlet. The tip leakage vortex caused by the preceding blade was in the downstream of the PS when t = 0.288133 sec. In addition, the impingement with the approaching blade's PS resulted in the dissipation of the structure of the tip leakage vortex, which was produced by the preceding blade; and this produces "*D*" that is the complicated static pressure distribution when t = 0.289161 sec Consequently, the tip leakage vortex was formed in the anterior region of the chord, where x/C_x = 0.2 ~ 0.4, because of the static pressure distribution, which is increased by the interaction between the approaching blade and the vortex occurred previously.

Based on the noise source location of the Base model, flow structure and flow field were investigated. It was determined that reduction of the vortex that was separated from the square edge by changing the shape of the shroud was more efficient in lowering the noise compared to changing the blade shape. Therefore, the fan performance and the flow noise reduction were to be predicted after changing the shape of the shroud inlet.

4.4 Noise reduction by changing the shape of shroud

In figure 4-6, the models with the shroud in modified shape for reduction of fan noise reduction are shown. While the Base model had a perpendicular shape of the shroud's cross-section, that in Case 1 was rounded shape with the curvature in length of L_{collar}. The same radius of curvature as Case 1 but half-length of arc was presented by that in Case 2; and Case 3 had semi-circle shape with the length of the diameter as L_{collar}.

Figure 4-7 is showing the predicted sound pressure spectra that represents the effect of the modification of the shroud inlet for noise reduction. Similar trend was observed in the noise spectrum of each model. No big difference was observed in tonal noises of BPF and its harmonic frequencies; on the other hand, the broadband noise of all models with modified shroud inlet shape was predicted to be lower than the Base model. The OASPL predicted for each of Base model, Case 1, Case 2, and Case 3 at noise measurement point H2 that is the noise measuring location was 60.1, 57.6, 58.5, and

57.4 dB(A), respectively.

Table 4-1 Specific noise level at axial flow fans

	OASPL	Q/Q_{Base}	$\Delta p_t/\Delta p_{t,Base}$	K_{sa}
Base, *Ref.*	60.1	1.0000	1.0000	60.1
Case 1	57.6	1.0667	1.1222	56.4
Case 2	58.5	1.0434	1.0607	57.8
Case 3	57.4	1.0512	1.0814	56.5

In figure 4-8, the distribution of static pressure on the cross-section with r/R = 0.78313 ~ 1.02400 and 10° interval and the distribution of vorticity on the cross-section of yz plane at x = 0 are described. When looking at the distribution of vorticity within the black rectangle in figure 4-8(a), interaction between the vortex that is separated from the inlet of each shroud and the blade's leading edge tip causes difference in downstream flow field. Among the models other than Base model, the high OASPL in Case 2 was due to the complicated pressure distribution that was caused by the structure of the tip leakage vortices (β2) that were disrupted by the preceding blade as described in figure 4-8(b). Such phenomenon is well-known as the vortex blade interaction (VBI) between the tip leakage vortex and the following blade. In Case 1, the tip leakage vortices (β1 and β2) lasted in the flow field relatively longer in Case 1. This can be explained by that the large pressure difference (α region) between the SS and PS of the blade produced a strong tip leakage vortex (β3) in the blade tip. In contrast, the tip leakage vortex of Case 1 occurs slowly and relatively in the posterior region of the tip blade compared to that of the other models.

Meanwhile, the modification of shroud shape causes changes in the flow field of the low noise model. Compared to Base model, the flow rate was increased by 6.77%, 4.34%, and 5.12%, respectively. Increase in total pressure rise was found by 12.22%, 6.07%, and 8.14%, respectively; and the fan efficiency ($\eta = \Delta pQ/\omega T$) was enhanced by 4.38%, 2.71 %, and 3.16%, respectively. Hence, noise reduction due to the shape of the shroud was compared by calculating specific noise level equation. This equation is used for prediction of the change in flow noise depending on the change in fan performance. Specific noise level equation is defined as follows.

$$K_{sa} = SPL - 10log\left(\frac{Q}{Q_{Base}}\left(\frac{\Delta p_t}{\Delta p_{t,Base}}\right)^2\right) \quad (4\text{-}2)$$

According to equation (4-2), specific noise level was predicted to be 56.4 dB(A) for Case 1, 57.8 dB(A) for Case 2, and 56.5 dB(A) Case 3 (Table 4-1). For low noise models, OASPL were obtained by using specific noise level and were predicted to be lower than 60.1 dB(A), which is the OASPL of Base model. This indicated the reduced broadband noise due to stabilized flow field in the inlet; thus, the modification of the shape of the shroud inlet is confirmed to be the factor for noise reduction.

Figure 4-9 is presenting the noise source location of the low noise models. In the low noise models, the main noise sources (*a* ~ *f*) that were presented in Base model shown in figure 4-3 were disappeared or weakened. The noise source was decreased the most in Case 1 that showed the most stable inlet flow; but strong noise source was found in the blade tip. Case 2 presented the noise source that is similar to what observed in Base model; however, the strong noise source in the blade tip was reduced. In Case 3, the noise was reduced the most as the strength of the noise source got weakened. Thus, the modification of shroud inlet was verified to be a major factor influencing on noise reduction.

4.5 Summary

Materials in this chapter were rewritten based on the paper [54]. In this study, the characteristics of the aeroacoustic noise and the reduction of such noise in a small axial flow cooling fan were predicted by using unsteady three-dimensional flow analysis and the Ffowcs Williams and Hawkings equation. LES model was applied for further accuracy in prediction of the unsteady flow field in axial flow fan. In addition, the static wall pressure distribution over time, which was the input data of CAA, was obtained after fully developing the unsteadiness of the unsteady flow. The predicted noise spectrum was compared with the experimental value. This study was conducted in following sequence: identification of the noise sources by analyzing aeroacoustic noise, analysis of unsteady flow that causes noise sources, and noise reduction simulation with the construction of low noise models. Here are the results of this study.

(1) The noise spectrum predicted by numerical analysis was compared with that

measured by the microphone. The tonal noise in BPF and its harmonic frequencies, and the broadband noise presented the spectrum that was considerably consistent with the experimental value at less than 1300 Hz. On the other hand, discrepancy was presented at more than 1300 Hz. The reason of this was the neglected effect of the irregular broadband noise including turbulent boundary layer, vortex shedding, flow separation, and tip leakage vortex while considering the dipole only.

(2) The noise sources from Base model were showed at the blade's leading edge tip, blade surface, region neighboring each strut, and region of the inner shroud that is close to the rotation trajectory of the blade's leading edge tip. By unveiling the noise source location, the unsteady flow field produced by the interaction between the vortex and the blade was verified.

(3) By confirming the unsteady flow, the control of the vortex that is separated on the perpendicular cross-section of the shroud was revealed to be the efficient solution for acoustic noise reduction. Therefore, noise was reduced by modifying the inlet shape of the shroud of low noise models in order to produce stable inflow.

(4) The performance of the low noise models was also improved by the stable inflow; thus, noise reduction was reviewed by using specific noise level. Compared to OASPL of Base model, reduction of the noise approximately by 3.7 dB was resulted in the low noise models. In conclusion, the shroud shape modification was verified to be one of the major factors for noise reduction in axial flow fan.

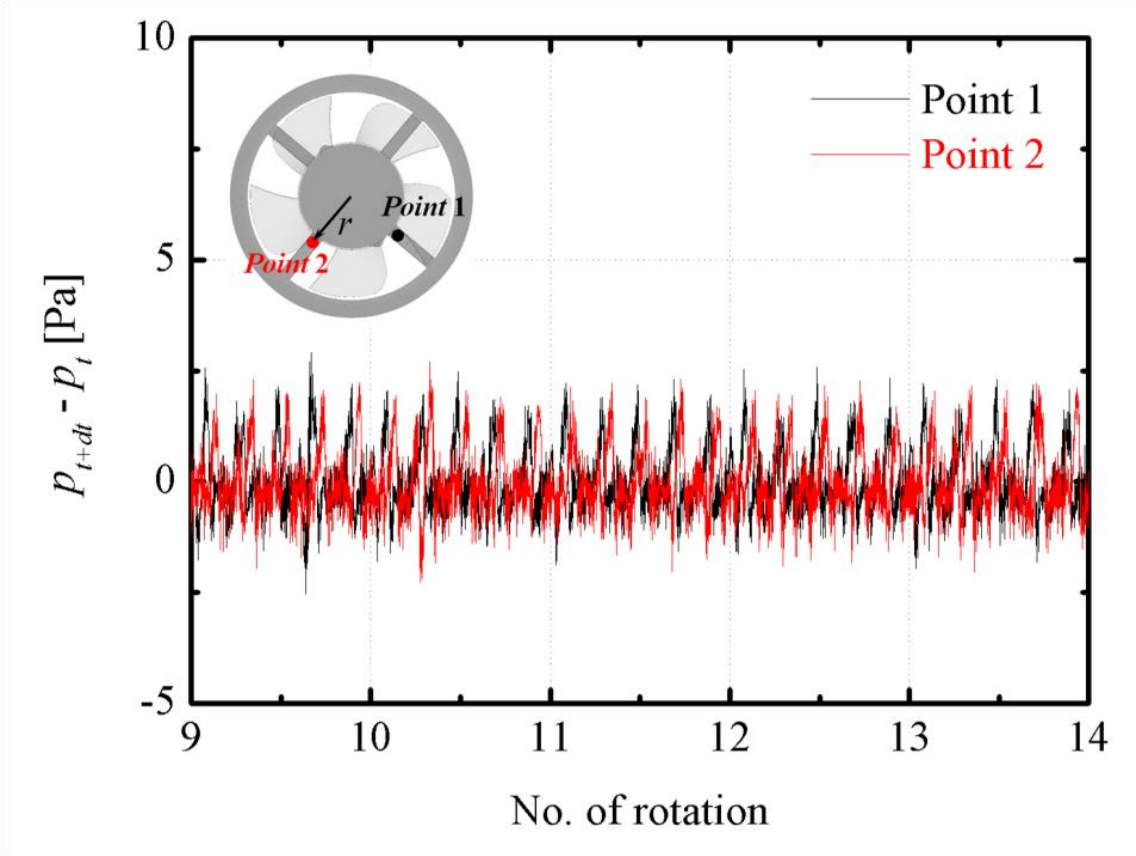

Fig. 4-1 Fluctuation of static wall pressure on the strut of the shroud

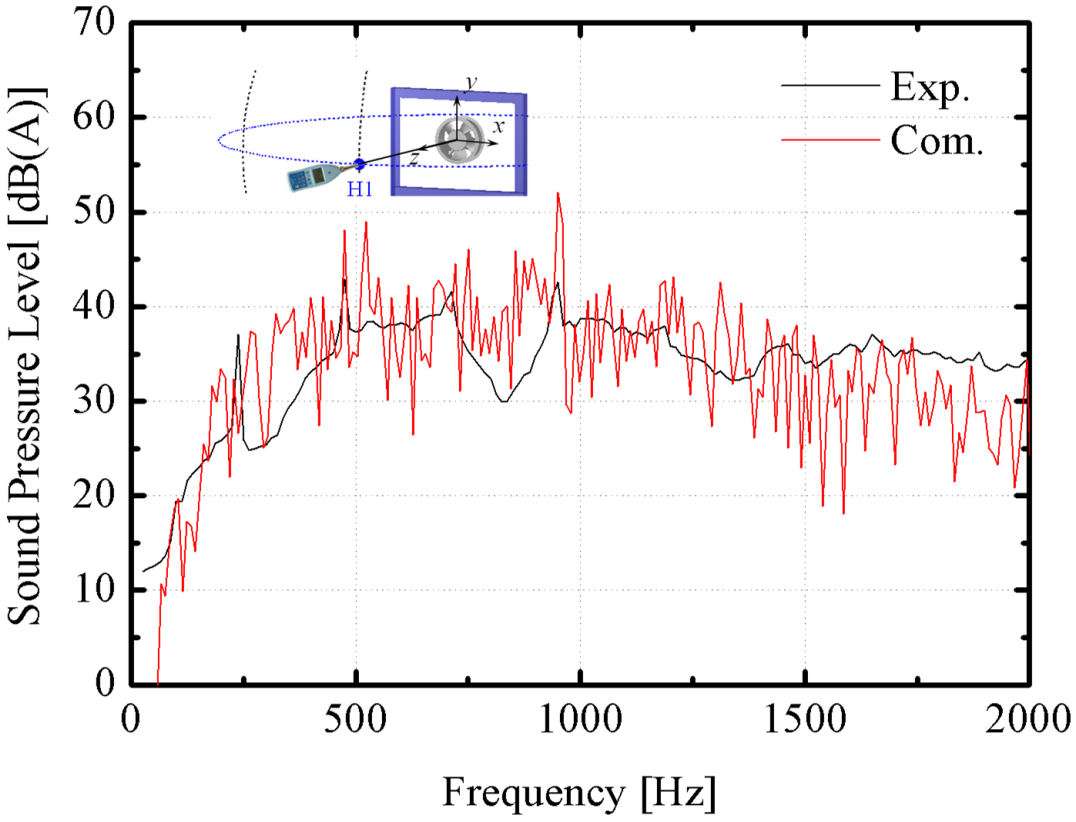

(a) At H1

Fig. 4-2 Comparison of aeroacoustic sound spectra obtained by the numerical simulation and the experimental measurement (continue)

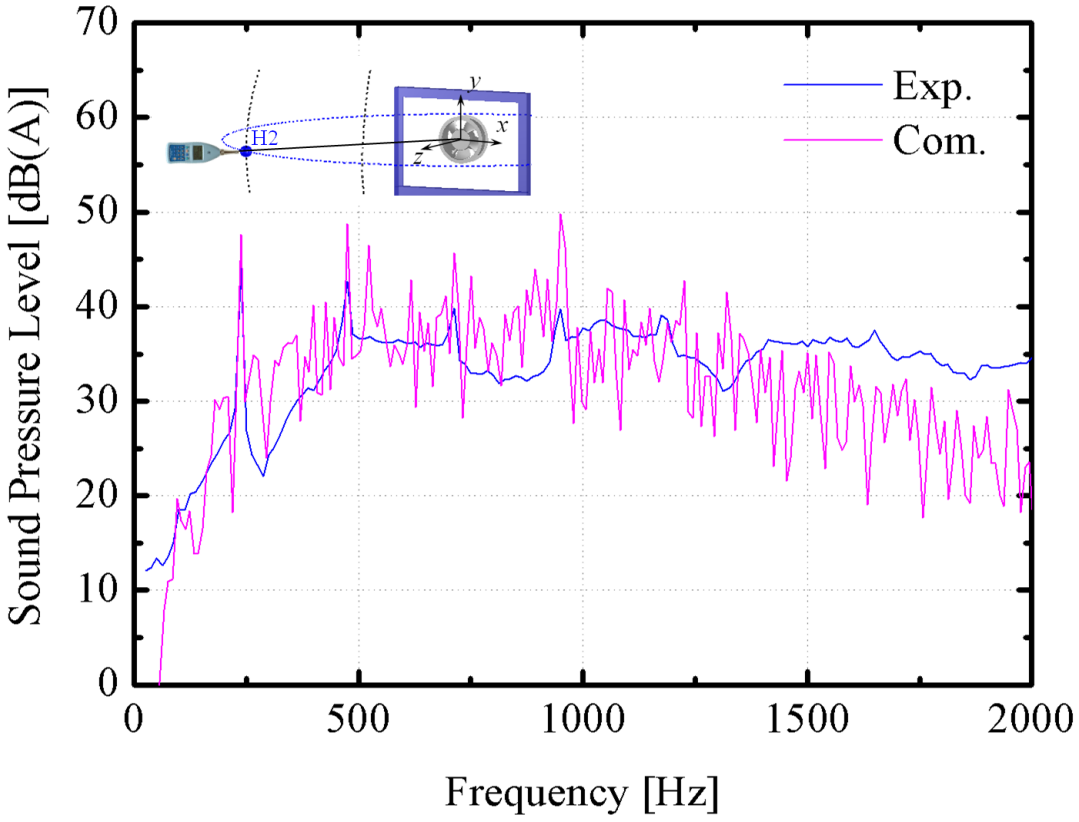

(b) At H2

Fig. 4-2 Comparison of aeroacoustic sound spectra obtained by the numerical simulation and the experimental measurement (continue)

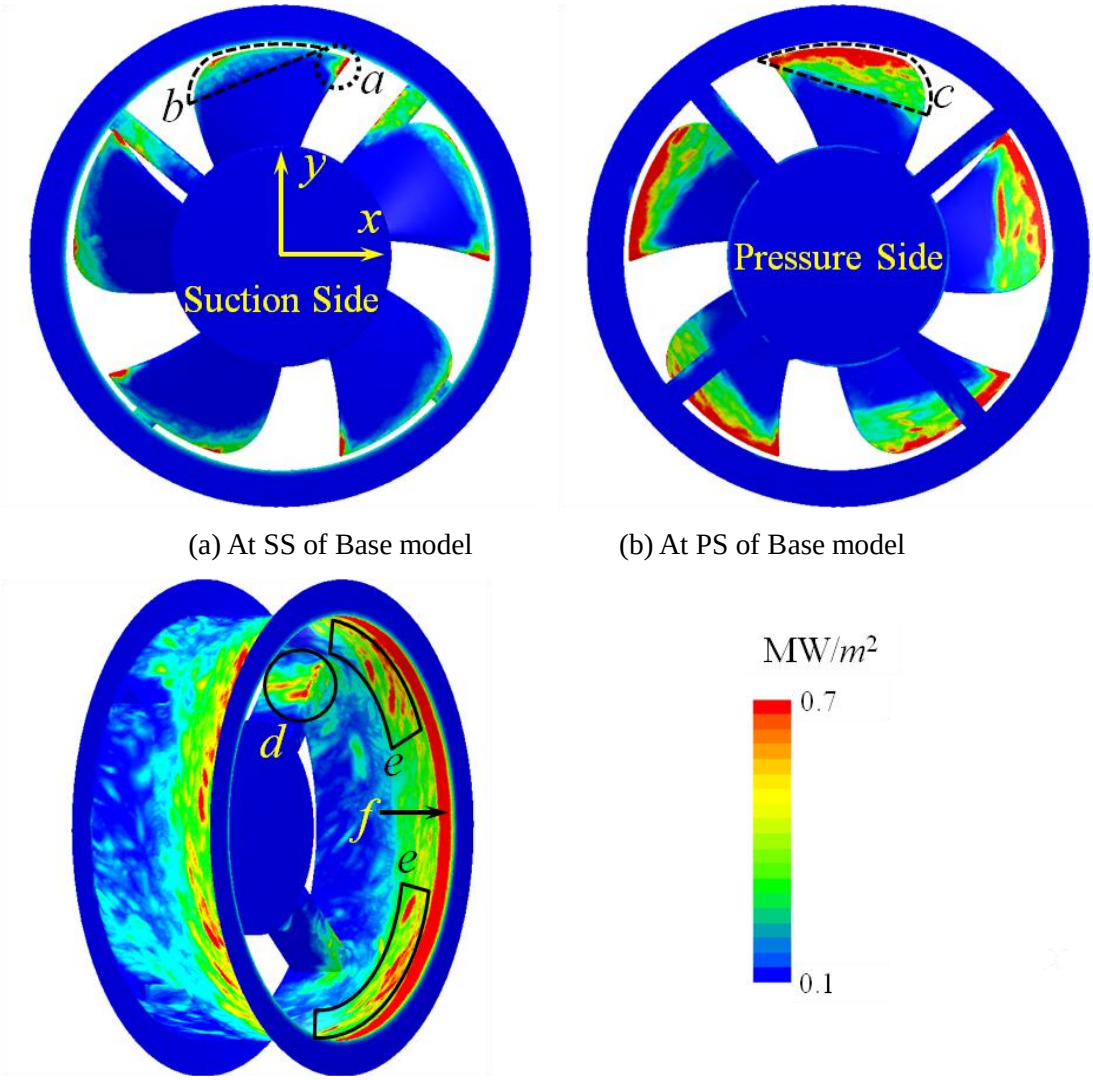

(a) At SS of Base model (b) At PS of Base model

(c) At perspective view of shroud

Fig. 4-3 Distribution of the aeroacoustic source strength in Base model

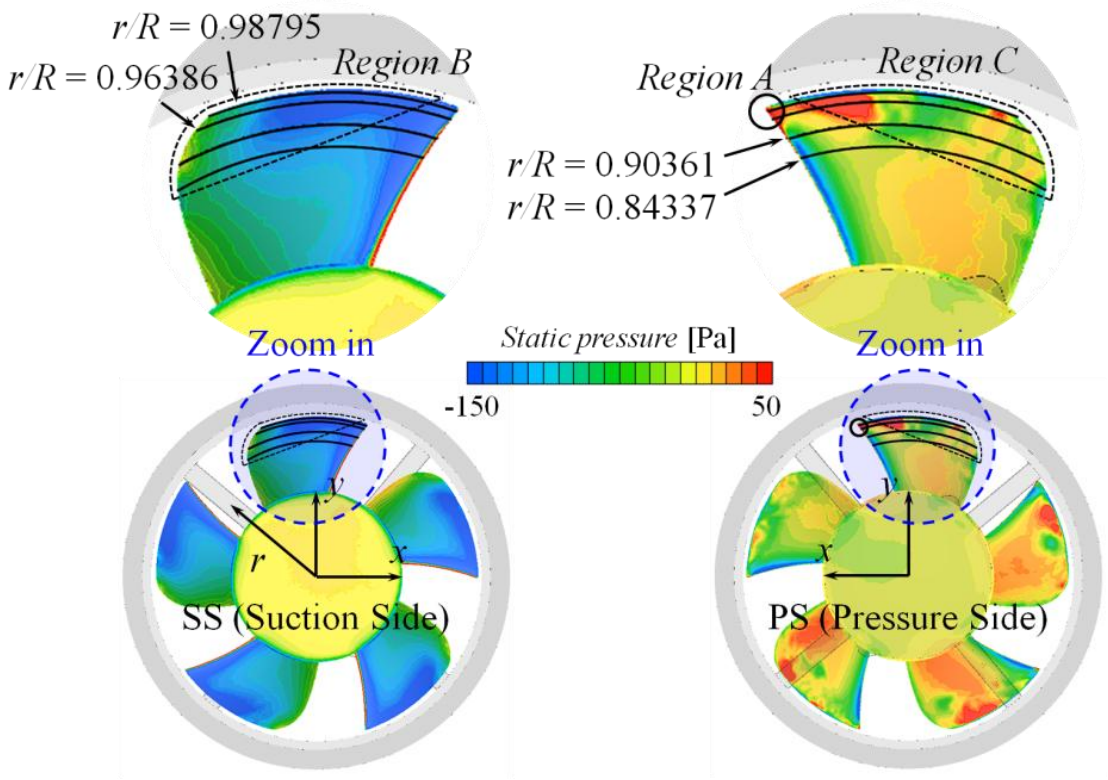

(a) Static wall pressure contours on the rotor

Fig. 4-4 Distribution of the static wall pressure on the rotor of Base model (continue)

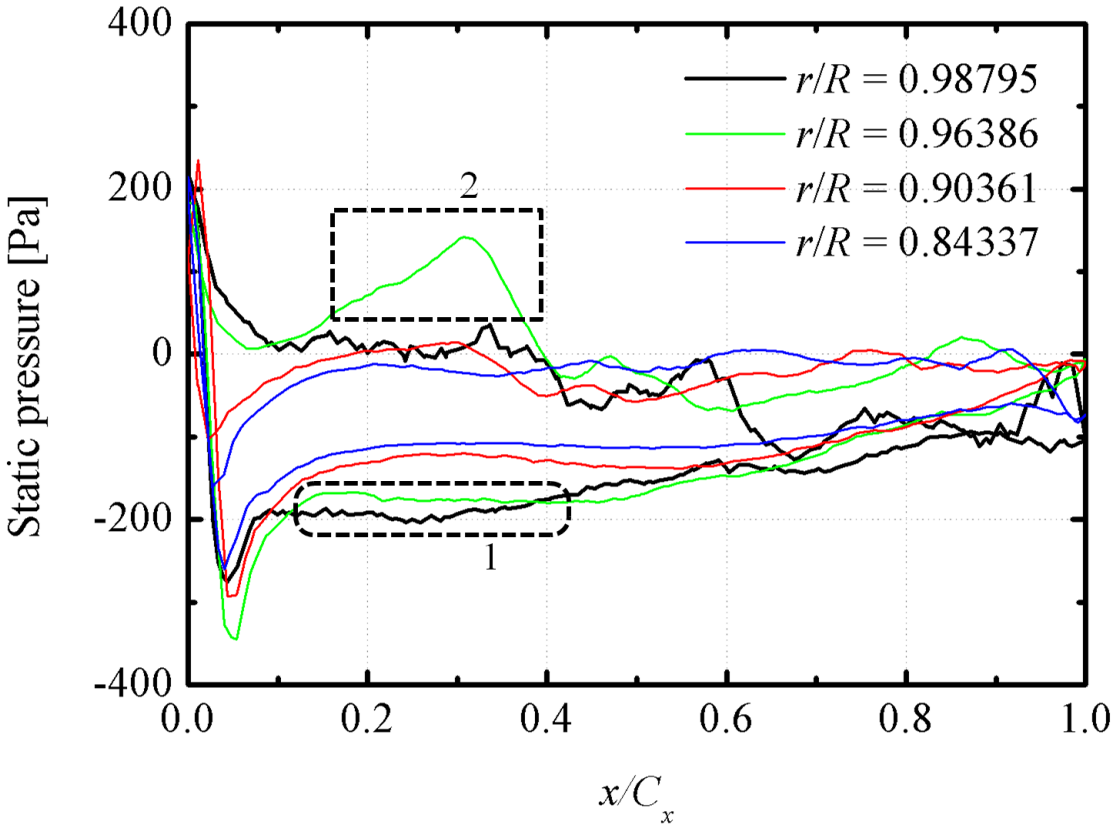

(b) Distribution of the static wall pressure depending on *r*/*R*

Fig. 4-4 Distribution of the static wall pressure on the rotor of Base model (continue)

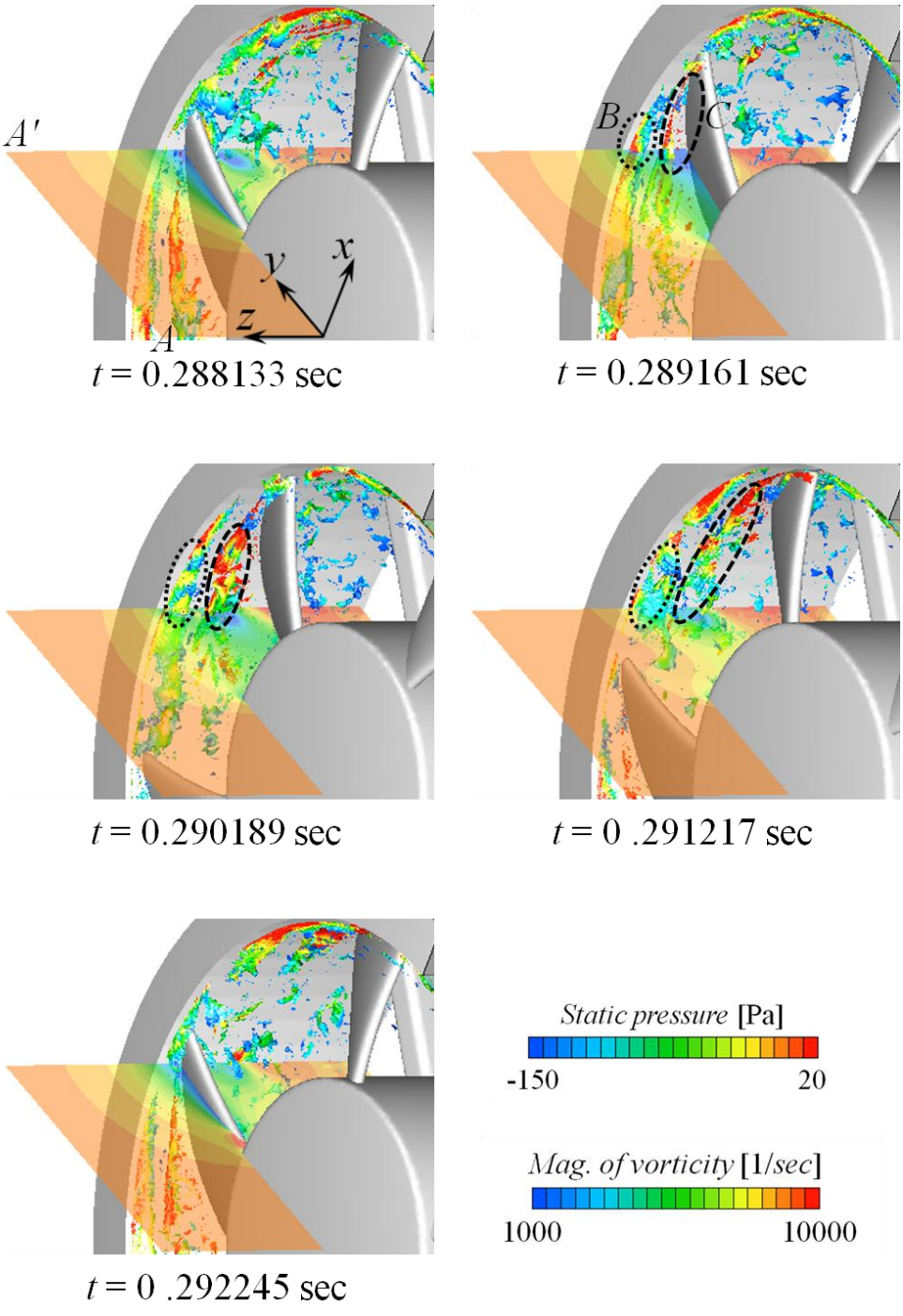

(a) Magnitude of vorticity on the iso-surface of helicity(H_n) -0.95

Fig. 4-5 Distribution of the vorticity at iso-surface of the helicity and the static pressure at cross-section depending on time (continue)

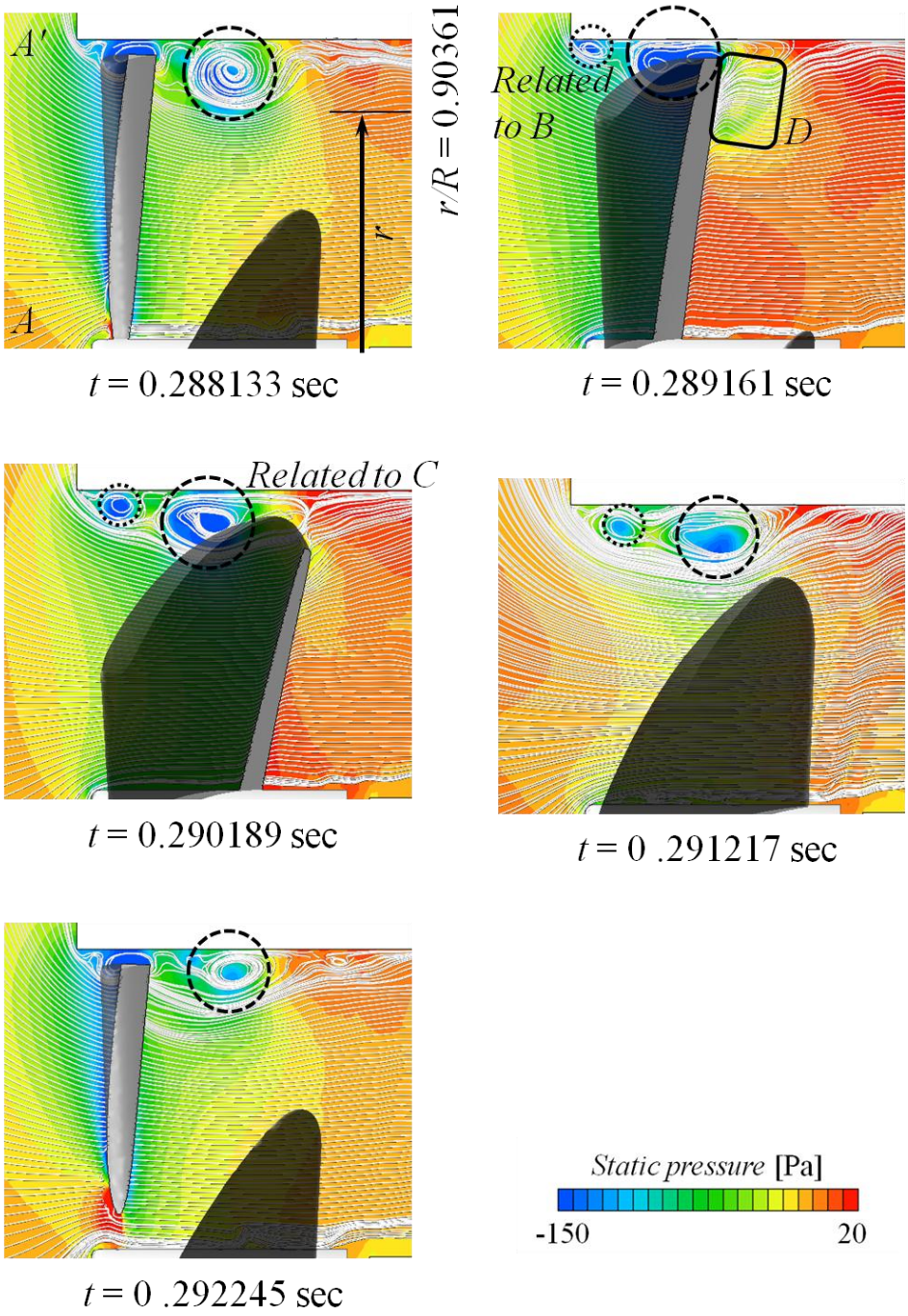

(b) Static pressure at cross section A-A′

Fig. 4-5 Distribution of the vorticity at iso-surface of the helicity and the static pressure at cross-section depending on time (continue)

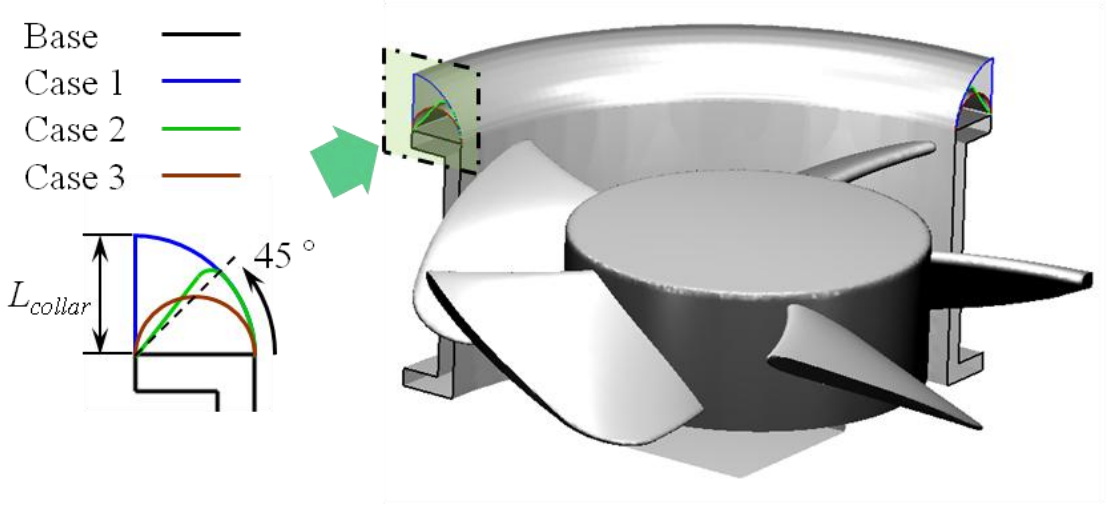

Fig. 4-6 Comparison of the shroud shapes between models

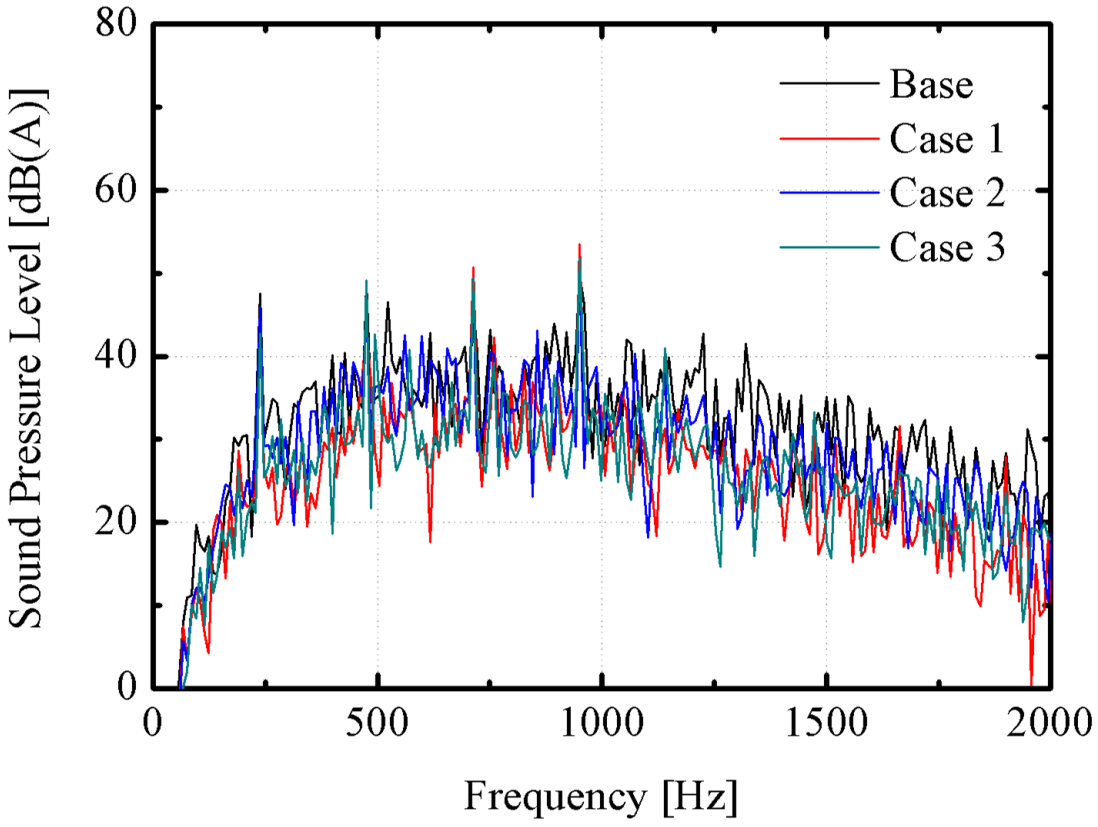

Fig. 4-7 Comparison of the aerodynamic sound spectra between models

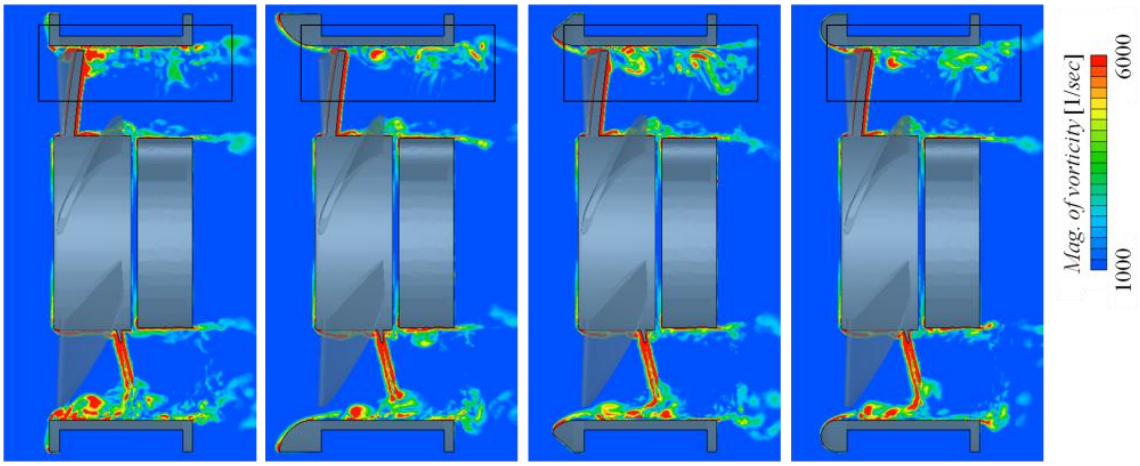

(a) Magnitude of the vorticity in *yz* plane at $x = 0$ *m*

Fig. 4-8 Distribution of the vorticity and the static pressure at $t = 0.288647$ sec (continue)

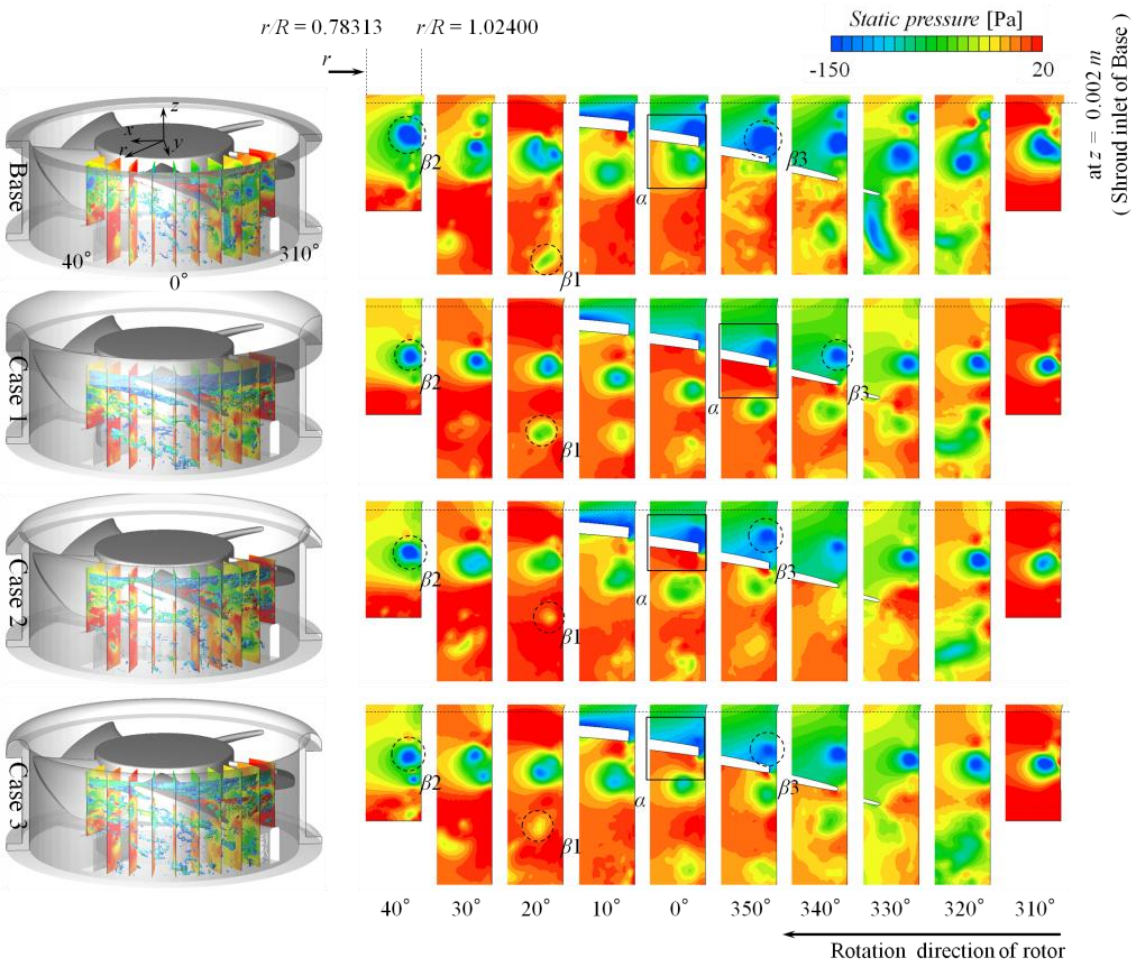

(b) Magnitude of the vorticity on the iso-surface of H_n = -0.95 and static pressure distribution at cross-section

Fig. 4-8 Distribution of the vorticity and the static pressure at t = 0.288647 sec (continue)

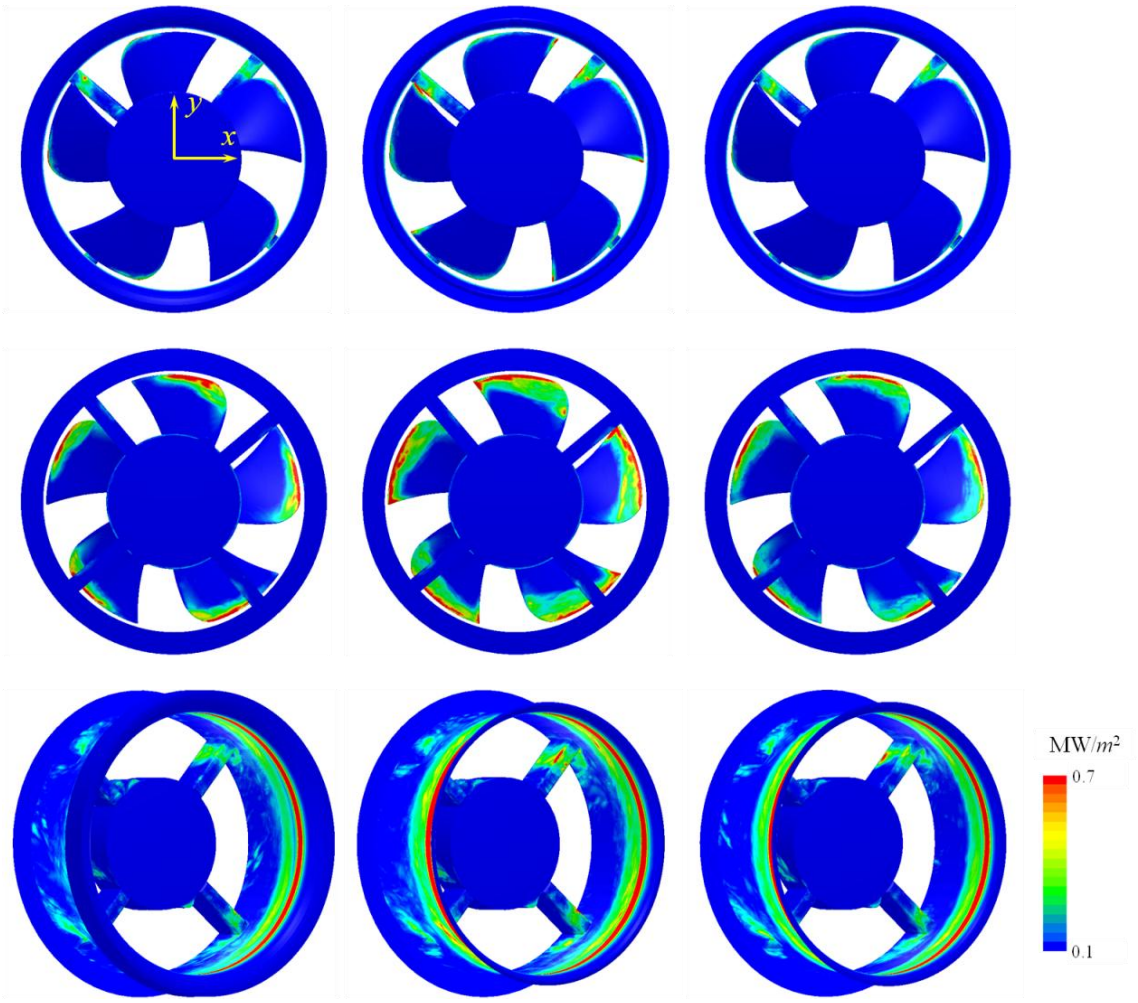

(a) Case 1 (b) Case 2 (c) Case 3

Fig. 4-9 Distribution of the aeroacoustic source strength in low noise models

Chapter 5. Prediction of the noise for a small axial flow fan

5.1 Introduction

Recently, the space density by the internal parts in the server computer has rapidly increased because of the competition among manufacturers for size and weight reduction. The increase in the space density by parts inside the product causes difficulties in release of the heat that is generated inside to outside; thus, small and high-performance fans are needed to release the heat easily. However, the rpm of the fan must be increased to maintain the cooling performance of a small fan. Consequently, issues of increased aeroacoustic noise are arisen. As a result, the standardization of noise measurement for small fans was required recently as a part of researches. The results from small fans have been reported from studies related to standardization and validation about the results has also been conducted [83, 84].

5.2 Characteristics of the unsteady flow field and the noise

To analyse the aeroacoustic noised of an axial flow fan, the static wall pressure fluctuations of unsteady flow field were used. For the unsteady state analysis, the steady-state results that were obtained by calculating Reynolds-averaged Navier-Stokes equations in a steady state were used as an input data. After rotating the axial flow fan twice, the characteristics of static pressure fluctuations in the unsteady flow field was observed. However, the fan was rotated twice more that is a total of four rotations in order to achieve more fully-developed unsteadiness in the flow field. Thereafter, the static pressure fluctuations were acquired while rotating the fan three more rounds. For each iteration, the time step was 23.8095 μsec. For accurate solution, sub-iteration was done for each iteration. The setting for the residual of each velocity component and pressure with regard to the convergence condition of each iteration was 0.000001. The next iteration was allowed only after the convergence was achieved.

In figure 5-1, the distribution of relative velocity and vector velocity in the axial flow fan are shown. Figure 5-1(a) is the schematic diagram showing the cross-sectional location of the velocity vector. Figure 5-1(b) shows the relative velocity distribution presented on the cylindrical surface with the radius r/r_{fan} = 0.9895 projected from the

rotation axis. Depending on the location of the leading edge of the blade and of the planes of the bell mouth, the velocity field close to the blade was varied. The velocity vector field shown on plane 3 is the upstream position near the leading edge passing the bell mouth's plane. In that velocity field, in particular, decrease in the velocity at the fore of the leading edge was found. In addition, a backward flow that was heading back to the upstream of the casing because of the blade was observed from the velocity vector in the plane 3. The clearance between the bell mouth and the blade tip was reduced by approaching each blade to the plane of the bell mouth, occurring the counter-flow toward upstream.

In figure 5-2, the vorticity distributed on the cylindrical surface at r/r_{fan} = 1.0000 is shown. A vortex generated in the leading edge of each blade by the rotor rotation is seen. A vortex was developed over the leading edge while the leading edge passes each plane of bell mouth. The vortex generated by the counter-flow toward upstream affects and disturbs repeatedly the flow field adjacent to each plane of bell mouth.

In figure 5-3, the static pressure distribution on the casing and the velocity distribution on the iso-surface of vorticity were shown with the same value ζ = 11,000 sec^{-1} depending on time. The static pressure on the plane of bell mouth changed continuously with the blade tip passing the plane of bell mouth by time. This was owing to the decrease in clearance between the bell mouth and the blade. And it was thought to be a noise source because the sudden and periodic change in static wall pressure causes aeroacoustic noise.

Figure 5-4 shows the velocity distribution on the cylindrical surface with the radius r/r_{fan} = 1.00000 by time. The analysis time for each figure was 0.060262 sec, 0.060500 sec, 0.060738 sec, 0.060976 sec, 0.061214 sec, 0.061452 sec, 0.061690 sec, and 0.061929 sec, respectively. Velocity distribution in each plane (1~4) was changed with time variation as shown in the figure. It was also notable that the variation of velocity over time resulted in static pressure fluctuations.

5.3 Prediction of the flow-induced noise and coherence analysis

Figure 5-5 presents the axial flow fan's sound spectra acquired from the numerical analysis and the experimental measurement. The aeroacoustic pressure was calculated by using the Ffowcs Williams and Hawkings equation. The total noise level was

measured by using a microphone that was installed 1 *m* ahead of the axial flow fan's rotation center. The sound spectrum and tonal/broadband noise, which were predicted by the numerical analysis, presented distributions that are similar to those of the noise measured by the experiment. In particular, 4x tonal noise at 467 Hz that is smaller than 583 Hz, which corresponds to the first BPF in the sound spectrum, was predicted and found to be consistent with the result obtained from the experiment. This noise was thought to be due to the planes that are located on the bell mouth of the casing. Likewise, the 2nd and 3rd 4x tonal noise as well as the 2nd and 3rd BPF were predicted in an appropriate manner. On the contrary, the predicted broadband noise beyond 1500 Hz was smaller than the experiment data. This was because only dipole was considered. In general, random broadband noise is produced by phenomena including turbulent boundary layer, flow separation, tip vortex, vortex shedding, and so on. In this study, however, the influence of the scattering that is caused as the turbulent boundary layer passes each blade's trailing edge was ignored, and the reflection of noise that is produced by the fan structure was not considered as well. Hence, the discrepancy in the noise prediction was presented at high frequency. However, the predicted OASPL was consistent with the measured OASPL within a margin of 1dB. In this study, the measured OASPL was 52 dB(A) whereas the predicted OASPL was 51 dB(A).

In figure 5-6, the axial flow fan's aeroacoustic source strength is shown. The aeroacoustic source strength is expressed with the aeroacoustic power that is generated per unit area and the unit is W/m^2. The dominant noise sources were at the leading edge tip in the rotating blade, whereas those on the casing were on the planes of the bell mouth and the struts that were installed for uniform flow.

In figure 5-7, the consistency between the acoustic pressure fluctuations obtained from the aeroacoustic noise analysis and the static wall pressure fluctuations of each point by the flow obtained from Point A on a plane of the bell mouth and from Point B on a strut were presented, respectively. Point A and Point B were ones of the dominant noise sources. Here, the coherence between the fluctuation of static wall pressure by fluid flow and the fluctuation of the acoustic pressure for the same time is defined as follows [85].

$$\gamma_{xy}^2(f) = \frac{|S_{xy}(f)|^2}{S_{xx}(f)S_{yy}(f)} \quad (5\text{-}1)$$

where, $S_{xy}(f)$ is the cross spectrum. $S_{xx}(f)$ and $S_{yy}(f)$ are the auto spectra for the fluctuation of static wall pressure by fluid flow and those for the fluctuation of acoustic pressure, respectively. Normally, the value of coherence is the range of $0 \leq \gamma^2_{xy} \leq 1$. In the case that the value of coherence is close to "1", there is high coherence between two data.

The coherence for 4x and 5x tonal frequencies was found to be high as shown in the figure. It was predicted that the coherence for the plane of bell mouth, which is located near the upstream of the blade, is distinguished to be each tonal noise of 4x and 5x; however, the reason why the coherence for the strut was overlapped and united was thought to be due to complicated flow field resulted from the mutual interaction with the rotating blade and the strut. The two location points were verified to be the major noise sources in the axial flow fan based on the coherence analysis.

5.4 Summary

Materials in this chapter were rewritten based on the paper [52]. By using three-dimensional flow analysis and the Ffowcs Williams and Hawkings equation, this study predicted the characteristics of unsteady flow field and aeroacoustic noise produced in a small axial flow cooling fan that is installed in a rack mount server. Below are the results of this study.

(1) According to the unsteady flow analysis, the interaction between the strut and the blade increased the static pressure on the pressure side; hence, a tip vortex was generated by the clearance between the blade and the casing. The strut of casing was found to be the one of dominant aeroacoustic sources based on the aeroacoustic source strength.

(2) Fluctuation of the static pressure was induced on the casing whenever the leading edge tip passes the flat of the bell mouth. Repetitive velocity increase and decrease due to the interaction between the strut and the blade, and the interaction between the separated vortex and the leading edge was found to occur near the cylindrical surface of a shroud.

(3) The predicted sound spectrum revealed the 4x tonal component, which is smaller than the 1st BPF. This was considered to be due to the interaction between the shape of the casing and the rotation of the blade. Then, prediction of the 2nd and 3rd 4x tonal components and BPF components was performed in an appropriate manner; and the comparison of the overall sound pressure level between the prediction and the measurement presented an error as 1dB in approximation. In addition, the aeroacoustic sources that are dominant in the axial flow fan were presented on the planes at bell mouth and the struts based on the acoustic sound strength. The coherence analysis confirmed the validity of the locations of the aeroacoustic sources that are dominant in the axial flow fan. The noise produced at Point A of bell mouth was found to be 4x and 5x tonal noise; however, that at Point B in downstream was found to be the tonal noise that is an overlap of both 4x and 5x.

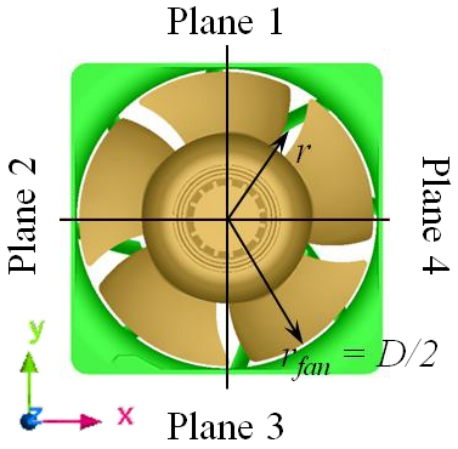

(a) Schematic diagram of cross section views

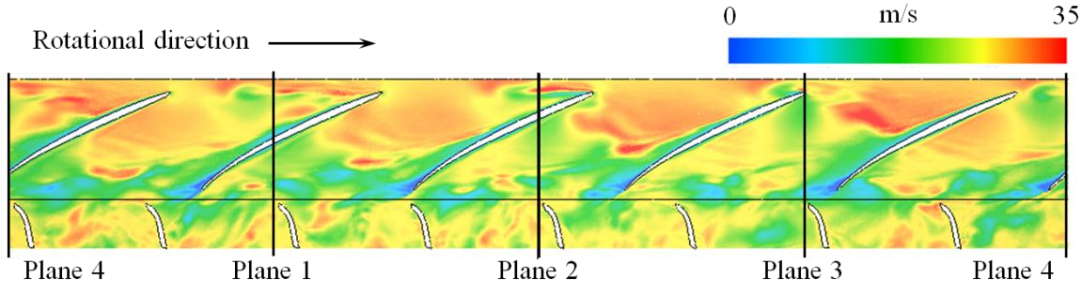

(b) Velocity distribution at the radius r/r_{fan} = 0.9895

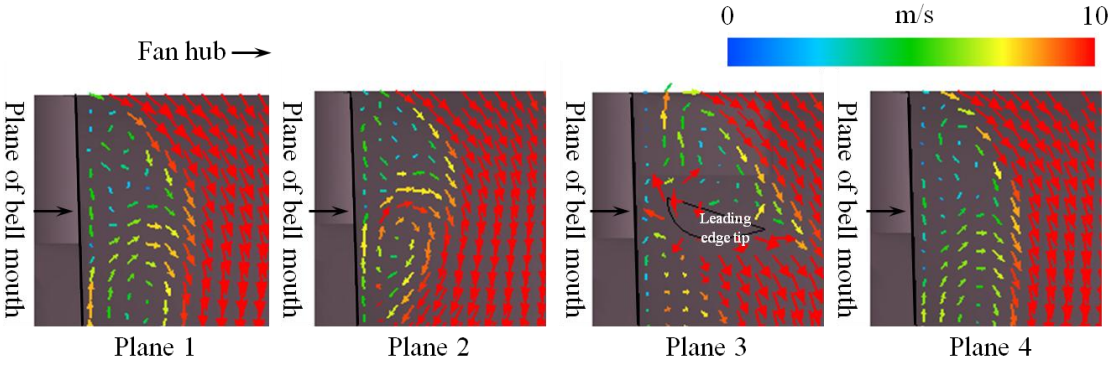

(c) Velocity vector at each plane near the flat of bell mouth

Fig. 5-1 Distribution of relative velocity and velocity vector

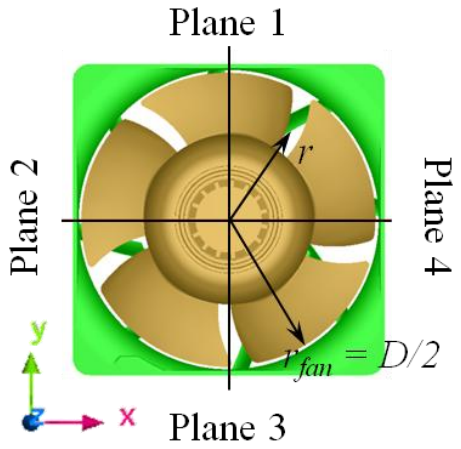

(a) Schematic diagram of cross section views

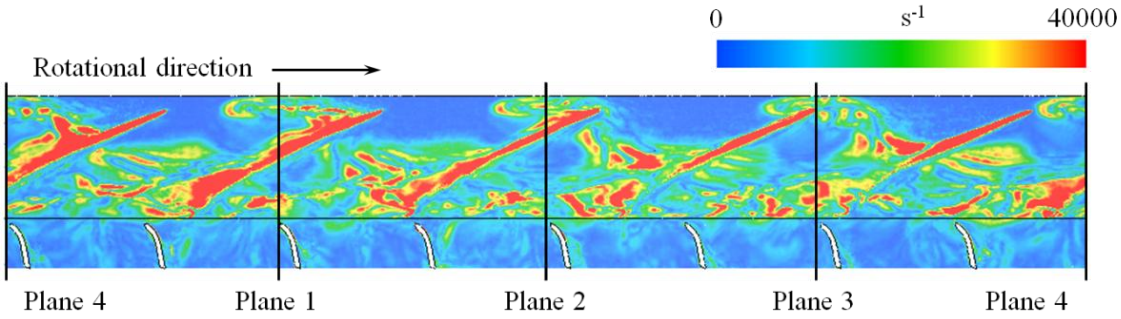

(b) Vorticity distribution on the cylindrical surface at r/r_{fan} = 1.0000

Fig. 5-2 Vorticity distribution on the cylindrical surface at r/r_{fan} = 1.0000

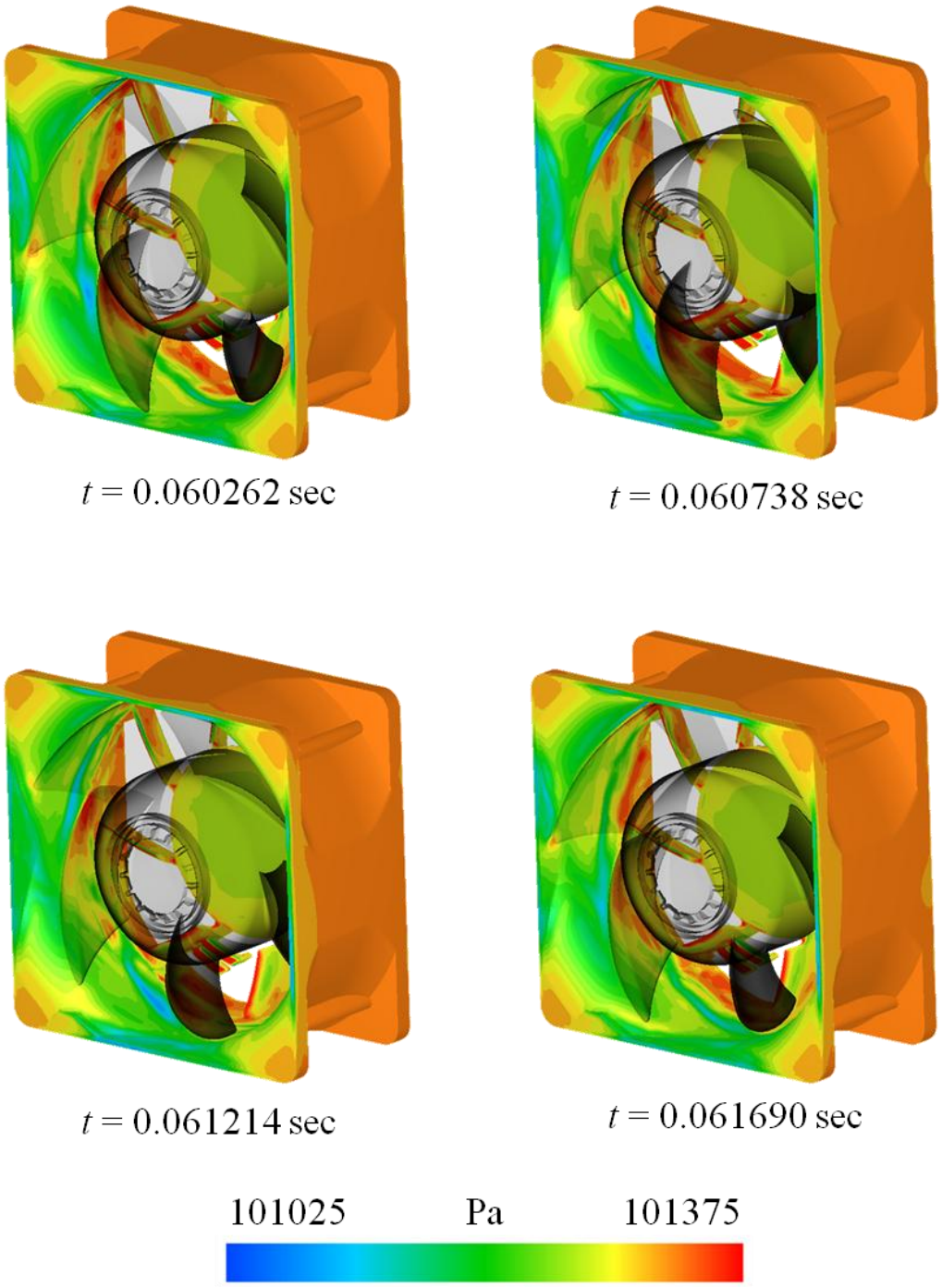

(a) Static wall pressure distribution on the casing

Fig. 5-3 Static pressure and velocity magnitude distribution (continue)

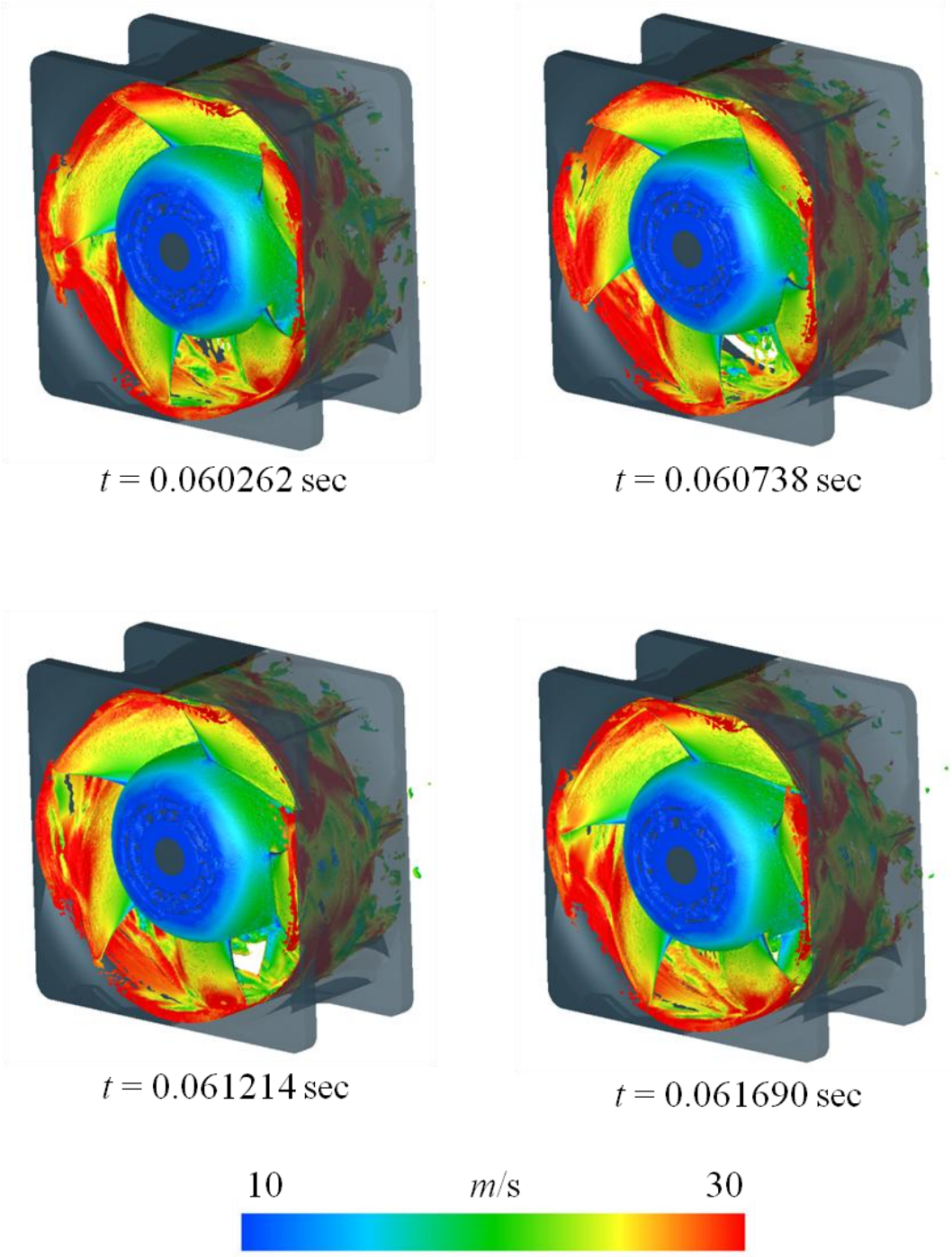

(b) Velocity magnitude distribution on the iso-surface of vorticity ζ = 11,000 sec^{-1}

Fig. 5-3 Static pressure and velocity magnitude distribution (continue)

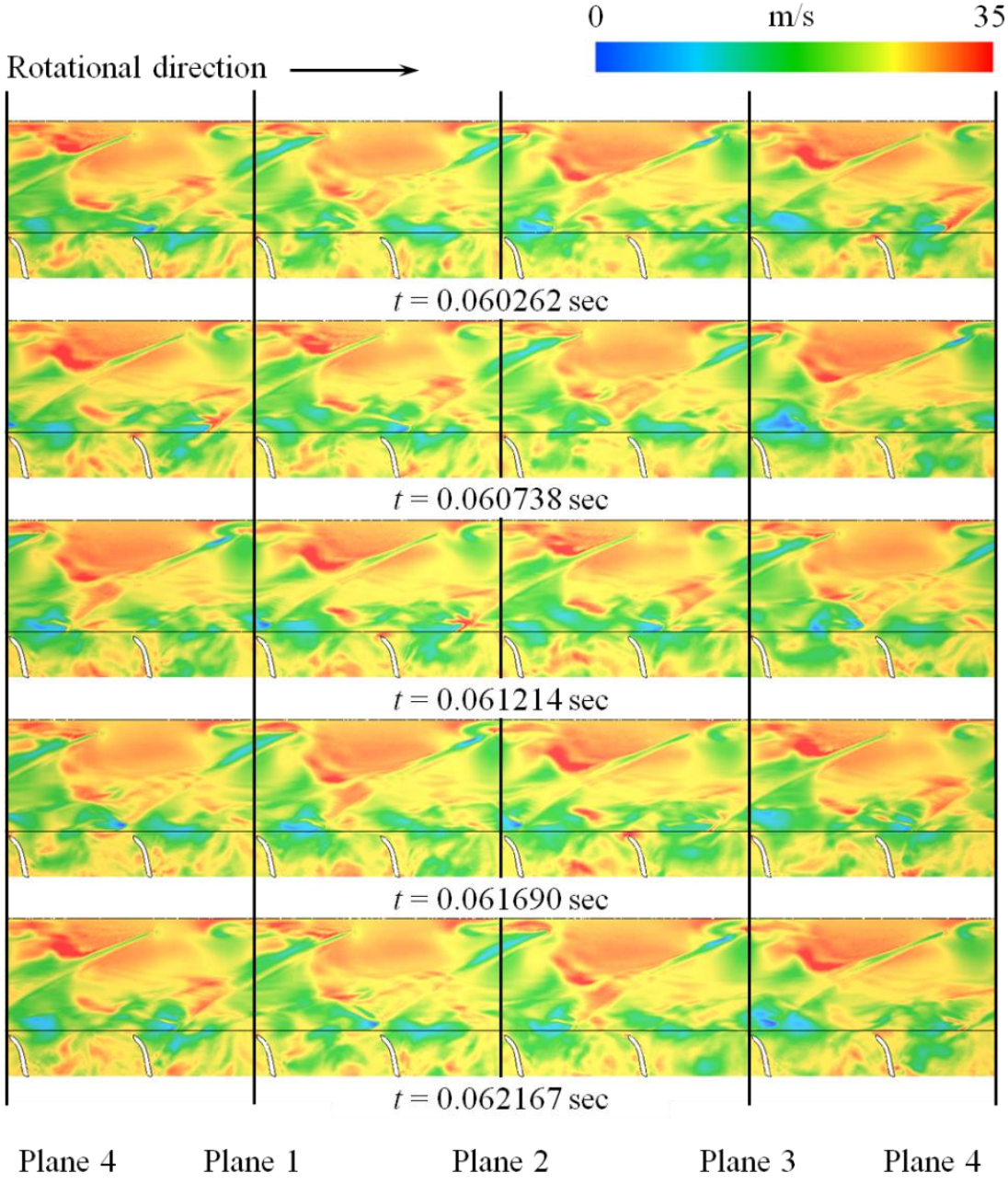

Fig. 5-4 Velocity magnitude distribution depending on time at cylindrical surface r/r_{fan} = 1.0000

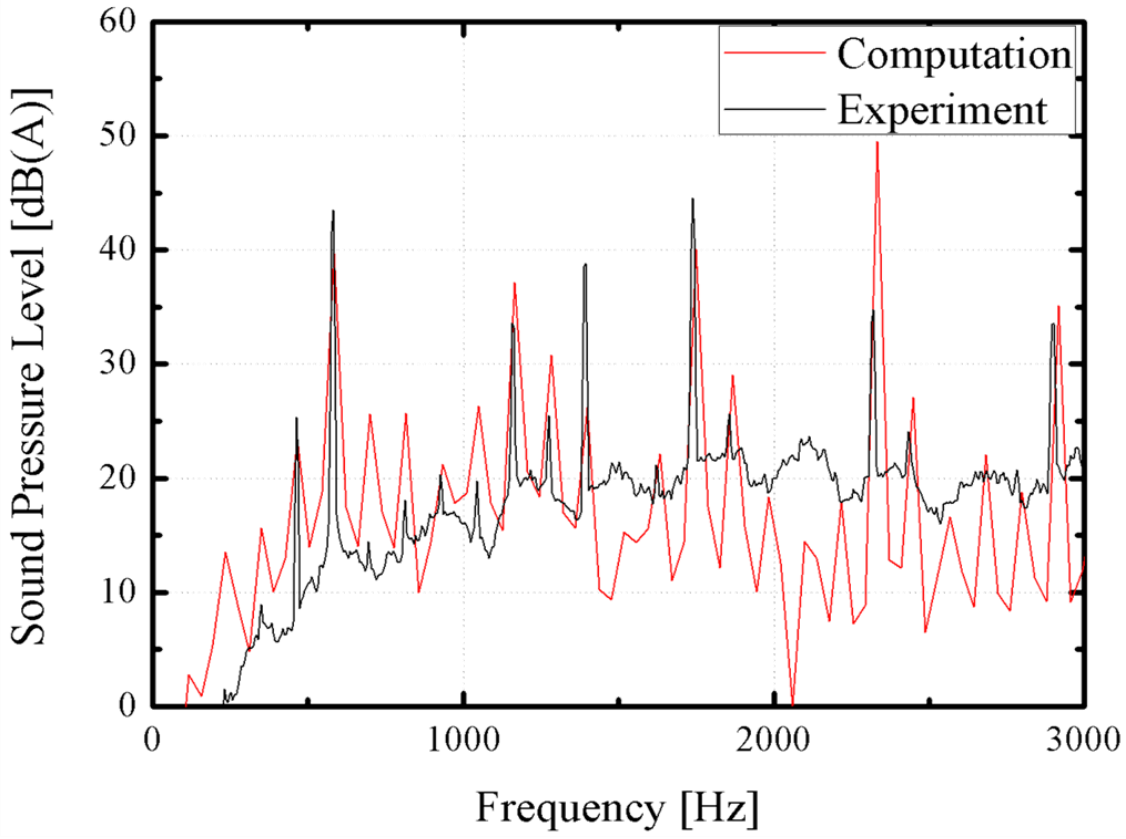

Fig. 5-5 Comparison of aeroacoustic sound spectra obtained by numerical simulation and experimental measurement

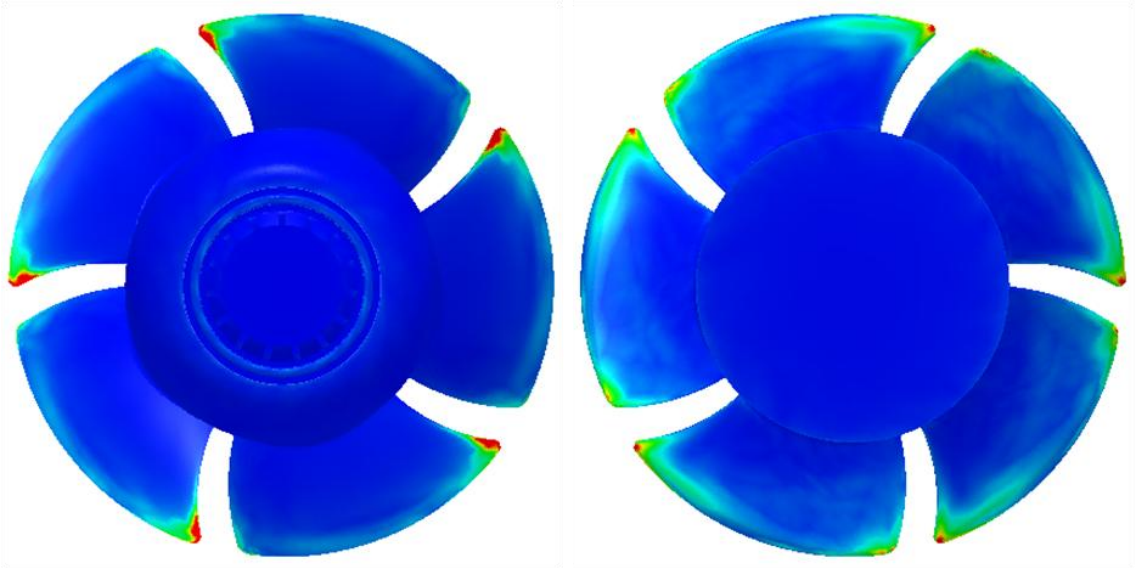

(a) Suction side and pressure side of a fan

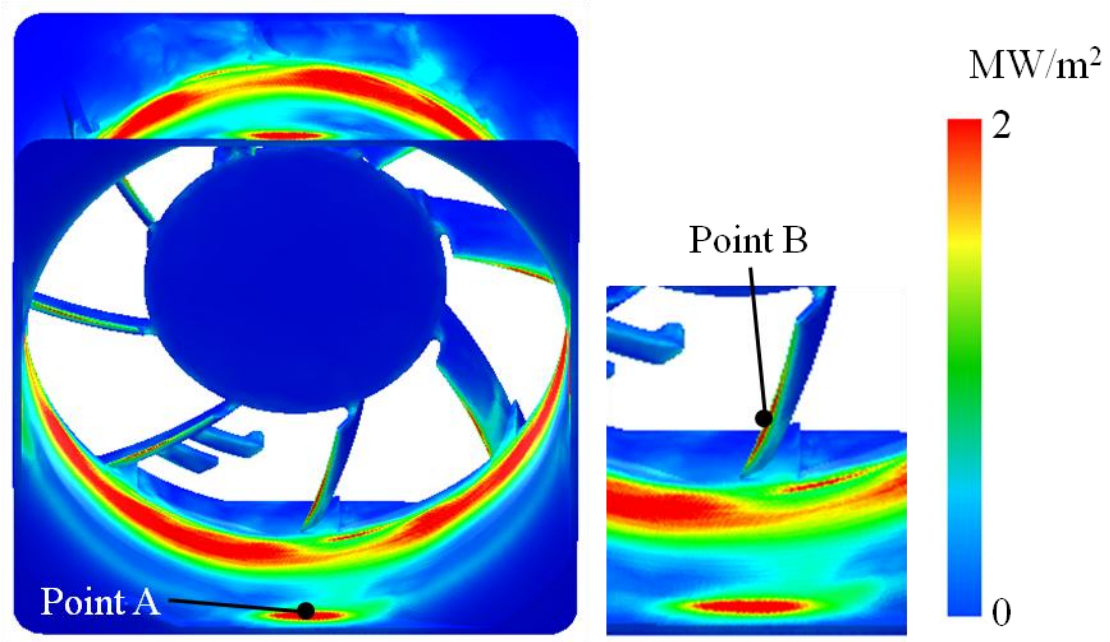

(b) Casing

Fig. 5-6 Aeroacoustic source strength distribution

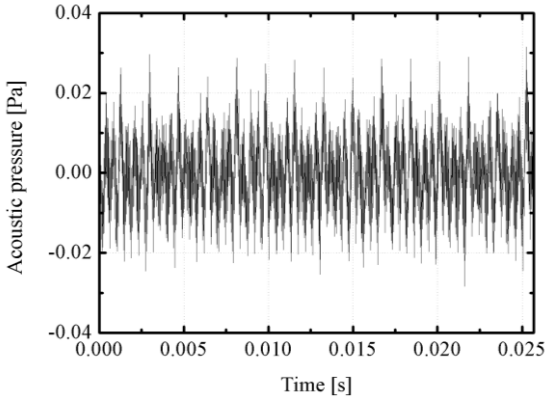

(a) Acoustic pressure distribution

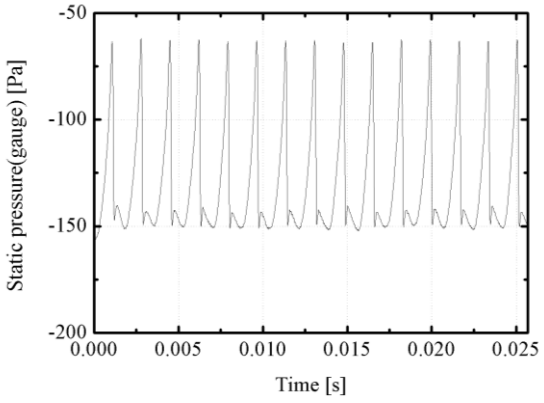

(b) Static pressure at Point A

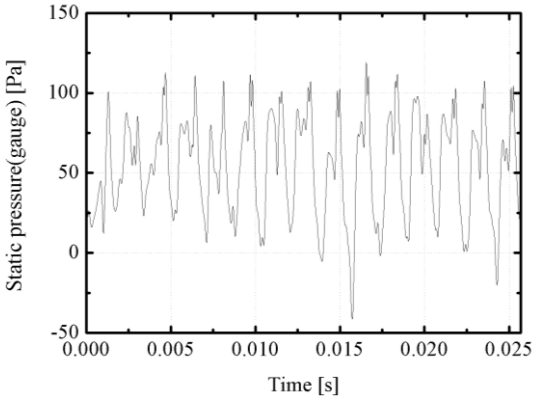

(c) Static pressure at Point B

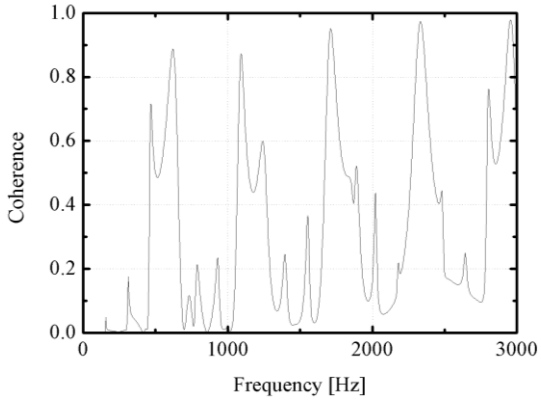

(d) Coherence between (a) and (b)

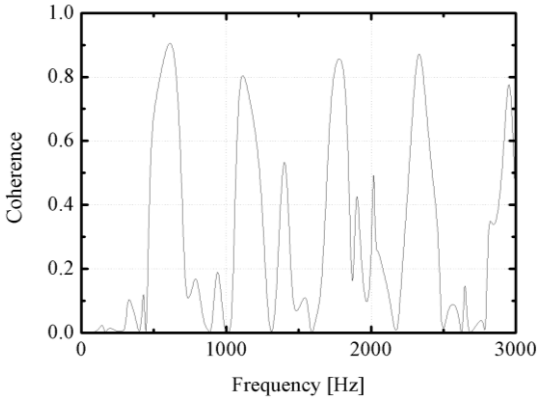

(e) Coherence between (a) and (c)

Fig. 5-7 Coherence analysis between sound pressure and static pressure

Chapter 6. Application for the noise reduction of a small centrifugal fan

6.1 Introduction

To cool the main part that generates heat, a cooling module is used in most electronic devices. Since the heat flows within the device, a cooling module is comprised of three units. The three units are a heat collection unit absorbing the heat, which is generated by a heat-generating part, a heat transfer unit delivering the heat to a heat dissipation unit, and a heat dissipation unit cooling down the heat. Generally, a fan is the fluid machinery that has been used to cool a heat dissipation unit in the electronics. The centrifugal fan, in particular, has been used for size-restricted electronics including ultra laptops, tablet-type personal computers (PC), and laptop computers due to users demand on miniaturization and lightweight to enhance mobility.

The radiation of heat from the inside to the outside of the electronics is not easy since a small mobile device has the highly dense space by parts. Consequently, a fan with high performance that is small so as it can be installed in a narrow space is required to cool down the heating parts. When considering the fact that size of the fan is a crucial factor for fan performance and the size need to be small due to the limited space of small mobile devices, the fan’s rotation speed needs be increased in order to maintain or enhance the cooling performance in comparison with the existing fans. However, the performance improved in such manner can cause higher flow-induced noise and it is able to have significant influence on the quality of products. Therefore, many researched have been conducted to study how to maximize the fan performance while reducing flow noise in the restricted-sized fan.

The previous study conducted with the aim for reduction in flow noise that is produced from a small fan was an experiment-based study that may carry limitations due to the difficulties in verification of the transient flow in fluid machinery such as small fans regardless of the use of a state-of-the-art equipment. Hence, new technique along with conducting experiment is needed in order to understand the phenomena of unsteady flow. Recently, approaches with numerical analysis including Computational fluid dynamics (CFD) and Computational aeroacoustics (CAA) have been utilized for evaluation and prediction of the flow field and the noise in small fans; and the

validation of the approach is ongoing [51-53, 83].

6.2 Characteristics of the unsteady flow field and the flow-induced noise

For analysis of aerodynamics noise in the small centrifugal fan, the static pressure fluctuations in the unsteady flow field were used. The unsteady state analysis was performed with the input data of the result that was obtained from the steady state analysis on RANS model. Due to the complexity/narrowness of the internal structures and configurations contained in small-sized electronics, for example laptops, the flow field generated by each rotation of the impeller while rotating the impeller eight rounds was examined to set full development of unsteadiness in the flow field. Thereafter, the unsteady state analysis was performed during five rotations of the impeller in order to obtain the data of static pressure fluctuations on the surfaces that are needed for aeroacoustic analysis.

The static wall pressure distributions recorded at two points on the inner casing during 5 rotations after 8 rotations were shown in figure 6-1. Point 1 was located on the upper casing whereas Point 2 was located on the lower casing. The static pressure that is repetitively distributed with similar amplitude at the two points during the 5 rotations indicates the full development of unsteadiness. In order to secure the accurate solutions, sub-iteration for each iteration was performed and the time step per iteration was 15.9337 μsec. The convergence condition with respect to each residual for velocity and pressure was set as 0.000001 or below and 0.00001 or below, respectively. The convergence condition was imposed for each iteration and the next iteration was allowed after reaching convergence.

Figure 6-2 shows the contour of static pressure on the casing's inner surface by time. The gage pressure used here was zero-referenced with respect to the atmospheric pressure. With the rotation of the impeller, a complex flow field was produced by the interaction between the casing and impeller. The consequent changes in static pressure distribution due to the interaction were verified on the surface of the casing. When bisecting the *yz* plane based on the center as $x = 0$ in figure 6-2 into "Area A" where $x > 0$ (left side) and "Area B" where $x < 0$ (right side), the static pressure was observed to be asymmetrically distributed. The flow structure of the centrifugal fan can explain the asymmetric pressure distribution. In the centrifugal fan, the flow is introduced from the

inlet in the upper region of the impeller and pressurized in “Area A” due to the impeller rotation and the casing. Then, the flow is finally discharged from “Area B” to the atmosphere due to the pressure difference between the pressurized flow field in “Area A” and the outside flow field. In addition, the static pressure difference between the upper and lower surfaces of the casing was occurred by the inertia of the fluid and the change of flow direction which the flow introduced through the inlet was discharged toward the radial direction.

In figure 6-3, the *z*-directional velocity distribution was described on *zx* plane with y = 0. Because of the impeller rotation and the shape of the casing, *z*-directional velocity gradient in “Area B” was observed greater than those in “Area A”. This was understood to be due to the flow structure in the centrifugal fan.

Figure 6-4 presents the velocity (Figure 6-4(a)) and total pressure (Figure 6-4(b)) distribution with streamlines at z = -0.00145 *m* that is the height of the center plane of the centrifugal fan’s outlet when t = 0.073996 sec. As described in figure 6-3, the flow toward “A” direction and the flow toward “B” direction were observed. The flow toward “A” direction was produced by the pressure that is relatively higher than that of the outside whereas the flow toward “B” direction was produced by the impeller rotation. Pressure reduction near the outlet, which is the spot between the impeller blades in “Area B”, was recognized easier than that between the impeller blades in “Area A”; this was understood to be the reduced pressure due to the discharge of the flow to the outside.

In figure 6-5, the vorticity distribution depending on time was illustrated on a cylindrical section between 0° and 180° of r/r_{fan} = 1.00625 (Figure 6-5(a)) and on cross sections of z = -0.0145 *m* and z = -0.0235 *m* (Figure 6-5(b)). Due to the rotation of the impeller, increased vorticity was found in the spot between blades, in the gap between the casing and impeller, and near each blade’s tip. The random turbulence was produced in the spot in between blades and in the region downstream of the blade’s tip. Especially, in the section between 45° and 135°, the vorticity was increased by the flow that was discharged to the atmosphere. Furthermore, dissipation of the turbulence structure around the blade tip was found as the impeller rotated through the cut-off region (near 135°). Therefore, the region between 45° and 135° and the region around the cut-off region were predicted to be the noise sources.

In figure 6-6, the sound spectra of the centrifugal fan are shown that were obtained from the numerical analysis and the experimentally measured data using a microphone. From the numerical analysis, the aerodynamic sound pressures were obtained from the FW-H equation. The numerical analysis predicted the tonal noises of BPF at 2964 Hz and its harmonics very well as shown in the figure. For the broadband noise at frequency domain, the predicted values were consistent with the experimental value. Some difference was found in the flow noise within the frequency range of 850 ~ 1350 Hz between the predicted value and experimental value. Due to the fact that this computational study considered noise radiation only, the noise occurred by the casing shape that was gradually increased and reduced within the range was considered to cause such discrepancy between noises.

The locations of aeroacoustic source strength in Base model are shown in figure 6-7. In centrifugal fans, the noise sources were not usually found in the impeller; and most of those were found in the casing along the impeller's rotational region. The complicated flow field produced by the aforementioned impeller rotation was confirmed to generate the region marked as "An" on the upper and lower surface of the casing. To be specific, the noise sources on the casing's upper surface were found in the section between 70° ~ 220°. However, the noise sources on the casing's lower surface were found in the section between 50° ~ 180°. Also, the noise sources with higher strength were indicated on the lower surface of casing but distributed on narrower region. Especially, the distribution of the noise sources on the casing's upper surface was found to be along the impeller tips. Hence, reduction in noise was predicted through modification of the impeller tips. On the lower surface of the casing, on the contrary, the distribution of the noise source locations was found to be within the diameter not along the impeller tips. The interaction between the impeller and the cylindrical step that is 0.0003 *m* tall and is located at the spot where r/r_{fan} = 0.8125 on the casing's lower surface toward +*z* direction. Hence, both impeller configuration and casing configuration should be considered for noise reduction in the casing's lower surface. Since the purpose of this study was not the noise reduction in every aspect, this study only focused on the noise reduction by modifying the impeller tips.

6.3 Prediction for low noise through modification of impeller tip

Figure 6-8 is showing the modification made in the shape of the impeller tips for noise reduction. As shown in top view of the impeller, the diameter of the impeller was not changed. When the difference in the shapes of the impeller was examined by looking at the side views, the tip of the impeller blade in Base model was perpendicular whereas each tip of the impeller blade in low noise models was cut by 30° as shown in figure 6-8(b) and (c), respectively. As described in figure 6-7, the low noise models were proposed with the purpose of reduction in noise sources that are generated in the upper surface of the casing.

In figure 6-9, the sound spectra for the frequency of the Base model and of the low noise models with their impeller tips partially modified for noise reduction are presented. For the distributions of tonal and broadband noise in each sound spectrum, similar trend was commonly observed. However, the tonal noises of BPF and its harmonic frequencies, and the broadband noise predicted for low noise models were lower than those that the base model. Each OASPL for Base model, Case 1 and Case 2 was predicted by performing the numerical analysis; and that was 52.2 dB(A), 51.8 dB(A), and 51.4 dB(A), respectively. Fan performance was changed because of the modification made in the impeller tips. Therefore, reduction in flow noise with respect to the performance was examined by using specific noise level equation. Below is the specific noise level equation described in Sec. 4.4.

$$K_{sa} = SPL - 10log\left(\frac{Q}{Q_{Base}}\left(\frac{\Delta p_t}{\Delta p_{t,Base}}\right)^2\right) \quad (4\text{-}2)$$

Compared to the base model, quantitative changes were found in the flow field of the low noise models: decreased flow rate by 5.3% in Case 1 and by 3.8% in Case 2, and decreased total pressure rise (Δp_t) by 8.3% in Case 1 and 7.1% in Case 2. The specific noise level for the low noise models was drawn from the calculation of equation (4-2); and that was 51.8 dB(A) for Case 1 and 51.4 dB(A) for Case 2 (Refer to Table 6-1). Since OASPL of the low noise models predicted by the specific noise level was lower compared to the Base model, partial modification made for the impeller tips was confirmed to play an important role in noise reduction.

Table 6-1. Specific noise level at centrifugal fans

	OASPL	Q/Q_{Base}	$\Delta p_t/\Delta p_{t,Base}$	K_{sa}
Base, *Ref.*	52.2	1	1	52.2
Case 1	50.8	0.94729	0.91721	51.8
Case 2	50.6	0.96197	0.92870	51.4

In figure 6-10, the vorticity distribution on the cylindrical surface of r/r_{fan} = 1.00625 at t = 0.074252 sec are shown for all models. Clear distinction in the vorticity distribution was seen depending on the shapes of impeller tips. In particular, relatively smaller and weaker vorticity structure was observed in Case 1 and Case 2 because of the partially removed impeller tips in the low noise models. The removed tips were thought to weaken the vorticity and thereby reduce the noise.

The locations of aeroacoustic noise sources for the low noise models are shown in figure 6-11. The low noise models presented weaker strength and reduced area of the noise sources in both upper and lower surface of the casing compared to the Base model. The partially modified tip shape was confirmed to weaken the strength and reduce the domain of the noise sources remarkably on the casing's upper surface. The diameters of the noise sources located on the surface of the casing were reduced depending on how the partial change was made in the tip. In addition, the strength of the noise sources on the casing was found to be decreased differently depending on how the partial change was made in the tip as well. In other words, the normal of the plane cut affected the strength of the noise sources; the cutting pattern adopted for Case 1 resulted relatively weakened noise sources on lower surface of the casing whereas the cutting pattern adopted for Case 2 resulted relatively weakened noise sources on the upper surface of the casing.

6.4 Summary

Materials in this chapter were rewritten based on the paper [53]. The characteristics of unsteady flow field and noise from a small centrifugal fan were predicted by using three-dimensional numerical analysis in this study. To simulate the similar environment, a model device with narrow flow channels that are similar to what in a real laptop was prepared and the fan was installed in there. LES model was applied to predict the unsteady flow field accurately. The centrifugal cooling fans are linked to considerably

narrow and complex flow channels in portable electronics. Hence, unsteady flow was analyzed following to the full development of unsteady flow field in order to obtain an input data for CAA. The noise spectrum was compared to the experimental values. Thereafter, the CAA results presented the locations of noise sources. The locations were verified from the Base model; and then, the noise was reduced by adopting the low noise models. The conclusions drawn in this study are below.

(1) In the flow structure of the centrifugal fan, the outlet and inlet are placed perpendicularly to each other. Hence, the flow field is inconsistent due to the rotational axis. Consequently, the flow fluctuates vertically in the casing because of the inertia of the fluid created as the impeller rotates. There are two types of the flow that is discharged to the radial side: the flow that is discharged due to pressurization caused by the impeller and casing, and the flow that is discharged due to the rotation of the impeller.

(2) The comparison of the noise spectrum between the prediction and measurement in a frequency domain revealed the agreement of tonal noises at BPF and its harmonics, and broadband noise. Since the prediction in this study was done only for the noise radiation, the increase of the noise, which is due to the centrifugal fan configuration, presented within some frequency ranges was not predicted.

(3) The major aeroacoustic noise sources of the Base model were mostly presented around the casing of the centrifugal fan and the distribution of the locations on the casing were existed along the rotational direction of the impeller. However, the locations of the noise sources on the upper surface of the casing and on the lower surface did not match each other. In particular, the noise sources that were caused by the blade tip were observed on the upper surface of the casing in contrast to the noise sources that were produced by the centrifugal fan's complex flow structure were observed on the lower surface of the casing.

(4) For minimization of the noise sources that are located on the upper surface of the casing, noise reduction was performed by modifying the shape of the impeller's blade tips. In addition, the noise reduction using the low noise models was discovered by using specific noise level. Compared to the Base model's OASPL, the noise reduction by around 0.8 dB was accomplished.

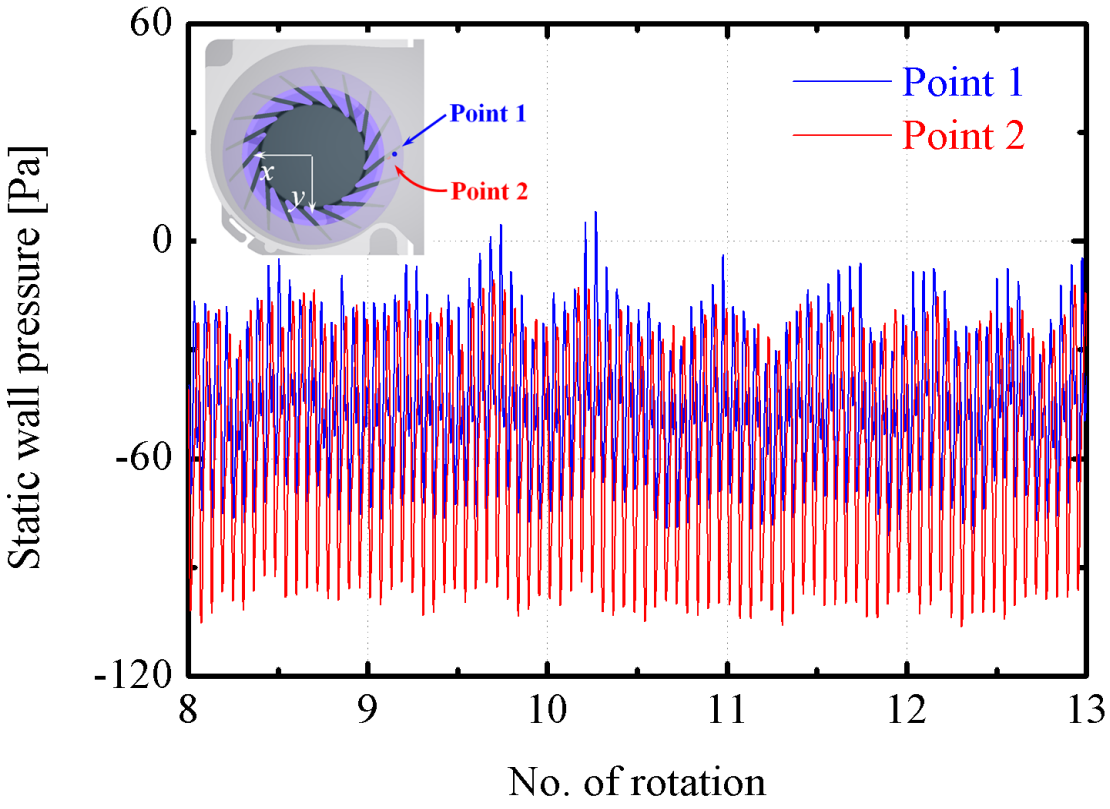

Fig. 6-1 Time-dependent static pressure distribution at two points on the inner casing

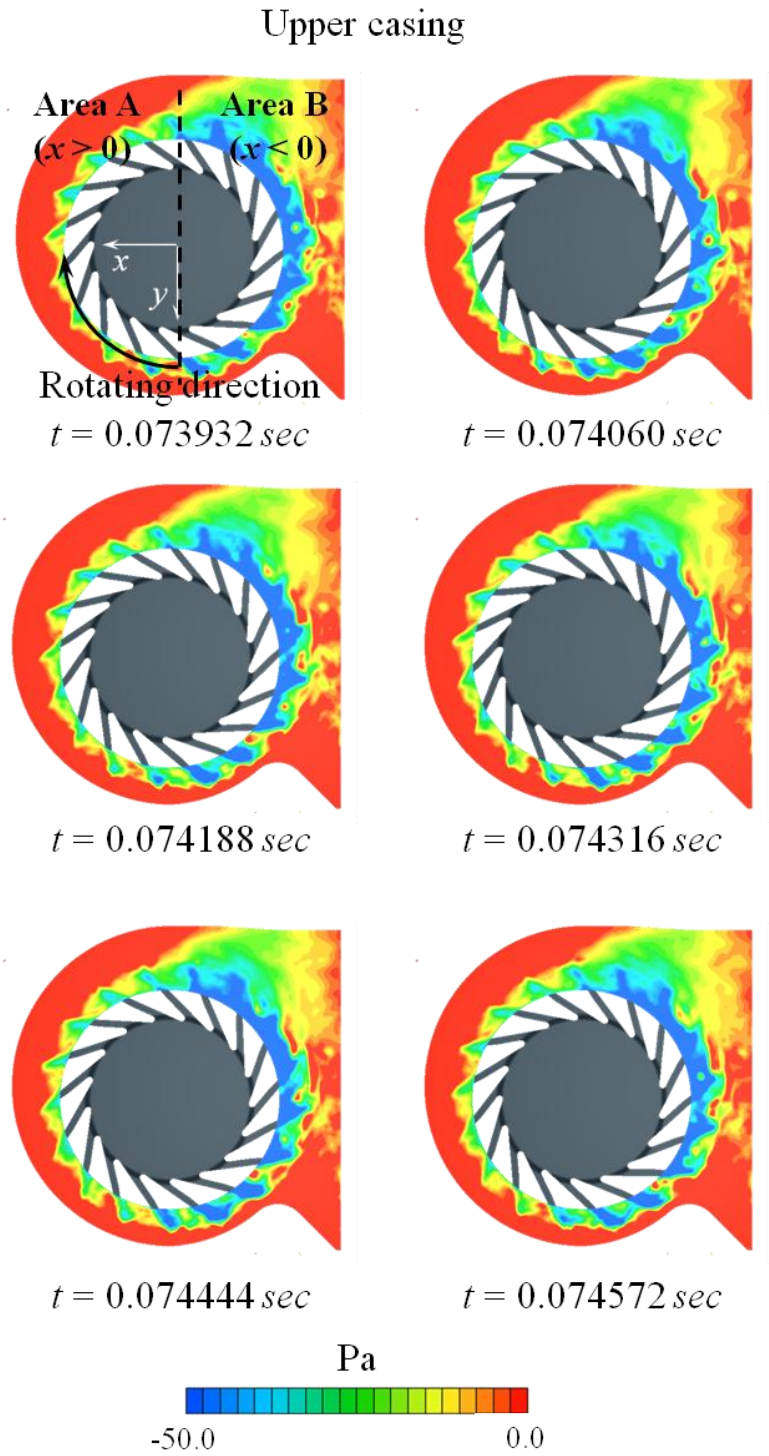

(a) Static wall pressure at upper casing

Fig. 6-2 Distribution of static wall pressure on the inner casing (continue)

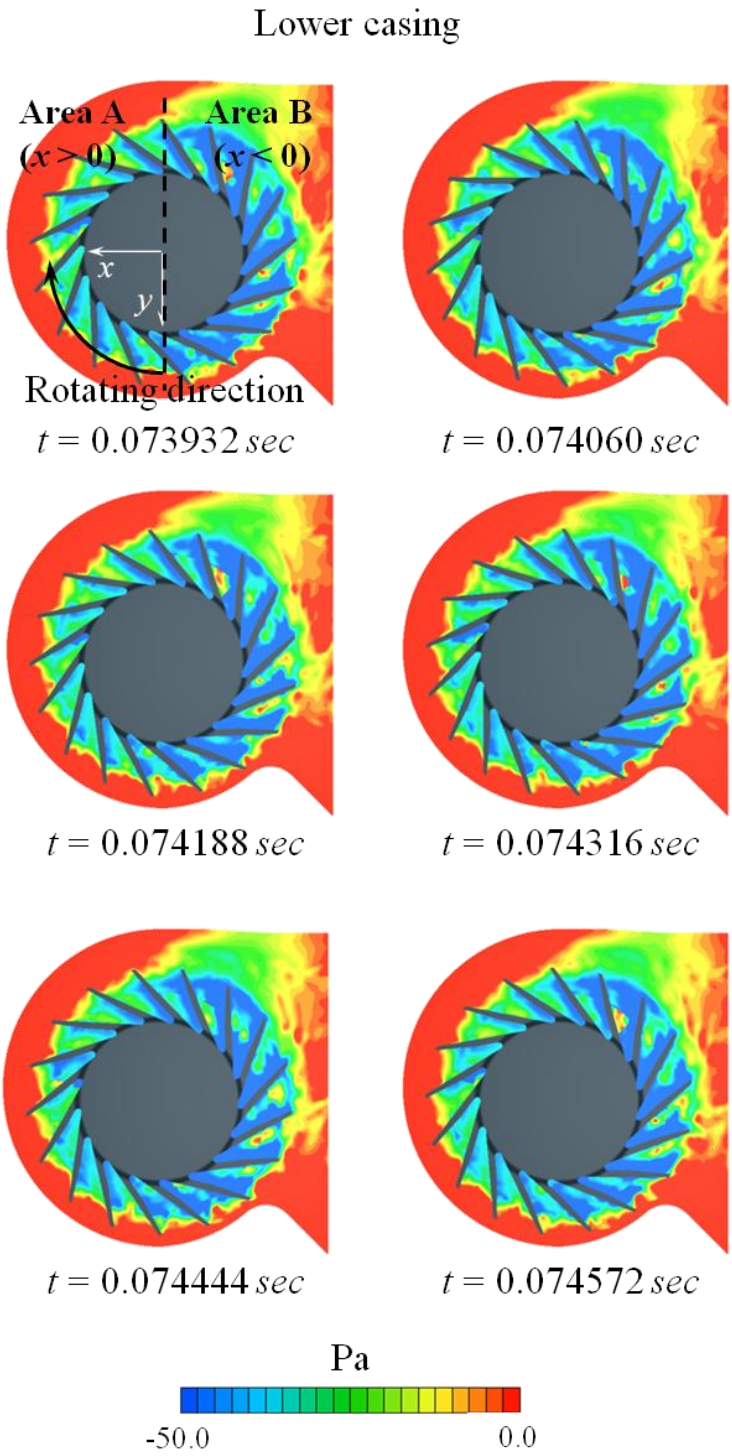

(b) Static wall pressure at lower casing

Fig. 6-2 Distribution of static wall pressure on the inner casing (continue)

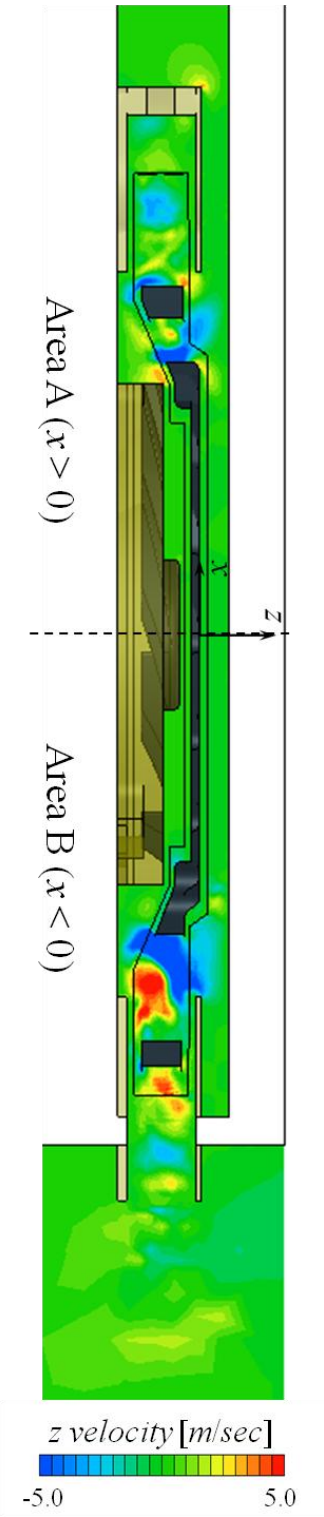

Fig. 6-3 *z*-directional velocity distribution on the *zx* plane with $y = 0$

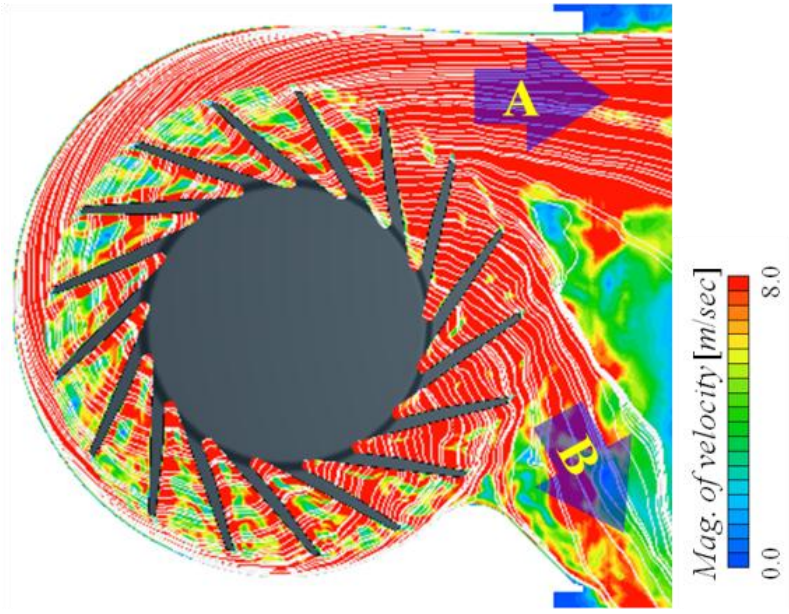

(a) Magnitude of velocity

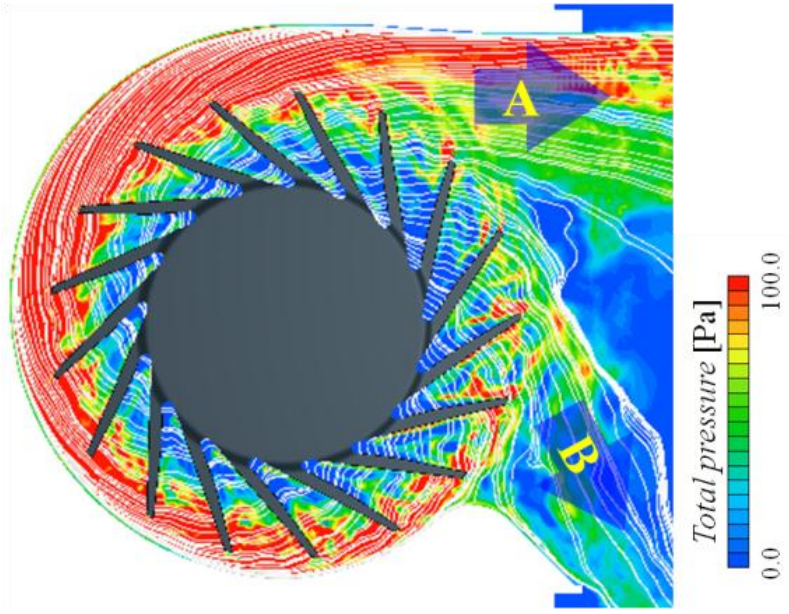

(b) Total pressure

Fig. 6-4 Distribution of flow properties and streamline at z = -0.00145 m and t = 0.073996 sec

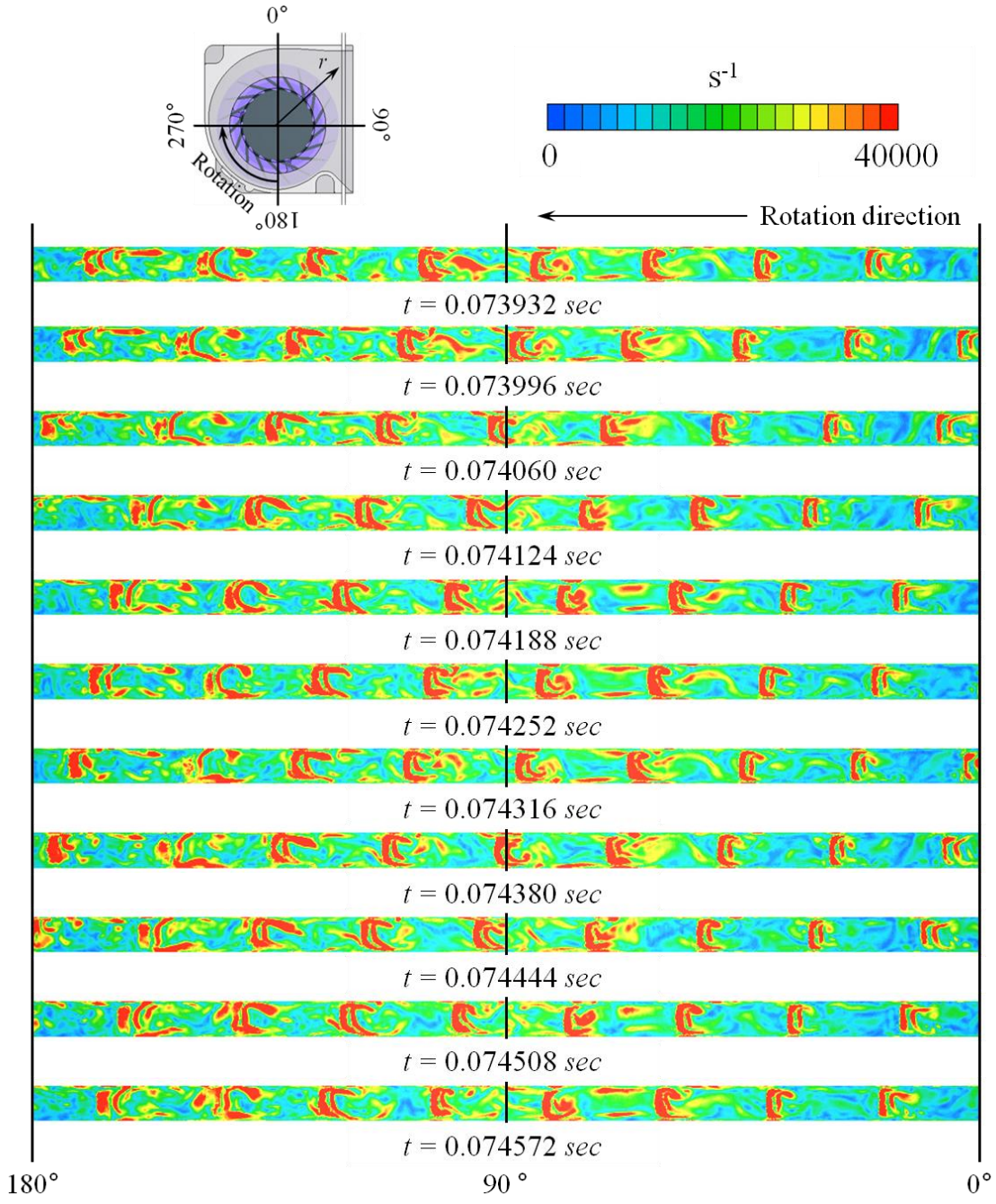

(a) At cylindrical plane r/r_{fan} = 1.00625

Fig. 6-5 Vorticity distribution depending on time (continue)

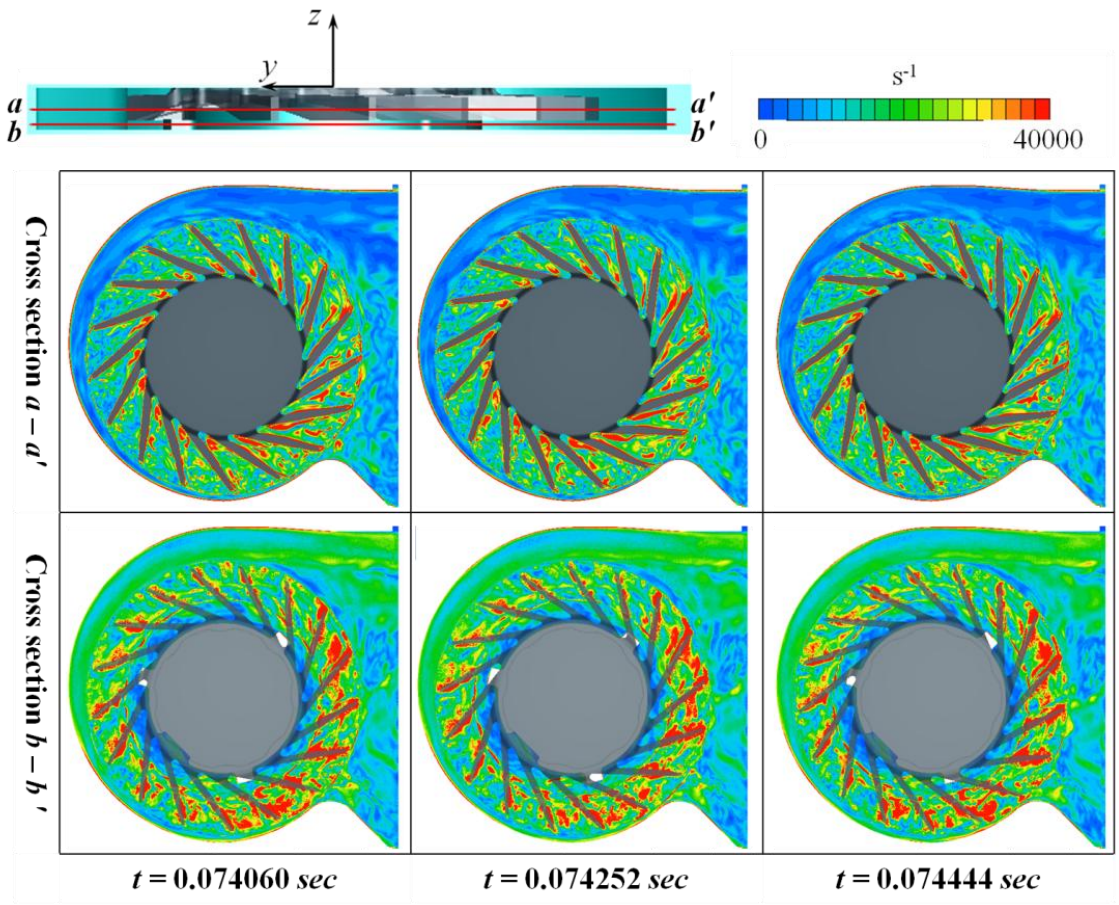

(b) At z = -0.0145 *m* and -0.0235 *m* (cross section *a* - *a′* and *b* - *b′*)

Fig. 6-5 Vorticity distribution depending on time (continue)

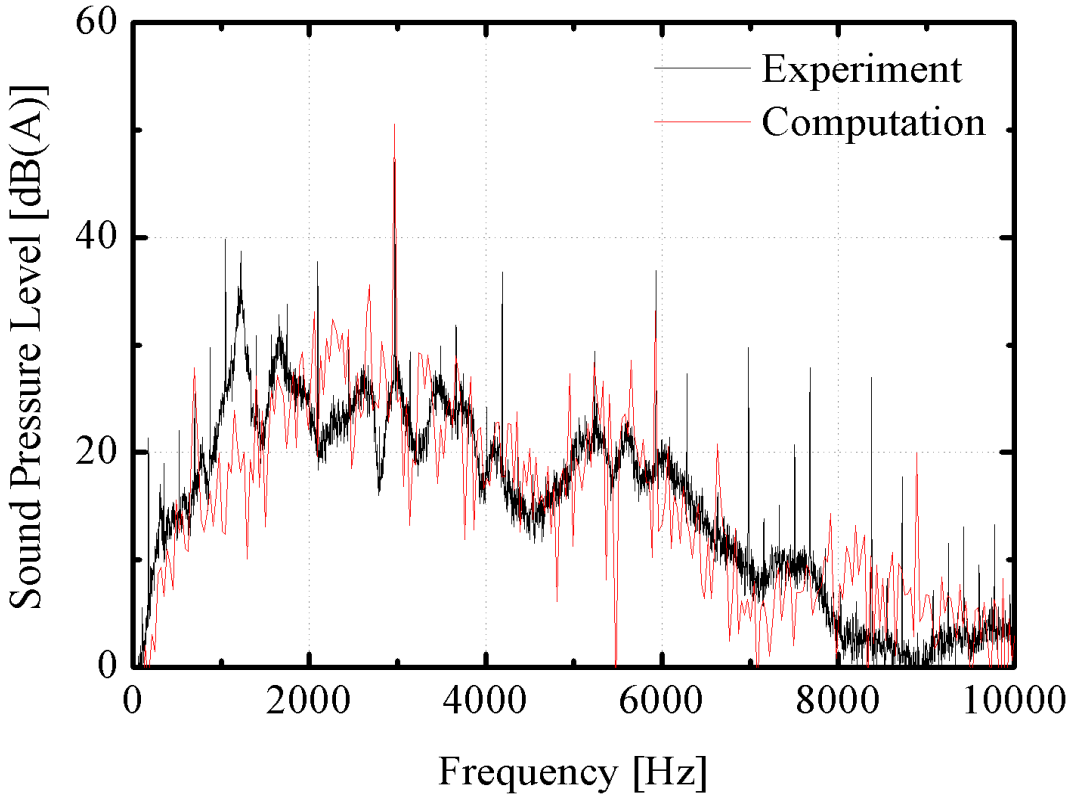

Fig. 6-6 Comparison of aerodynamic sound spectra of Base model

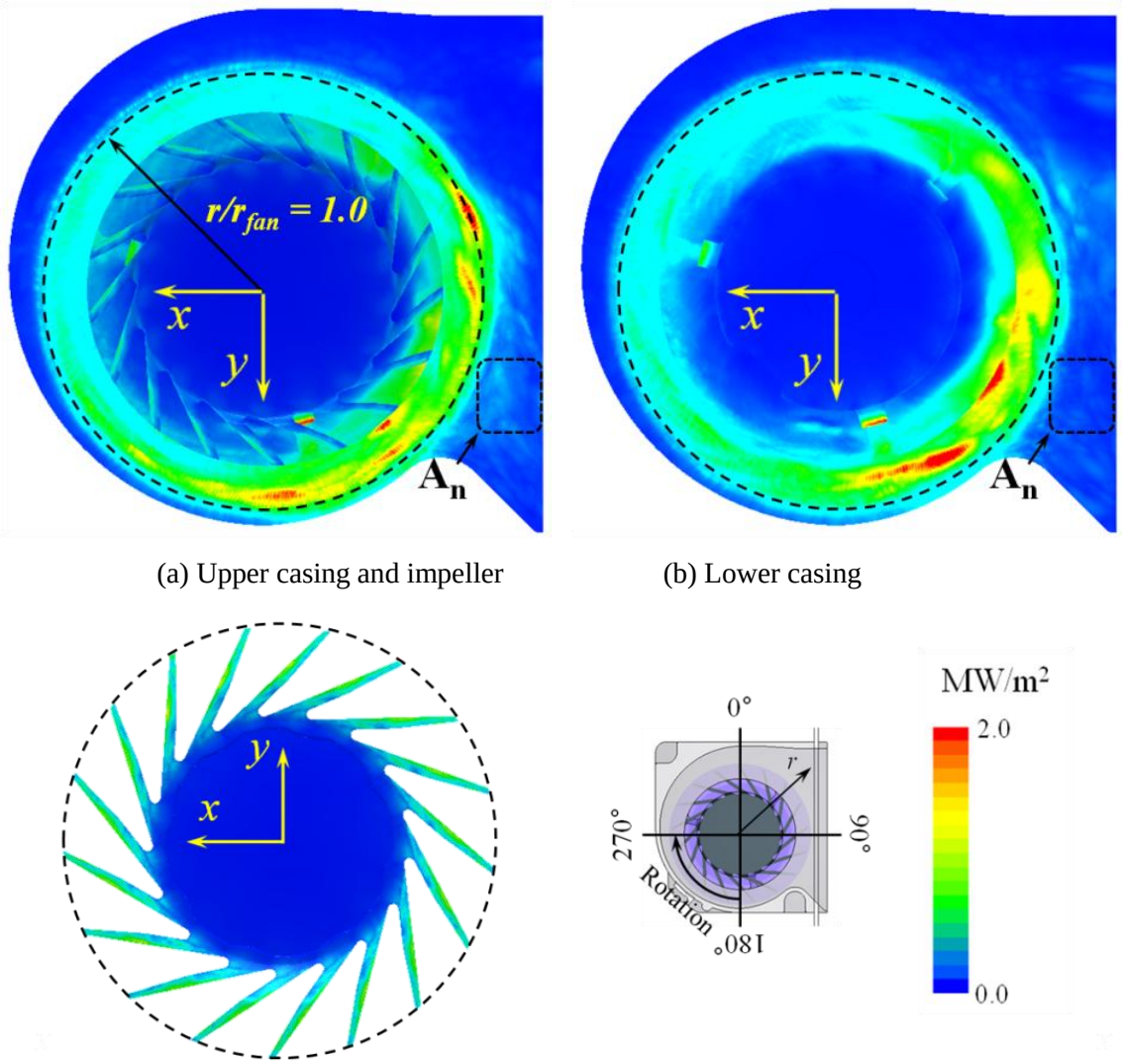

(a) Upper casing and impeller (b) Lower casing

(c) Bottom view of impeller

Fig. 6-7 Aeroacoustic source strength distribution of Base model

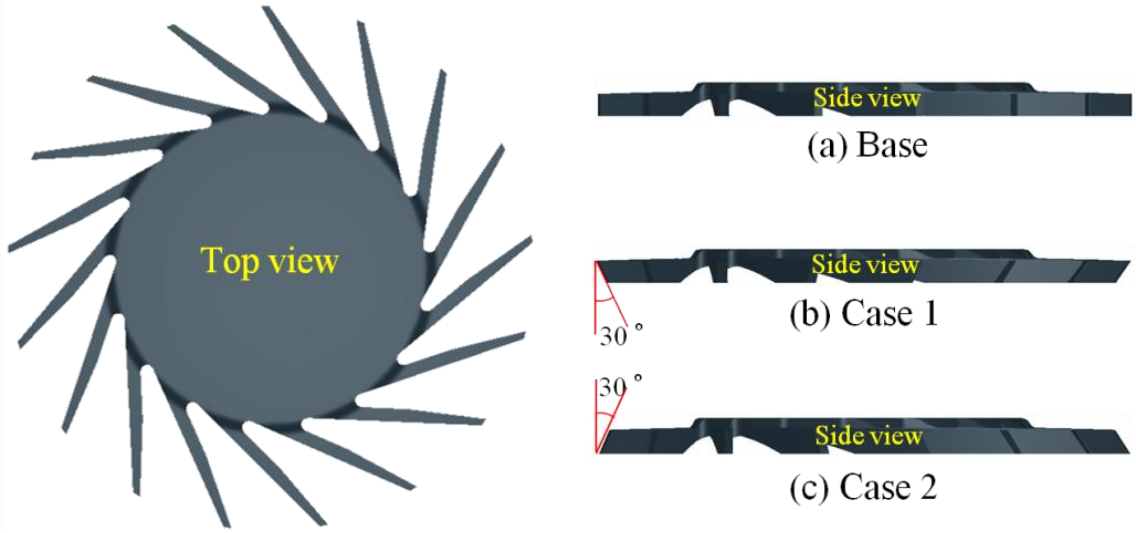

Fig. 6-8 Modification of impeller shapes for low noise

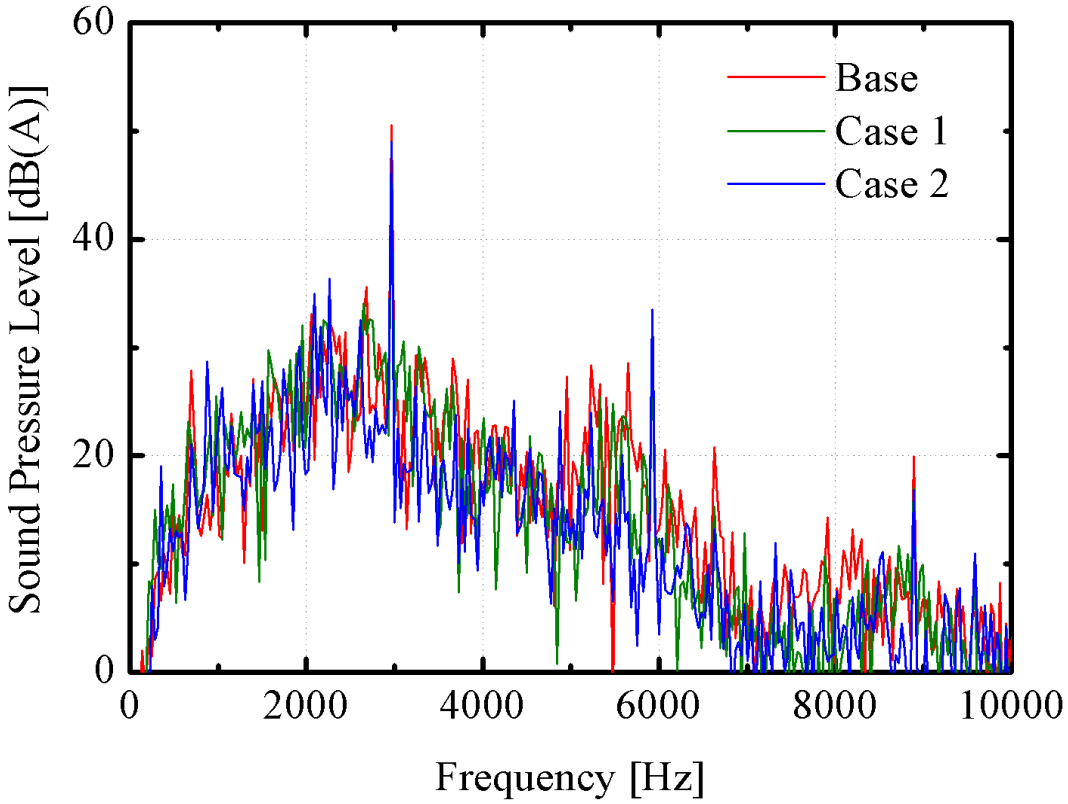

Fig. 6-9 Comparison of aerodynamic sound spectra between Base model and modified impeller models

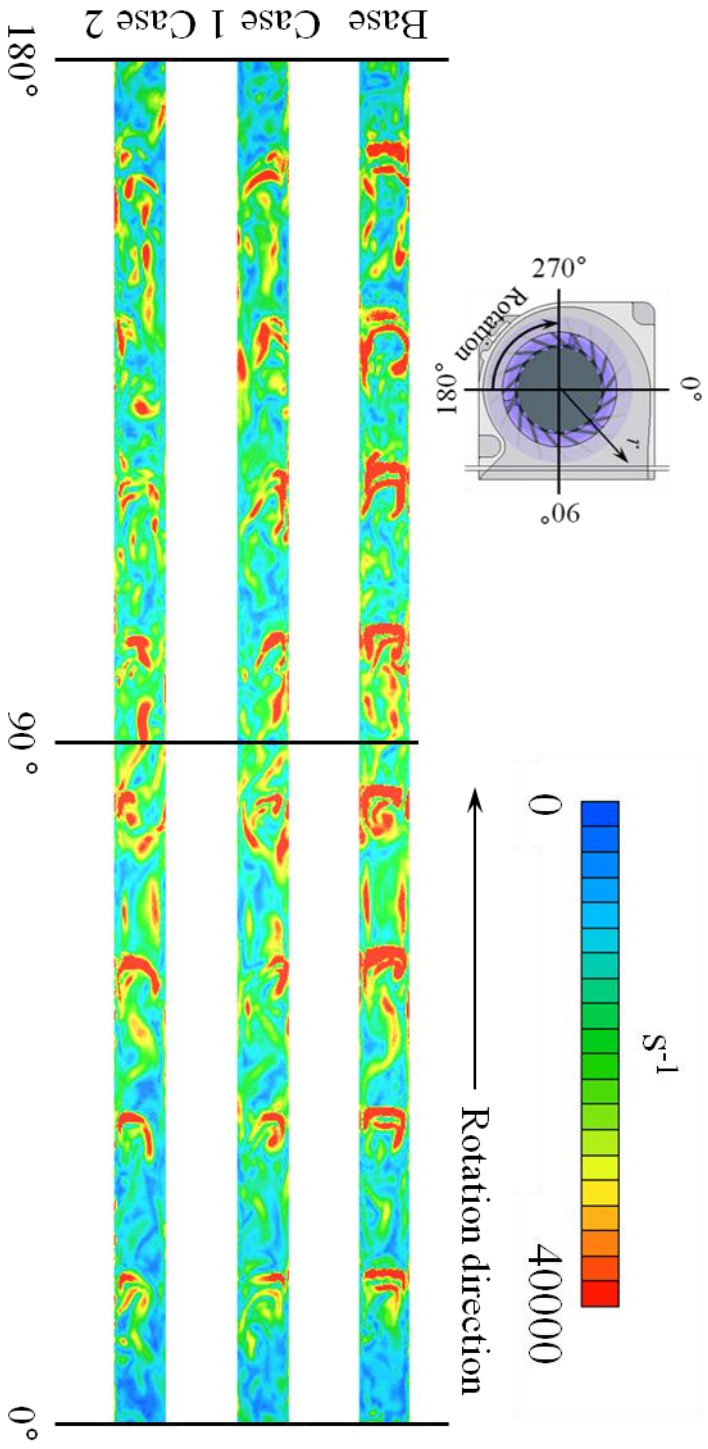

Fig. 6-10 Vorticity distribution of r/r_{fan} = 1.00625 and t = 0.074252 sec

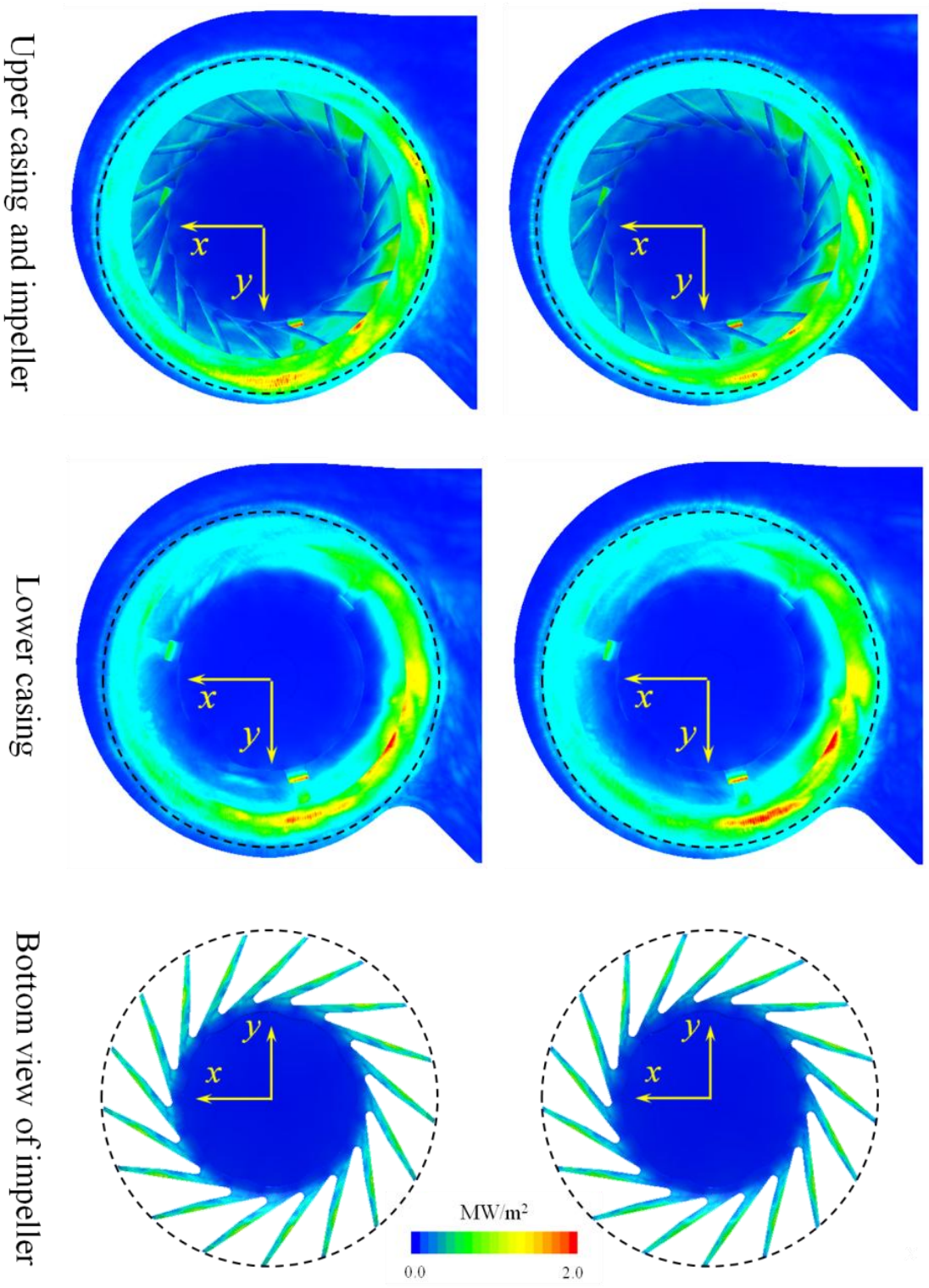

(a) Case 1 (b) Case 2

Fig. 6-11 Aeroacoustic source strength distribution in low noise models

Chapter 7. Conclusions

In this study, numerical analysis method by using CFD and aeroacoustic analogy was utilized for noise reduction in the turbomachinery that is used in home electronics. To predict the flow field produced by the rotation of the turbomachinery, the three-dimensional unsteady Navier-Stokes equations were solved. The turbulence model used for the flow field prediction was SST k–ω model that thoroughly simulates the adverse pressure gradient and separation in the boundary layer and LES model presenting the excellence in modeling of the turbulence intensity. In order to increase the accuracy of the unsteady state flow analysis, double precision solver and sub-iteration in each time step were adopted, the convergence condition was given for each time step, and the next step was conducted only after the condition was satisfied.

The method used for prediction of the flow noise in this study was acoustic analogy method that is one of the hybrid methods in which CFD and CAA are combined together. The grid used to predict the noise with the acoustic analogy was the surface grid that is used in CFD. Numerical algorithm was adopted for prediction of the noise at the location identical to the location of the microphone that was used to measure the noise. Consequently, the use of the surface grid that was identical to what was used in CFD and expresses the shape of the turbomachinery enabled to predict the location and the distribution of the noise source in a more accurate manner. In addition, aeroacoustic analogy was conducted in this study to predict the flow noise by solving Lowson equation that is easy for numerical application and can be used to predict the sound pressure on a point force which is moving in a free field based on Neise research reporting that the major noise sources of the turbomachinery operating in subsonic domain are caused by the dipole.

Each of the noise predicted by the numerical analysis was compared with the corresponding noise measured through the experiment. Observation on the noise spectrum revealed considerable agreement in the tonal noise of BPF and its harmonic frequency and the broadband noise at low frequency between the predicted noise and the measured noise. However, the disagreement at high frequency was determined to be that the broadband noise due to the random broadband noise was not able to be

predicted since the noise radiation at a free field in which only dipole was considered was calculated.

In the small axial flow fan with cylindrical shroud, the noise source was found to be located in the pressure side of the blade. As a result of the investigation on the unsteady state flow field based on the location of the noise source, the flow structure in which the flow that was separated from the right-angled cross-section of the shroud inlet causes the tip leakage vortex by interacting with the blades of the rotor and the caused tip leakage vortex produces noise as it hits the following blades was confirmed. For reduction of the flow noise, the shape of the shroud inlet was altered to the nozzle shape with various radius of the curvature; and noise reduction by 3.7 dB was predicted.

To verify that the approach of numerical analysis is possible for noise prediction in a small turbomachinery, the flow noise of a small axial flow fan used as a cooling fan in a rack mount server computer with smaller rotor diameter and higher rotation speed than the small axial flow fan with the cylindrical shroud that was predicted above was predicted in advance. Agreement was confirmed by comparing the predicted noise spectrum with the measured noise spectrum. In particular, the tonal noise that occurs by the irregular clearance that is the interval between the blade tip and the shroud due to the shroud shape was well predicted. In addition, the correlation between the surface pressure fluctuation obtained by the flow analysis and the sound pressure predicted at the location of the microphone from the noise analysis was confirmed through the coherence analysis.

For the centrifugal fan with smaller size of the impeller, higher rotation speed, and different flow structure compared to the two axial flow fan predicted above, the flow noise was predicted and its characteristics were understood. Due to the structure of the centrifugal fan that is operated for cooling of the electronics as embedded inside the electronics such as portable laptops, asymmetric flow field was observed. The locations of the noise source were also distributed asymmetrically by unsteady flow and stronger noise sources were found in the casing rather than in the impeller of the centrifugal fan. After analyzing the distribution of the noise source, the method of numerical analysis was applied for reduction of the flow noise and the impeller tip was cut obliquely to minimize the noise sources produced by the impeller tip; and noise reduction by 0.8 dB was predicted. In the low noise models applied for noise reduction above, fan

performance was changed by altering the shape of the shroud or the rotating part. Hence, specific noise level was used to determine the noise reduction in the low noise models.

In this study, the flow noise caused by the turbomachinery was predicted by combining CFD and CAA, and the method of numerical analysis was utilized to reduce flow noise. Since the random broadband noise at high frequency was not predicted well as this study focused on the radiation of the dipole noise in a free field, accurate sound pressure at the measuring point where the microphone is located in the space was not predicted. However, the location and characteristics of the noise source were predicted well. As a result, the unsteady flow related to the noise sources was confirmed and understood; hence, the shape of the low noise model that can reduce the flow noise can be drawn. The results of this study are believed to be sufficient to motivate the use of the numerical analysis for reduction of flow noise in the turbomachinery through the understanding on the noise sources.

References

[1] Dixon, S. L. and Hall, C. A., 2010, "Fluid mechanics and thermodynamics of turbomachinery", Butterworth-Heinemann, 6th edition.

[2] Wright, T. and Gerhart Philip M., 2010. "Fluid machinery", CRC Press, 2nd edition.

[3] Needham, J., 1986, "Science and Civilization in China: Volume 4, Physics and Physical Technology, Part 2, Mechanical Engineering, Taipei, Caves Books.

[4] Morfey, C. L., 1972, "The acoustics of axial flow machines", Journal of Sound Vibration, Vol. 22, Iss. 4, pp. 445-466.

[5] Goldstein, M. and Rosenbaum, B., 1973, "Effect of anisotropic turbulence and aerodynamics noise", J. Acous, Soc. Am. Vol. 54, No. 3, pp. 630-645.

[6] Wright, S. E., 1976, "The acoustic spectrum of axial flow machines", Journal of Sound and Vibration, Vol. 45, Iss. 2, pp. 165-223.

[7] Maskew, B., 1982, "Prediction of subsonic aerodynamic characteristics: A case for low-order panel method", Journal of Aircraft, Vol. 19, No. 2, pp. 157-163.

[8] Neise, W., 1992, "Review of fan noise generation mechanisms and control methods", An International INCE Symposium, CETIM, France, 1992, pp. 45-56.

[9] Crighton, D. G., Dowling, A. P., Ffowcs Williams, J. E., Heckl, M. and Leppington, F. G., 1992, "Modern methods in analytical acoustics: Lecture notes", Springer-Verlag.

[10] Lighthill, M. J., 1952, "On Sound Generated Aerodynamically. I. General Theory", Proc. R. Soc. Lond. Ser. A 211, pp. 564-587.

[11] Lighthill, M. J. 1954, "On Sound Generated Aerodynamically. II. Turbulence as a source of sound", Proc. R. Soc. Lond. Ser. A 222, pp. 1-32.

[12] Curle, N., 1955, "The influence of solid boundaries upon aerodynamic sound", Pro. R. Soc. Lond. Ser. A 231, pp. 505-514.

[13] Lowson, M. V., 1965, "The sound field for singularities in motion", Pro. R. Soc. Lond. Ser. A. 286, pp. 559-572

[14] Ffowcs Williams, J. E. and Hawkings, D. L., 1969, "Sound generation by turbulence and surfaces in arbitrary motion", Phil. Trans. Proc. R. Soc. Lond. Ser. A264, No. 1151, pp. 321-342.

[15] Wiesner, F. J., 1967, "A review of slip factors for centrifugal impellers", J. Eng.

Power, Vol. 89, Iss. 4, pp. 558-566.

[16] Weissgerber, C. and Carter, A. F. 1980, “Comparisons of hydraulic performance prediction and test data for a range of pumps”, In Symposium on Performance prediction of centrifugal pumps and compressors, Louisiana, March, ASME, pp. 219-226.

[17] Takagi, T., Kobayashi, J., Miyashiro, H. and Morimoto, M., 1980, “Performance prediction of single-suction centrifugal pumps of different specific speeds”, In Symposium on Performance prediction of centrifugal pumps and compressors, Louisiana, March, ASME, pp. 227-234.

[18] Rathod, M. S. and Donovan, F. M., 1980, “Performance evaluation of a centrifugal cardiac pump”, In Symposium on Performance prediction of centrifugal pumps and compressors, Louisiana, March, ASME, pp. 235-243.

[19] Wu, C. H., 1952, “A general theory of three-dimensional flow in subsonic and supersonic turbomachines of axial-, radial-, and mixed-flow types”, NACA TN 2604.

[20] Katsanis, T., 1964, “Use of arbitrary quasi-orthogonals for calculating flow distribution in the meridional plane of a turbomachine”, NASA TN 2546.

[21] Tsukamoto, H and Ohashi, H., 1982, “Transient characteristics of a centrifugal pump during starting period”, J. Fluids Eng., Vol. 104, Iss. 1, pp. 6-13.

[22] Imaichi, K., Tsujimoto, Y. and Yoshida, Y., 1982, “An analysis of unsteady torque on a two-dimensional radial impeller”, J. Fluids Eng., Vol. 104, Iss. 2, pp. 228-234.

[23] Tsukamoto, H., Matsunaga, S., Yoneda, H. and Hata, S., 1986, “Transient characteristics of a centrifugal pump during stopping period," J. Fluids Eng., Vol. 108, Iss. 4, pp. 392-399.

[24] Shoji, H. and Ohashi, H., 1987, “Lateral fluid forces on whirling centrifugal impeller (1st Report: Theory)”, J. Fluids Eng., Vol. 109, Iss. 2, pp. 94-99.

[25] Kiya, M. and Kusaka, A., 1989, “Numerical analysis of separated unsteady flow in a centrifugal impeller”, Transactions of the Japan Society of Mechanical Engineers Series B, Vol. 55, No. 510, pp. 290-297.

[26] Panigrahi, D. C. and Mishra, D. P., 2014, “CFD simulations for the selection of an appropriate blade profile for improving energy efficiency in axial flow mine ventilation fans”, Journal of Sustainable Mining, Vol. 13, Iss. 1, pp. 15-21.

[27] Zhang, S., MacManus, D. G. and Luo, J., 2016, “Parametric study of turbine NGV

blade lean and vortex design", Chinese Journal of Aeronautics, Vol. 29, Iss. 1, pp. 104-116.

[28] Pogorelov, A., Meinke, M. and Schröder, W., 2016, "Effects of tip-gap width on the flow field in an axial fan", International Journal of Heat and Fluid Flow, Vol. 61, Part B, pp. 466-481.

[29] Lynam, E. J. H. and Webb, H. A., 1919, "The emission of sound by airscrews", Reports and memoranda 624 Aeronautical research committee.

[30] Gutin, L., 1948, "On the sound field of a rotating propeller", Technical Memorandum 1195 NACA

[31] Tyler, J. M. and Sofrin, T. G., 1962, "Axial flow compressor noise studies", Society of Automotive Engineers Transactions, 70 pp. 309-332.

[32] Embleton, T. F., 1963, "Experimental study of noise reduction in centrifugal blowers", Journal of the Acoustical Society of America, Vol. 35, Iss. 5, pp. 700-705.

[33] Lyons, L. A. and Platter, S., 1963, "Effect of cut-off configuration on pure tones generated by small centrifugal blowers", Journal of the Acoustical Society of America, Vol. 35, Iss. 9, pp. 1455-1456.

[34] Neise, W., 1976, "Noise reduction in centrifugal Fans: A literature survey", Journal of Sound and Vibration, Vol. 45, Iss. 3, pp. 375-403.

[35] Neise, W. and Koopmann, G.H., 1980, "Reduction of centrifugal fan noise by using resonators", Journal of Sound and Vibration, Vol. 73, Iss. 2, pp. 297-308.

[36] Neise, W., 1982, "Review of noise reduction methods for centrifugal fans", J. of Engineering for Industry, Vol. 104, Iss. 2, pp. 151-161.

[37] Koopmann, G. H., Fox, D. J. and Neise, W., 1988, "Active source cancellation of the blade tone fundamental and harmonics in centrifugal fans", Journal of Sound and Vibration, Vol. 126, Iss. 2, pp. 209-220.

[38] Chen, M. Z. and Wu, X. H., 1999, "Vortex simulation of rotor/stator interaction in turbomachinery", Journal of Turbomachinery, Vol. 121, Iss. 2, pp. 358-364.

[39] Jang, C. M., Furukawa, M. and Inoue, M., 2001, "Analysis of vortical flow field in a propeller fan by LDV measurements and LES-Part I: Three-dimensional vortical flow structures", Journal of Fluids Engineering, Vol. 123, Iss. 4, pp. 748-754.

[40] Jang, C. M., Furukawa, M. and Inoue, M., 2001, "Analysis of vortical flow field in a propeller fan by LDV measurements and LES-Part II: Unsteady nature of vortical flow

structures due to tip vortex breakdown", Journal of Fluids Engineering, Vol. 123, Iss. 4, pp. 755-761.

[41] Jang, C. M., Furukawa, M. and Inoue, M., 2003, "Frequency characteristics of fluctuating pressure on rotor blade in a propeller fan", JSME International Journal Series B, Vol. 46, No. 1, pp. 163-172.

[42] Jang, C. M., Fukano, T., and Furukawa, M., 2003, "Effects of the tip clearance on vortical flow and its relation to noise in an axial flow fan," JSME International Journal, Series B, Vol. 46, No. 3, pp. 356-365.

[43] Carolus, T., Schneider, M. and Reese, H., 2007, "Axial flow fan broad-band noise and prediction", Journal of Sound and Vibration, Vol. 300, Iss. 1-2, pp. 50-70.

[44] Rafael Ballesteros-Tajadura, Sandra Velarde-Suárez and Juan Pablo Hurtado-Cruz, 2008, "Noise prediction of a centrifugal fan: Numerical results and experimental validation", Journal of Fluids Engineering, Vol. 130, Iss. 9, 091102, pp. 1-12.

[45] Scheit, C., Karic, B. and Becker, S., 2012, "Effect of blade wrap angle on efficiency and noise of small radial fan impellers-A computational and experimental study", Journal of Sound and Vibration, Vol. 331, No. 5, pp. 996-1010.

[46] Jeon, W. H. and Lee, D. J., 1999, "An analysis of the flow and aerodynamic acoustic sources of a centrifugal impeller", Journal of Sound and Vibration, Vol. 222, Iss. 3, pp. 505-511.

[47] Kim, W., Jeon, W. H., Hur, N., Hyun, J. J., Lim, C. K. and Lee, S. H., 2011, "Development of a low-noise cooling fan for an alternator using numerical and DOE methods," International Journal of Automotive Technology, Vol. 12, No. 2, pp. 307-314.

[48] Jeon, W. H., 2003, "A numerical study on the effects of design parameters on the performance and noise of a centrifugal fan," Journal of Sound and Vibration, Vol. 265, Iss. 1, pp. 221-230.

[49] Jeon, W. H. and Lee, D. J., 2003, "A numerical study on the flow and sound fields of centrifugal impeller located near a wedge", Journal of Sound and Vibration, Vol. 266, Iss. 4, pp. 785-804.

[50] Jeon, W. H., Baek, S. J. and Kim, C. J., 2003, "Analysis of the aeroacoustic characteristics of the centrifugal fan in a vacuum cleaner", Journal of Sound and Vibration, Vol. 268, Iss. 5, pp. 1025-1035.

[51] Lim, T. G., Lee, S. M., Jeon, W. H. and Jang, C. M., 2015, "Characteristics of

unsteady flow field and aeroacoustic noise in a regenerative blower," Journal of Mechanical Science and Technology, Vol. 29, No. 5, pp. 2005-2012.

[52] Lim, T. G., Jeon, W. H. and Minorikawa, G., 2016, "Characteristics of unsteady flow field and flow-induced noise for an axial cooling fan used in a rack mount server computer," Journal of Mechanical Science and Technology, Vol. 30, No. 10, pp. 4601-4607.

[53] Lim, T. G., Jeon, W. H. and Minorikawa, G., 2017, "Computational study for noise reduction and characteristic of unsteady flow field/flow-induced noise generated in a small radial fan", Journal of Mechanical Science and Technology, Vol. 31, No. 11, pp. 5337-5345.

[54] Lim, T. G., Jeon, W. H. and Minorikawa, G., 2017, "Prediction of the noise reduction by shroud shape and the characteristics of flow-induced noise generated in an axial flow fan", International Journal of Fluid Machinery and System. (submitted on Nov. and revised).

[55] Myeong, H. K., 2002, "CFD Introduction", Munundang (in Korean).

[56] Ferziger, J. H. and Peric, M., 2002, "Computational methods for fluid dynamics", Springer.

[57] Myeong, H. K., 2012, "CFD", Munundang (in Korean).

[58] Software Cradle, 2015, "Basics of CFD analysis, User's guide manual of SC/Tetra Ver.12", Japan.

[59] Mavriplis, D. J., 1997, "Unstructured grid techniques", Annual Review of Fluid Mechanics, Vol. 29, pp. 473-514.

[60] Kim, W., 2010, "A study on computational aeroacoustic noise of fans by numerical analysis method", Sogang University Press. (in Korean)

[61] Patankar, S. V. and Spalding, D. B., 1972, "A calculation procedure for heat, mass and momentum transfer in three-dimensional parabolic flows", Int. J. Heat Mass Transfer, Vol. 15, Iss. 10, p. 1787-1806.

[62] Versteeg, H. K. and Malalasekera, W., 2006, "An introduction to computational fluid dynamics: The finite volume method", Longman Scientific & Technical.

[63] Van Doormal, J. P. and Raithby, G. D., 1984, "Enhancements of the SIMPLE method for predicting incompressible fluid flows", Numerical Heat Transfer, Vol. 7, Iss. 2, pp. 147-163.

[64] Menter, F. R., 1993, “Zonal two equation $k-\omega$ turbulence models for aerodynamic flows”, AIAA Paper No. 93-2906, Proc. 24th Fluid Dynamics Conf., July 6-9, Orlando, Florida, USA.

[65] Menter, F. R., 1994, “Two-equation eddy-viscosity turbulence models for engineering applications”, AIAA Journal, Vol. 32, No. 8, pp. 1598-1605.

[66] Menter, F. R., Kuntz, M. and Langtry, R., 2003, “Ten years of industrial experience with the SST turbulence model”, Turbulence, Heat and Mass Transfer 4, Begell House, Inc., pp. 625-632.

[67] Wilcox, D. C., 1988, “Reassessment of the scale-determining equation for advanced turbulence models”, AIAA J., Vol. 26, No. 11, pp. 1299-1310.

[68] Wilcox, D. C., 2006, “Turbulence Modeling for CFD”, DCW Industries.

[69] Wilcox, D. C., 2008, “Formulation of the $k-\omega$ turbulence model revisited”, AIAA Journal, Vol. 46, No. 11, pp. 2823-2838.

[70] Launder, B. E. and Spalding, D. B., 1974, “The numerical computation of turbulent flows”, Computer Methods in Applied Mechanics and Engineering, Vol. 3, Iss. 2, pp. 269-289.

[71] Donea, J., Huerta, A., Ponthot, J.-Ph. and Rodr´ıguez-Ferran, A., 2004, “Encyclopedia of Computational Mechanics”, Vol. 1, John Wiley & Sons, Ltd.

[72] Sagaut, P., 2001, “Large eddy simulation for incompressible flows”, Springer.

[73] Leonard, A., 1974, “Energy cascade in large eddy simulation of turbulent fluid flows”, Advances in Geophysics, Vol. 18, Part A, pp. 237-248.

[74] Smagorinsky, J., 1963, “General circulation experiments with the primitive equations. I. The basic experiment”, Monthly Weather Review, Vol. 91, No. 3, pp.99-164.

[75] Davidson, L., 2009, “Large eddy simulations: how to evaluate resolution”, International Journal of Heat and Fluid Flow, Vol. 30, Iss. 5, pp. 1016-1025.

[76] Margnat, F. Fortuné, V., 2010, “An iterative algorithm for computing aeroacoustic integrals with application to the analysis of free shear flow noise”, The Journal of the Acoustical Society of America, Vol. 128, Iss. 4, pp.1656-1667.

[77] Brentner, K. S., 1996, “Numerical algorithms for acoustic integrals – The devil is in the details.”, 2nd AIAA/CEAS Aeroacoustics conference, May 6-8, State College, PA.

[78] Ito, T., Minorikawa, G. and Fan, Q., 2009, “Experimental research for performance

and noise of small axial fan," International Journal of Fluid Machinery and Systems, Vol. 2, No. 2, pp. 136-146.

[79] Cattanei, A., Ghio, R., Bongiovì, A., 2007, "Reduction of the tonal noise annoyance of axial flow fans by means of optimal blade spacing," Applied Acoustics, Vol. 68, No. 11-12, pp. 1323-1345.

[80] Cai, N., Xu, J. and Benaissa, A., 2003, "Aerodynamic and aeroacoustic performance of a skewed rotor," in Proceedings of ASME Turbo Expo, International Gas Turbine Institute Conference (IGTI '03), Vol. 6A, pp. 497-504, Atlanta, Ga, USA.

[81] Neise, W., 2010, "Noise reduction in centrifugal fans: A literature survey", Journal of Sound and Vibration, Vol. 45, Iss. 3, pp. 375-403.

[82] Ren, G., Heo, S., Kim, T. H. and Cheong, C., 2013, "Response surface method-based optimization of the shroud of an axial cooling fan for high performance and low noise", Journal of Mechanical Science and Technology, Vol. 27, No. 1, pp. 33-42.

[83] Minorikawa, G. and Muto, H., 2011, "Study on fan noise reduction for small fan using commercial CFD software", Proceedings of Internoise 2011, Osaka, Japan, pp. 153-159.

[84] Jeon, W. H., Kobayashi, T., Kodama, T. and Hamada, S., 2011, "Study on the CFD method for noise source identification and aeroacoustic analysis of an axial fan", Proc. of Internoise2011, Osaka, Japan, pp. 160-169.

[85] Sheng, G., 2012, "Vehicle noise, vibration, and sound quality", SAE international, Warrendale, Pennsylvania, USA.

Acknowledgements

I would like to express my deepest gratitude to my supervisor Prof. Gaku Minorikawa who gave me the opportunity to tread the path of knowledge again and supported me to keep walking without stopping during following the path of knowledge under detailed guidance as well as warm encouragement. I would also like to heartily thank Dr. Wan-Ho Jeon, who gave me the opportunity to pass the unfinished graduate school and helped me to take my psychological and academic composure even though my busy life. Their kind consideration and encouragement about me have been greatly helpful to tread the path of knowledge again.

I also appreciate sincerely CEDIC Co. Ltd. CEO Jang-Hyung Cho, who understand the necessary of researches and recommend continuously us to conduct the researches, and co-workers including my team members.

Thanks for my old friends (Jin-Hyong Kwon, Bum-Jin Kim, Seung-Hyo Lyu, Hyung-Tak Moon, Sang-Hyun Park, Yoon-Seok Hong) who have always encouraged by just keeping watching me during more than 30 years. And special thanks for Dr. Ho-Joon Lee who often called me to relieve my stress and gave me a lot of advices from his experience. In addition, I'm sorry that I could not express my thanks to all people who helped me and ask for their understanding.

Finally, I would like to express sincere thanks my wife’s family including my parents-in-law who have prayed for me and my family. Also thanks to my reliable younger sister, Soo-Jeong, and my younger brother, Tae-Hyung, and only my mother’s sister and her family. My family deserves my gratitude more than adequately because it was impossible for my dream to come true without their love, support and patience. I owe my profound gratitude to my beloved wife Mi-Hee Hwang, my lovely and cherished son Seo-Joon and daughter Ah-Yoon. Also, my special thanks and honor offer my parents who give me all they can do themselves for me.

Praying their happiness, I dedicate my work to my family and to people who helped for me.

The person who makes a success of living is the one who sees his goal steadily and aims for it unswervingly. That is dedication.

- Cecil B. DeMille -